A *C. elegans* model for X-linked adrenoleukodystrophy: roles of *pmp-4* fatty acid transporter in the nervous system

SANJIB KUMAR GUHA

TESI DOCTORAL UPF 2015

Thesis Supervisors: Dr. Aurora Pujol Onofre
Dr. Esther Dalfo Capella

Department: Neurometabolic diseases laboratory

IDIBELL- Institut d´Ínvestigacio´ Biomédica de Bellvitge

Acknowledgements:

I express my heartiest gratitude to my advisors Dr. Aurora Pujol and Dr. Esther Dalfo who have always provided me constant support and encouragement. A big thanks to Dr. Pujol first of all for giving me an opportunity to join her esteemed lab, do the PhD and also in getting the prestigious FI scholarship. Dr. Dalfo has been always with me throughout all these years both in terms of supervising the projects, helping me with this dissertation and also in helping an international student like me with bureaucracy.

I like to take the opportunity to thank my lab mates who have extended their help in carrying out my research, especially Andrea Coppa, my fellow lab mate who also worked with *C. elegans* and to Laia Morato with whom I used to share my bench space. Am lucky to have all the other PhD students starting from Jorge, Jone, Patri, Pablo, Devesh as my companions and also Janani who were always there stretching out their helping hands whenever needed. Thanks to all the technicians: Juanjo, Jordi, Chris, Laia, Barbara. Also a big thanks to the senior members of the group and the Post docs starting from Stephane, Montse, Nath, Xavi, Agatha and Hartmut, who always gave valuable suggestions during data clubs and seminars and always had answers to my questions. I can't forget the help of all the other members from Genetica Molecular Department, the secretaries and the people of Confocal microscope facility. I sincerely thank my committee members for their time and assistance in the preparation of the thesis.

And last but not the least I am extremely grateful to my family, my relatives, my Cricket group friends and last but not the least, my beautiful wife, Sreetama who have supported throughout my course of study and my duration of research. In short, thanks to all the lovely, beautiful and caring people in my life, without their upteen support this thesis wouldn't have been possible.

Summary

X-linked adrenoleukodystrophy (X-ALD) is an inherited neurodegenerative disorder. The genetic bases for all its different phenotypic variants are mutations in the gene encoding the peroxisomal ATP-binding cassette (ABC) transporter ABCD1, which transports very long chain fatty acids from the cytosol into the peroxisome for its degradation. The default manifestation of mutation in ABCD1 is adreno myeloneuropathy (AMN), a slow, progressive dying-back axonopathy affecting both ascending and descending spinal cord tracts as well as in some cases, peripheral neuropathy. In the present study, we use the invertebrate model organism *Caenorhabditis elegans* to generate a new nematode model of X-ALD. We reveal that the *pmp-4(ok396)* deletion mutant reproduces the main features of X-ALD such as lipid accumulation, increased mitochondrial oxidative stress, axonopathy and altered locomotion. Given the evidence that oxidative stress plays an important role in VLCFA-induced pathogenesis of ALD, therapeutic efforts aimed at the removal of free-radicals, prevention of their formation, or restoration of ETC function seem promising. Here we describe the mitochondria-specific pharmacological effects of MitoQ in protecting against VLCFA-induced toxicity and oxidative stress and its ability to rescue the observed X-ALD phenotypes on *pmp-4(ok396)* mutant worms.

Resumen

La adrenoleucodistrofia ligada al cromosoma X (ALD-X) es un trastorno neurodegenerativo hereditario, causado por mutaciones en ABCD1. Este gen codifica para un transportador peroxisomal que importa ácidos grasos de cadena muy larga (AGCML) del citosol hacia el peroxisoma para su posterior degradación. La adrenomieloneuropatía (AMN) es la variante fenotípica en adultos y se manifiesta como un axonopatia de progresión lenta en la médula espinal. En este estudio utilizamos el gusano *Caenorhabditis elegans* para generar un nuevo modelo de ALD-X. Observamos que el mutante *pmp-4(ok396)* reproduce las principales características de la ALD-X (acumulación de lípidos, incremento del estrés oxidativo mitocondrial, axonopatía y locomoción alterada). Basándonos en evidencias que el estrés oxidativo inducido por acumulación de AGCML juega un papel importante en la patogénesis,

estrategias enfocadas en la eliminación de radicales libres, prevención de su formación o normalización de la función de la cadena de transporte de electrones mitocondrial, poseen un prometedor potencial terapéutico. Aquí demostramos que el compuesto MitoQ actua a nivel mitocondrial protegiendo en contra del estrés oxidativo y rescata los fenotipos ALD-X en los gusanos *pmp-4(ok396).*

Resum

La adrenoleucodistròfia lligada al cromosoma X (ALD-X) és un trastorn neurodegeneratiu hereditari, causat per mutacions en ABCD1. Aquest gen codifica per un transportador peroxisomal que importa àcids grassos de cadena molt llarga (AGCML) del citosol cap al peroxisoma per a la seva posterior degradació. La adrenomieloneuropatía (AMN) és la variant fenotípica en adults i es manifesta com una axonopatia de progressió lenta en la medul·la espinal. En aquest estudi utilitzem el cuc *Caenorhabditis elegans* per generar un nou model d'ALD-X. Observem que el mutant *pmp-4 (ok396)* reprodueix les principals característiques de l'ALD-X (acumulació de lípids, increment d'estrès oxidatiu mitocondrial, axonopatia i locomoció alterada). Basant-nos en les evidències que l'estrès oxidatiu induït per acumulació d'AGCML juga un paper important en la patogènesi, estratègies enfocades en eliminar radicals lliures, prevenirla seva formació o normalitzar la funció de la cadena de transport d'electrons mitocondrial, posseeixen un prometedor potencial terapèutic. Aquí, demostrem que el compost MitoQ actua a nivell mitocondrial protegint en contra de l'estrès oxidatiu i rescatant els fenotips ALD-X en els cucs *pmp-4 (ok396)*.

Abstract

X-linked adrenoleukodystrophy (X-ALD) is a rare neurometabolic disease characterized by inflammatory demyelination in the brain and axonal degeneration in the spinal cord. The disease is caused by mutations in the ABCD1 gene, which codifies for the peroxisomal transporter of very long chain fatty acids (VLCFAs) (Ferrer et al., 2010). Accumulation of VLCFAs, increased oxidative stress and mitochondrial impairment are considered as the main etiological factor of this disease (Lopez-Erauskin et al., 2013; Morato et al., 2013).

The present thesis is focused on establishing a new *in vivo* model of X-ALD in the invertebrate model organism *Caenorhabditis elegans (C. elegans)*, a tiny ~1 mm size multicellular nematode, by using the mutant strain *pmp-4(ok396)* lacking the PMP-4 protein, which is the ortholog of mammals ABCD1 and ABCD2. The absence of PMP-4 reproduced the principal X-ALD phenotypes found in humans and mice. Indeed, the *pmp-4(ok396)* mutant worms display lipid accumulation, represented by enlarged lipid droplets, increased levels of ROS, originating mainly from mitochondria and high susceptibility to inhibitors of the mitochondrial electron transport chain. The neuronal phenotype in worms is represented by reduced locomotion ability via thrashing behaviour and morphological axonal defects, which arise during L4 developmental stage and become more severe with aging. We investigated the *in vivo* ability of a cellular anti-oxidant, Coenzyme Q (CoQ) and of a mitochondria-targeted antioxidant, MitoQ, to protect against ROS and oxidative stress in this *C. elegans* model of X-ALD. Our research reveals that MitoQ specifically improves severely reduced locomotion behaviour and ameliorates defects in GABA motor neurons and mechanosensory neurons.

X-ALD is being characterized as a glial disease (Pujol et al., 2010; Reiser et al., 2008). Glia-like cells in *C. elegans* are mostly located in the amphid organ, the main chemosensory organ in the worm (Parpura et al., 2014; Shaham et al., 2008). Apart from the X-ALD specific phenotypes, we have discovered that the *pmp-4* mutant worms are not only defective in AWB chemosensory neuron cilia structural integrity but also in some cilia-mediated sensory behaviour. Furthermore, these abnormalities are shared with other intra-peroxisomal mutants such as *daf-22* and *dhs-28*, the thiolase and bifunctional peroxisomal proteins respectively. Through superoxide staining and anti-oxidant treatments we have demonstrated that mitochondrial ROS are principal and

specific modulators of *pmp-4* mutants chemosensation defects whereas in case of peroxisomal mutants, chemosensation is not modulated by mitochondrial ROS.

Collectively, this thesis provides the proofs that this mutant *C. elegans* strain *pmp-4(ok396)* is robustly modelling X-ALD disease. Consequently this model might be used to deeper, investigate this disease. This nematode model is a more advantageous tool in comparison to the existing mouse models, because of its early onset of the phenotypes, easy maintenance and short life span. It also reveals the way of action of different anti-oxidants and paves the way for their use in higher model organisms. Moreover, in agreement with its design, the protective effects of MitoQ seem to be targeted specifically to the mitochondrial membrane and our findings confirm that MitoQ have strong therapeutic potential for oxidative stress-associated neurodegenerative disorders as shown by Halliwell et al., 2014 for the treatment of Alzheimer´s disease and also maybe for sensory cilia-related disorders.

Contents

R. Results (Chapter I)

R. Results (Chapter II)

M. Materials and Methods

INTRODUCTION

I. Introduction:

I.1 General features of X-ALD

X-linked adrenoleukodystrophy (X-ALD: McKusick no. 300100) is a rare neurometabolic genetic disorder of fatal outcome, characterized by a defective transport and subsequent degradation of saturated very long chain fatty acids (VLCFA), that ends up in axonal degeneration and / or demyelination within the central nervous system (CNS), axonopathy in spinal cords and adrenal insufficiency. The disease is caused by mutations in the *ABCD1* gene that leads to the loss of function of the ALD protein (ALDP). ALDP is an ATP – binding cassette (ABC) half-transporter, an integral peroxisomal membrane protein involved in the import of VLCFA into peroxisomes for degradation by β- oxidation. All X-ALD patients indeed accumulate saturated VLCFAs and to a lesser extent, monounsaturated VLCFAs in plasma and brain cortex. VLCFAs are incorporated in complex lipids in cell membranes and are thought to destabilize and break proteins, gangliosides and phospholipids.

X-ALD is the most common monogenic leukodystrophy and peroxisomal disorder with a minimum incidence of 1 in 17000 males. Four major disease variants have been described: - i) Adrenomyeloneuropathy (AMN), a late-onset form presenting a slow progression and characterized by a peripheral neuropathy and distal axonopathy in the spinal cord. This phenotype is most often associated with axonal or demyelinating peripheral neuropathy affecting both adult men and women. ii) AMN with cerebral demyelination or cAMN. This form mainly affects adult males and can turn into an inflammatory phenotype in many cases. iii) The cerebral inflammatory demyelination form (cALD) that affects boys, adolescents and adult males. iv) Adrenal insufficiency (Addison´s disease) that affects boys, adolescents and adult males and presents a partial penetrance.

The cardinal event of X-ALD is axonal damage. Demyelination appears to be the main cause of severe axonal damage and neuronal death in variants affecting the brain, whereas in AMN axonal damage in the spinal cord and peripheral nerve is the predominant feature, with demyelination as a secondary process (Powers et al., 2000; Ferrer et al., 2010; Galino et al., 2011; Lopez-Erauskin et al., 2011; Galea et al., 2012).

I.2 Biochemical aspects of X-ALD

Peroxisomes are ubiquitous subcellular organelles, derived from the endoplasmic reticulum. Their functions include hydrogen peroxide (H_2O_2) detoxification, plasmalogens, biosynthesis and degradation of amino acids, polyamines and purines. Moreover they are also responsible of β-oxidation of VLCFA (fatty acids with aliphatic tails longer than 22 carbons). This β-oxidation system involves four enzymatic steps – 1) dehydrogenation 2) addition of H_2O to the resulting double bond 3) oxidation of the β-hydroxyacyl-coA to a ketone and 4) thiolytic cleavage by coenzyme A (CoA). At the end of this cycle of four reactions, one acetyl-CoA is released from the end of FA, given a shortened acyl-CoA ester, which undergoes further rounds of β-oxidation (Fig I.1). Since peroxisomes are not able to degrade completely fatty acyl-CoA, the shortened acyl-CoA chain is transferred to mitochondria for full β-oxidation (Kemp and Wenders, 2010). In X-ALD, there is an increased percentage of VLCFA, mainly tetracosanoic acid (C24:0) and hexacosanoic acid (C26:0) acids in cholesterol esters and complex lipids such as gangliosides, sphingomyelin, cerebrosides and sulfatides. And this VLCFA accumulation is caused by mutations in ABCD1, which impair the import of VLCFA-CoA into the peroxisome (Fourcade et al., 2009; Singh et al., 1998).

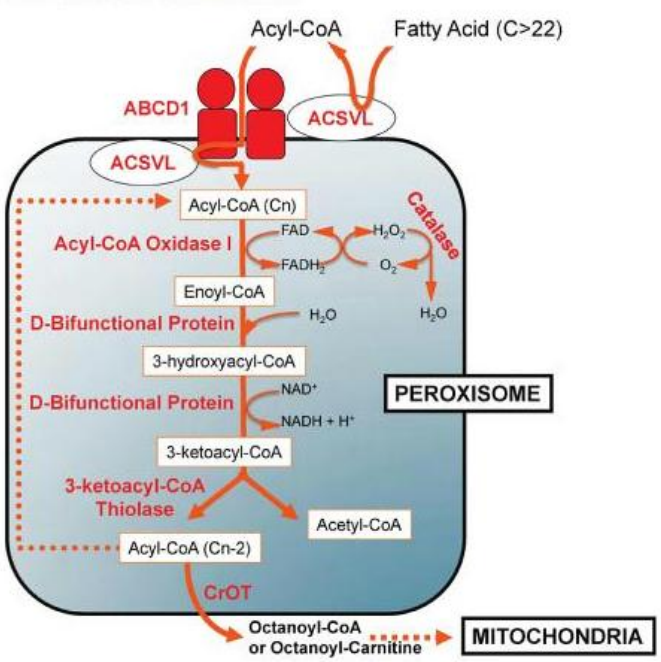

Fig.I.1: Schematic overview of the mammalian VLCFA peroxisomal β-oxidation VLCFA are esterificated to CoA (VLCFA-CoA) by acyl-CoA synthestase. VLCFA-CoA enters the peroxisome by using the ABCD1 transporter. Acyl-CoA oxidase I (ACOX1) catalyses the first

step, generating H_2O_2 that is then degraded by catalase. The D-bifunctional protein (DBP) catalyses the second and third steps, and the acetyl-CoA acyltransferase 1 (ACAA1) catalyses the last step. At the end of each cycle of four reactions, one acetyl-CoA is released from the end of the fatty acid, giving a shortened acyl-CoA ester. The shortened acyl-CoA, can undergo subsequent rounds of β-oxidation, or be shuttled to mitochondria to complete its degradation to CO_2 and H_2O (Petroni et al., 2013).

I.3 Therapeutic strategies for X-ALD

Researchers are trying different strategies for X-ALD, but so far mostly are unsatisfying or only suitable for small subset of patients, out of which the bone marrow transplantation and hematopoietic stem cell therapy are the most promising ones. The strategies which are tested are listed below:

a) Lorenzo´s oil: it is a 4:1 mixture of oleic acid (C18:1ω9) and erucic acid, extracted from rapeseed oil and olive oil designed to normalize the accumulation of VLCFAs in brain thereby halting the progression of the disease. After several years of clinical trials with patients it was concluded that although it is able to normalize the VLCFA levels but can't prevent the progression of the disease (Aubourg et al., 93).

b) Lovastatin: accumulation of VLCFA in X-ALD fibroblasts can be reduced by cholesterol-lowering drugs such as lovastatin. But finally it didn't elicit any clinical benefit neither in X-ALD mouse model nor in X-ALD patients (Berger at al., 2010).

c) Bezafibrate: this hypolipidemic drug has the capability to decrease VLCFA accumulation *in vitro* by inhibiting one of the seven elongases of VLCFA (ELOVL1), but clinical studies in X-ALD reported that it is unable to lower VLCFA levels in plasma or lymphocytes (Engelen et al., 2012).

d) Antioxidant strategies: axonal degeneration and locomotion deficits has been halted in *Abcd1*$^-$ mice by a combination of antioxidants (vitamin E, N-acetylcysteine and lipoic acid) (Lopez-Erauskin et al., 2011). These results proceed to phase II clinical trial in AMN patients with a cocktail of antioxidants (NCT01495260), with promising results.

e) Bone marrow transplantation (BMT): if in an early disease patient, allogeneic hemapoietic stem cell transplantation is performed, it is able to halt the neuroinflammatory demyelinating process. After the transplantation, the demyelination

process persists from 12 to 18 months before it is permanently arrested (Cartier et al., 2009).

f) Gene therapy: so far it has been tested in two ALD patients for whom there were no matched donors. Patients were injected with autologous CD34+ cells, genetically modified with a lentiviral vector encoding a wild type copy of ABCD1. The demyelinating process was successfully arrested after 14 months of the cell infusion and also both the patients showed a normal neurological examination 36 months after gene therapy (Cartier et al., 2009).

I.4 Oxidative stress and Role of VLCFA in X-ALD

I.4.1 Reactive oxygen species, oxidative stress and damage

Chemical reactions in nervous system are generally under strict enzyme control in a tightly regulated metabolic program to minimize unnecessary side reactions. However, even under physiological conditions, uncontrolled and potentially deleterious reactions occur with the production of ¨reactive oxygen species¨ - (ROS). It comprises a variety of molecules and free radicals (chemical species with one unpaired electron) physiologically generated from the metabolism of molecular oxygen. ROS include superoxide anion (O^{2-}), hydrogen peroxide (H_2O_2), hydroxyl radical (HO.), peroxyl radical ($RO.^2$), alkosyl radical (RO.), hydroperoxyl radical ($HO.^2$), hypochlorous acid (HOCL), hypobromous acid (HOBr) and singlet oxygen (O_2) (Galea et al., 2012). They are extremely reactive and have damaging effects. The main mediator in oxidative chain reactions and the precursor of most ROS is the superoxide anion, the product of a one-electron reduction of oxygen. Globally in cells of the nervous system, complex I and complex III of the mitochondrial electron transport chain are the major sites of physiological ROS generation as it contains several redox centers (flavins, iron-sulfur clusters and ubisemiquinone) which are capable of transferring electron to oxygen to form a superoxide anion. A condition of oxidative stress arises when net ROS production surpasses the above mentioned antioxidant barriers. It causes structural and functional changes in all cellular constituents including DNA, RNA, lipids and proteins. In X-ALD, VLCFA accumulation initiates oxidative stress that participates in the onset and progression of disease (Lopez-Erauskin et al., 2011).

I.4.2 Origin of VLCFA

Majority of the VLCFA come from the endogenous synthesis through elongation of long-chain fatty acids (LCFA) (FA with aliphatic tails of 13-21 carbons). Synthesis of polyunsaturated fatty acids (PUFA), monounsaturated VLCFA and saturated VLCFA takes place at the cytosolic side of the endoplasmic membrane and involves a four sequential reaction: i) condensation of a fatty acyl-CoA with malonyl-CoA ii) reduction to 3-ketoacyl-CoA iii) dehydration to trans-2enoyl-CoA and iv) reduction to fully elongated fatty acyl-CoA. The initial condensation step is carried out by one of the seven elongases of VLCFA (ELOVL). The synthesis of C24:0 and C26:0 requires two ELOVL. First, the elongation complex with ELOVL6 elongates to C16:0 to C20:0/C22:0. After, ELOVL1 elongates these FA to C24:0 and C26:0. So raised levels of C22:0/C24:0 are also the cause of VLCFA accumulation apart from the impaired peroxisomal β-oxidation pathway (Ofman et al., 2010) (Fig I.2).

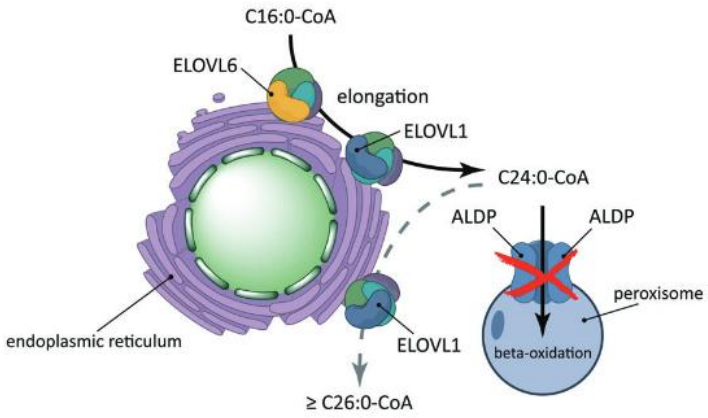

Fig.I.2: Illustration of how VLCFA are synthesized from elongation of LCFA via ELOVL6 (C18:C22:0) and ELOVL1 (C24:0-C26:0). ALDP imports VLCFacyl-CoA across the peroxisomal membrane, ALDP mutations impair peroxisomal β-oxidation and raise cytosolic levels of VLCFacyl-CoA, providing more substrate for elongation through ELOVL1 (Kemp and Wanders, 2010).

I.4.3 Consequences of VLCFA accumulation and Oxidative stress in X-ALD

Oxidative stress has been classically considered to be a common event in the neurodegenerative diseases. By using human fibroblasts our lab has shown that VLCFA accumulation induces levels of radical oxygen species (ROS), decreases reduced glutathione (GSH) levels and induces inner mitochondrial membrane

depolarization. Moreover, incubation of fibroblasts with C26:0 provoked oxidative damage to proteins and lipids in X-ALD fibroblasts and not in control fibroblasts (Fourcade et al., 2008). Also, mitochondria and in particular the mitochondrial electron transport chain (ETC) have been identified as main source of ROS in many neurodegenerative diseases. The leakage of electrons from the ETC located on the inner mitochondrial membrane causes the outflow of superoxide O^{2-}, leading to production of H_2O_2 by dismutation. As explained before, these ROS can then oxidize nearby macromolecules in the absence of antioxidant defences leading to mutations in DNA and structural and functional modifications to proteins and lipids. This leads to a pathological cascade of molecular damage which if not neutralized, may turn to cellular demise (Lopez-Erauskin et al., 2011). In type 2-diabetes or Refsum disease the accumulation of fatty acids causes the mitochondria dysfunction (Reiser et al., 2004). However the precise molecular mechanisms that drive the noxious interaction of C26:0 with mitochondria membranes and the consequent excessive mitochondria-derived ROS production in the context of X-ALD remain obscure. In the working model (Fig I.3) it describes as C26:0 interact with the phospholipid bilayer membrane provoking a perturbation of the bilayer organization by substituting other fatty acid species, polyunsaturated or monounsaturated fatty acids and interfering at the end with mitochondrial membrane structure and fluidity (Lopez-Erauskin et al., 2011).

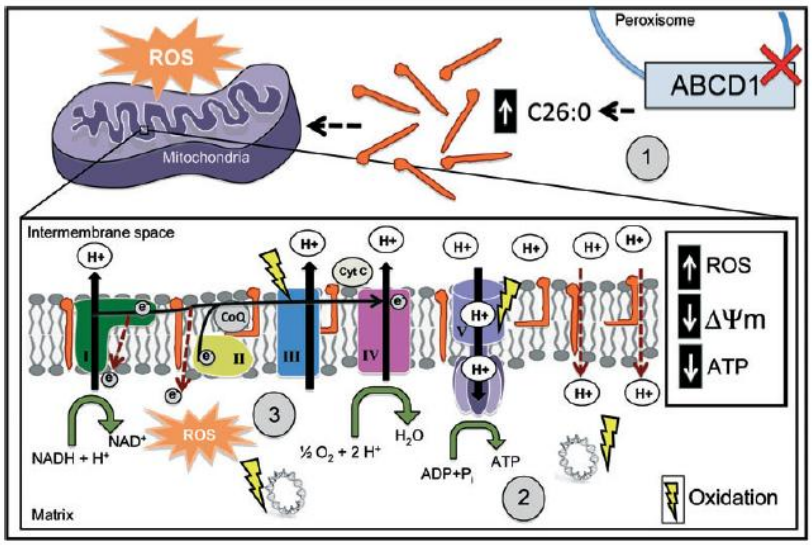

Fig.I.3: illustrates the working model mitochondrial impairment mediated by excess of C26:0. The model sheds light on the mechanisms of mitochondrial dysfunction in X-ALD, caused by loss of peroxisomal transporter ABCD1 (Lopez-Erauskin et al., 2013).

I.5 Animal models of X-ALD

Three mouse models for X-ALD were independently generated following a classical strategy of knocking out the *Abcd1* gene, which is located in the X chromosome of the mouse genome (Forss-Petter et al., 1997; Lu et al., 1997). Although all these three mouse models showed high levels of VLCFAs in the nervous tissue, adrenal glands and other organs, none of them had cerebral demyelination or inflammatory signs upto 6 months of age (Forss-Petter et al., 1997; Lu et al., 1997). However animals at 16 months of age with a pure C57BL/6J genetic background displayed histological signs of axonopathy in the sciatic nerves, and also at 20-22 months of age showed microglia activation, astrocytes and axonal swelling and damage (Pujol et al., 2002, 2004). Moreover, all these effects were concomitant with locomotor alterations and delays of motor nerve conduction velocities (Pujol et al., 2002; Ferrar et al., 2005). Thus this mouse model resembles the characteristic axonopathy in the spinal cord of patients with pure AMN (Pujol et al., 2002). A second peroxisomal transporter and the closest homolog, the ABCD2 protein, shares functions in the import of C26:0, the main VLCFA accumulated in X-ALD. In an attempt to induce a more severe phenotype, a double mutant of *Abcd1* and *Abcd2* gene was generated in mouse which displays a more severe and earlier onset axonopathy (Pujol et al., 2004; Fourcade et al 2009). Because of the neuropathology of the spinal cord and peripheral nerves, without an inflammatory component and without a cerebral demyelination, *Abcd1* and *Abcd1/Abcd2* null mutants are *bona fide* models of human AMN.

I.6 The nematode *Caenorhabditis elegans* as model organism

Caenorhabditis elegans (*C. elegans)* is a small nematode which dwells on the soil and feeds on microorganisms. This specie was first used in research by Sydney Brenner to study animal development and behaviour. Since then this nematode was extensively used as the most popular and well studied model organisms in biological research.

The main features and characteristics that make *C. elegans* an excellent model organism for biological research and for neurodevlopmental studies are listed as below:

- *C. elegans,* in the laboratory are easily maintained on agar plates with *Escherichia coli* OP50 as food source and can be grown at temperatures ranging from 15ºC to 25ºC.
- Worms are cryogenic; mutant stocks can be frozen and do not need to be maintained continually. Also when thawed, most of the worms frozen as starving L1 are viable.
- *C. elegans* has two sexes: self-fertilizing hermaphrodite (XX) and males (XO). (Figs I.4, I.5). Hermaphrodites are able to self-fertilize which allows for homozygous worms to generate genetically identical progeny. Males are not essentially required for reproduction but they are employed for the crossing of different mutants and thereby enable the combination of several genetic features in one strain.
- It is small (approx. 1mm) and has a short generation time and is therefore easy to propagate and maintain large numbers in a small space. The life cycle consists of embryonic stage, followed by four larval stages (L1 to L4) and adulthood (Fig I.4). This life cycle is temperature dependent and takes approximately 3.5 days at 20ºC. During unfavourable environmental conditions, such as food deprivation or over crowding late L1 larva enter dauer stage and get developmentally arrested can survive up to several months.
- It is a simple multicellular eukaryote with only 302 neurons and 50 glial cells of known shape and connectivity.
- Their body is transparent which is particularly useful in combination with the Green Fluorescent Protein (GFP) to visualize of cell morphologies and the subcellular localization of proteins in living animals (http://en.wikipedia.org/wiki/Caenorhabditis_elegans).
- By RNA-mediated interference (RNAi) technique the function of any specific gene can be disrupted and subsequently its phenotypic effects can be studied. RNAi afects sequence specific degradation of mRNA and consequently post transcriptional silencing of the gene of interest. In *C. elegans* RNAi can be performed by soaking or injecting with the solution containing double stranded RNA (dsRNA) or the worms can be feed on genetically transformed bacteria expressing the dsRNA of interest.

For these many reasons, *C. elegans* is uniquely suited for quick and efficient genetic manipulations for neurodevelopment studies (Bargmann et.al 1998).

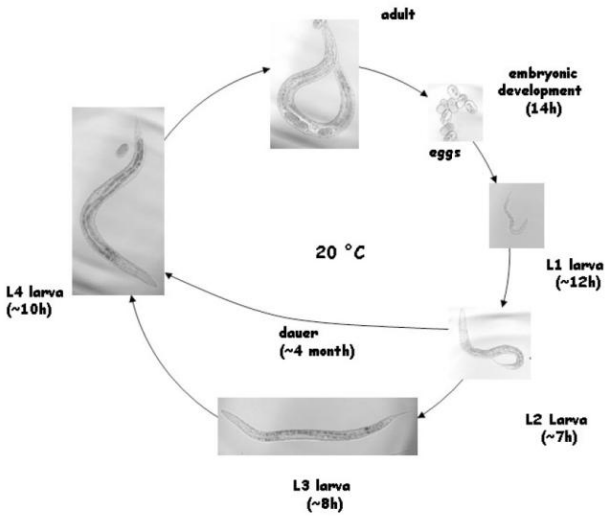

Fig.I.4: outlines the short generation cycle of *C. elegans* which facilitates genetic experiments and is a major advantage for researchers working with this organism. The numbers in brackets indicate hours after fertilisation at 20^0C.

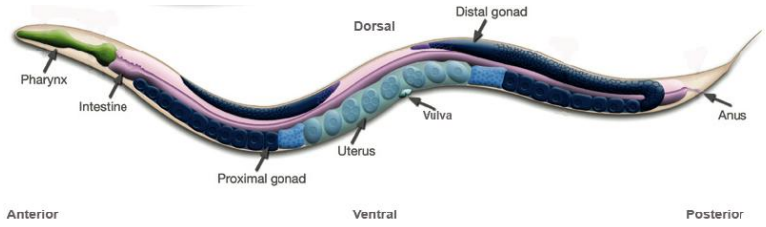

Fig.I.5: shows a schematic drawing of a *C. elegans* hermaphrodite. Anterior part consists of the pharynx, the head region, which is responsible for the uptake of food. It is connected with the intestine, which ends in the posterior part in the anus, where defecation occurs. The reproductive system is mainly the gonad consisting of a somatic gonad, the germ line and the egg laying apparatus. The eggs pass along the uterus and are released through the vulva, which penetrates the body wall in the ventral midsection (Modified from Wormatlas.org et al.)

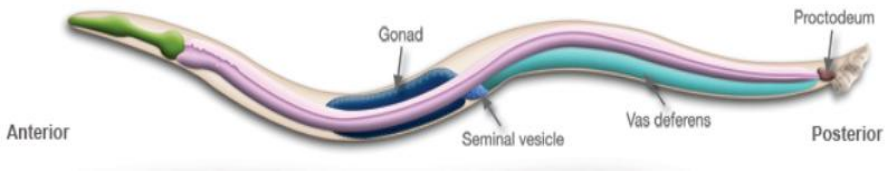

Fig.I.6: shows a schematic drawing of a *C. elegans* male. It has different body morphology compared to a hermaphrodite particularly at the posterior end where the sexual organ develops into a copulatory apparatus with 9 sensory rays that help transferring sperms into the vulva of a hermaphrodite (Modified from Wormatlas.org et al).

I.7 *C. elegans* as model organism for X-ALD

The nematode models of peroxisomal diseases existing so far are focused on peroxisomal biogenesis disorders (Thieringer, 2003; Petriv, 2002). Conclusions obtained are based mainly on RNAi silencing and controversial data were obtained among different groups regarding both, the role of peroxin genes in development and levels of ROS (Van Veldhoven, 2013). The only *C. elegans* models resembling better biochemically X-ALD are the deletion mutants of the peroxisomal β-oxidation in the nematode *daf-22(ok396)/thiolase* and *dhs-28(tm2581)/dehydrogenase* (Butcher, 2009; Joo, 2009). Both mutants are characterized by the accumulation of VLCFA. However oxidative stress consequences are not described nor the neurological consequences of the accumulation of VLCFA. In our research, we use the *C. elegans* model and try to reproduce the main phenotypes of X-ALD, such as VLCFA accumulation, oxidative stress and axonal damage and also try to pave the way for therapeutic approach for genetic and drug screenings to investigate human peroxisomal and/or neurometabolic diseases characterized by axonal damage.

I.7.1 Gene of interest, *pmp-4*

Phylogenetic analysis of ABCD family members indicate that ABCD1 and ABCD2 are paralogues that diverged rather late in evolution at the vertebrate lineage (Fig I.7). Indeed, the invertebrates *Ciona intestinalis,* a sea aquirt, the nematode *Caenorhabditis elegans* and insectae contain only one bona fide ABCD, similar to both ABCD1 and ABCD2 (Schluter, 2007; Fourcade 2009). The gene *pmp-4* (T02D1.5) (www.wormbase.org) is the nematode ortholog of *Abcd1* and *Abcd2* peroxisomal transporters and also its common ancestor (a comprehensive integrative phylogenetic tree of peroxisomal transporters is described in www.peroxisomedb.org (Schluter, 2007). Thus to examine the phenotypes resulting from the loss of *pmp-4* gene in worms, the null mutant strain *pmp-4(ok396)* consisting a deletion of 867bp was ordered from *Caenorhabditis* Genetics Center (CGC) and was used for the research.

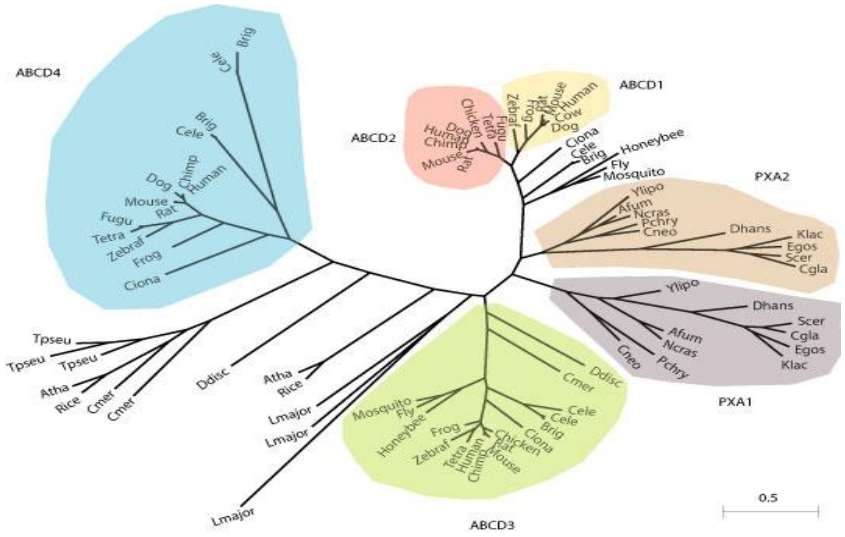

Fig.I.7: Phylogenetic tree of ABCDs. The philogenetic distribution for ABCD1, ABCD2, ABCD3, ABCD4, and the fungal PXA1 and PXA2 is displayed. The scale length indicates 0.5 substitutions per site. Human: *H. sapiens*, Ciona: *C. intestinalis*, Cele: *C. elegans*. Mosquito: *A. gambiae*, Honeybee: *A. Mellifera* (Fourcade, 2009).

I.8 *C. elegans* nervous system

C. elegans hermaphrodite nervous system consists of 302 neurons that belong to two distinct and independent nervous systems: a large somatic nervous system (282 neurons) and a small pharyngeal nervous system (20 neurons). The male has an additional 79 neurons that are mainly involved in the control of mating. *C. elegans* has 118 different neuron classes according to their topology and synaptic connection patterns, separating them into sensory, inter and motor neurons. The sensory neurons generally gather and transfer external sensory stimuli from the environment (chemical, mechanical and thermal), interneurons receive and transmit that information to other neurons and finally motor neurons transmit information to the motor cells and thus allowing the worm to respond to external stimuli and conditions (Fig I.8; Ferree et al., 1996).

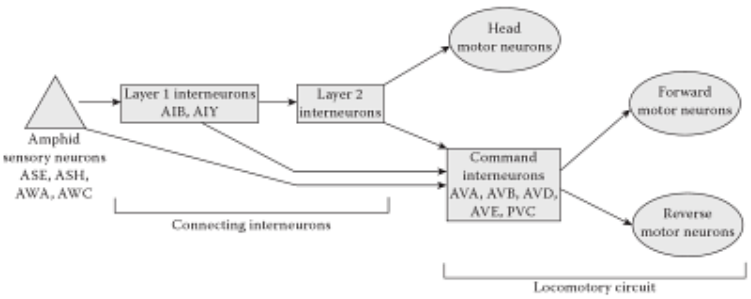

Fig.I.8: illustrates a simplified wiring of *C. elegans* nervous system. Most amphid sensory neurons synapse to the locomotory circuit via multiple layers of connecting interneurons.

The distribution of the nerve cells is mainly in the head, tail and along the ventral cord and build the somatic nervous system. The primary ganglia exist in the worms 'head and the nerve ring is a synapse rich band of processes which wraps around the pharynx anterior to the posterior bulb (Ward et al 1975; White et al 1986) (Fig 1.9).

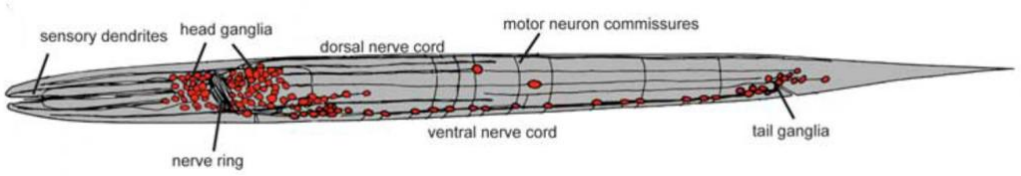

Fig.I.9: Schematic diagram of C. elegans nervous system consisting of the head and tail ganglia, nerve ring and the nerve cords (Reproduced from (White et al., 1986).

Each and every *C. elegans* neuron is designated with a unique name consisting of two or three uppercase letters (e.g. AWA, AWB) indicating class and sometimes a number indicating the neuron within one class. If the neurons are radially symmetrical, each cell has a three letter name followed by left (L), right (R), dorsal (D) or ventral (V) (*C. elegans* Atlas).

I.8.1 *C. elegans* for investigating axonal degeneration and ageing

C. elegans has emerged as a powerful model organism to study the molecular and cellular aspects of human disease *in vivo*. About 42% of the human disease genes have been estimated to have an ortholog in the *C. elegans* genome, including genes associated with Alzheimer´s disease (AD), Parkinson´s disease (PD), spinal muscular atrophy (SMA), hereditary nonpolyposis colon cancer and many other age related diseases (Halliwell et al., 2014; Caldwell et al., 2010; Baumeister et al., 2007). In these diseases, neurodegeneration have been found to have a profound effect on human health, but yet the mechanisms underlying neuronal injury and death remain unclear. For this purpose, *C. elegans* models of neuronal dysfunction have been established for a number of neurodegenerative diseases including AD, PD and polyglutamine expansion disorders. The use of this small nematode allows the dissection of complex molecular pathways into their component parts and provides a meaningful insight into the pathogenesis of a complex disease phenotype (Markaki and Tavernakis, 2010).

The neurotransmitter GABA has been proposed to play a role during nervous system development (Horvitz et al:, 1999). The structural integrity of GABaergic D-type motor neurons and their processes in *pmp-4 (ok396)* animals are examined by using the *Punc-25:: GFP* reporter. *unc-25* encodes the *C. elegans* ortholog of the GABA neurotransmitter biosynthetic enzyme, glutamic acid decarboxylase (GAD) and worms expressing this reporter show GFP labelling distributed along the axons and the GABaergic cell bodies of the ventral cord. The strain *Punc-25:: GFP* allows analyzing for defects in axonal outgrowth or navigation in individual neurons with neurites in both nerve cords as well as interconnecting commissural axons and has been widely used to investigate neurodegeneration in the nematode (Rawson, et al., 2014). Wild type worms expressing the *Punc-25:: GFP* reporter show both the dorsal and ventral nerve cords continuous and contain the normal complement of 19 inhibitory motor neurons (13 VD and 6 DD GABAergic neurons). In wild type animals, it is generally possible to score 16-17 commissures (two commissures often exit from the left side of the ventral cord and are out of the plane of focus or commissures may fasciculate and be counted as single commissure (Nix et al., 2014) (Fig I.10).

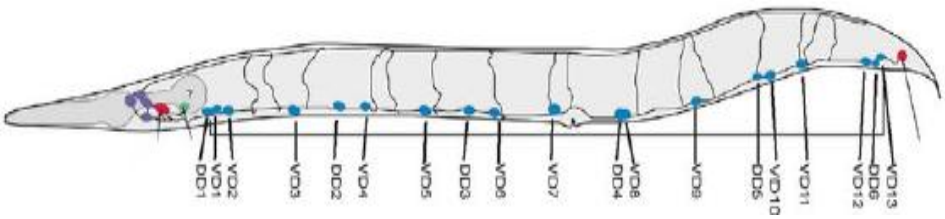

Fig.I.10: Image illustrating the fluorescence microscopy of GFP-labelled VD and DD class GABAergic neurons in living worm. It is oriented with anterior end left and ventral side down, as depicted in the schematic of normal GABAergic neurons and processes (Kraemer et al., 2010).

Specific mutations in the *Caenorhabditis elegans mec-7/β-tubulin* gene cause ectopic axon formation in mechanosensory neurons in vivo (Hilliard et al., 2012). *mec-7* in *C. elegans* is the homolog of the vertebrate β-tubulin gene and is expressed in the six touch receptor neurons existing in the nematode (ALML/ALMR, AVM, PLML/PLMR, and PVM) (Fig I.11). In *mec-7* mutants, the ALM mechanosensory neuron forms a long ectopic neurite that extends posteriorly and it severes as the worms age. To ascertain the specificity of the axonal damage, we also studied the mechanosensory strain *Pmec-7:: gfp.*

Fig.I.11: Schematic diagram of *C. elegans* touch receptor neurons, lateral view. Only of the bilateral ALM and PLM neurons are shown for simplicity (Pan et al., 2013).

In *C. elegans,* the anterior and posterior mechanosensory neurons are organized into precise and non-overlapping anterior and posterior sensory fields (Gallegos and Bargmann, 2004). Specifically, two pairs of mechanosensory neurons, the Anterior Lateral Microtubule left and right (ALM L/R) and the Posterior Lateral Microtubule left and right (PLM L/R) divide the body into two mechanosensory fields (Fig I.18). As a result of the anterior/posterior arrangement of ALM and PLM dendrites, a gentle touch on the anterior half of the animal mediates backward movement, and a gentle touch on the posterior end of the animal mediates forward movement (Chalfie et al., 1985). ALM (left and right) each have a cell body (soma) located near the centre of the animal's long axis with a sensory neurite that extends along the anterior half of the body surface whereas each PLM (left and right) has a cell body at the posterior end of the animal's long axis with a sensory neurite that extends along the posterior half of the body surface (Fig I.12).

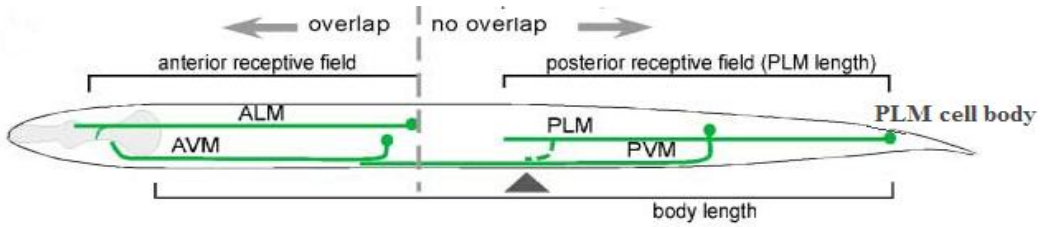

Fig.I.12: shows the morphologies of four distinct types of mechanosensory neurons (ALM, AVM, PLM and PVM) in a wild type *C. elegans* hermaphrodite (image taken from Gallegos and Bargmann, 2004). The arrowhead indicates the position of the developing vulva. The green circles are the cell bodies. The PLM dendrite typically terminates posterior to the ALM cell body as shown. PLM neurite that terminates anterior to the ALM cell body (vertical dashed line) is considered mutant. Thus the dashed line is simply an arbitrary boundary that is used for scoring wt and mutant phenotypes, an alternative way to characterize mutants used in place of measuring normalized PLM lengths. Posterior ventral and anterior ventral mechanosensory neurons PVM and AVM are not essential for mechanosensation and are not discussed further.

I.8.2 *C. elegans* chemosensory nervous system

Chemosensation is the process by which a worm is able to find food, avoid noxious conditions, find mates, makes decisions about development and going to dauer stage and most importantly sense many volatile or soluble chemicals or odorants with the help of the chemosensory neurons embedded in the amphid organ. There exist 16 pairs of anatomically bilaterally symmetric neurons (i.e. 32 neurons or 10% of the nervous system) which have been confirmed to be chemosensory based on functional studies or anatomy. These chemosensory neurons respond to a wide variety of soluble and volatile odorants and mediate either attraction or repulsion behaviour in the worm (Table 1). There exist four types of visible *C. elegans* chemosensory organs: the amphid, phasmid, inner labial and outer labial organs (Fig I.13).

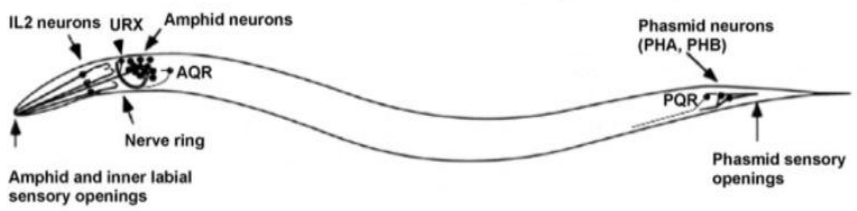

Fig.I.13: illustrates the distribution of chemosensory neurons. Amphid contains 12 pairs of chemosensory or thermosensory neurons whereas phasmid contains two pairs (PHA, PHB). Each inner labial organ contains one IL2 chemosensory and one IL1 mechanosensory neuron (unmodified from Wormbook).

Chemosensory Neuron	Function	Compound(s) Sensed
AWB	Volatile avoidance	2-nonanone, 1-octanol
ASH	Osmotic Avoidance	SDS, 1-octanol, Quinine, Cd^{2+}, Cu^{2+}
ASI	Dauer formation, Chemotaxis	Na^{+}, Cl^{-}, Lysine, Biotin, cAMP
ASJ	Dauer formation and recovery, Chemotaxis	Lysine
ASK	Avoidance, Chemotaxis	Lysine
ADL	Volatile Avoidance	1-octanol, Cd^{2+}, Cu^{2+}

The table lists the main chemosensory neurons, their respective functions and the chemicals sensed used for its functional investigations. Complete list can be found in Wormbook (www.wormbook.org/chapters/chemosensation).

I.8.2.1 Chemosensory organs in *C. elegans*

Amphid is the main chemosensory organ of *C. elegans* where mainly the chemosensory neurons reside. This chemosensory organ is well supported by two support cells: sheath and socket cells, which form a pore through which the sensory neuron endings are exposed to the external environment. Apart from being the support system, they play a critical role in response to chemical stimuli. They are located at the tip of the head and contain the sensory endings of 11 chemosensory neurons and one thermosensory neuron (Fig I.14.A). There are 24 sheath cells and 26 socket cells and their processes are sealed to each other by electron-dense adherens junctions. The former regulate dendrite extension and the latter is involved in navigating sensory dendrites to specific sensory organs.

Amphidial neuronal cell bodies are located in the anterior part of the worm in the pharyngeal bulb area and connect through axons to the nerve ring. Their dendrites reach to the anterior tip of the animal, terminating in ciliated structures in the amphids. The ciliated sensory endings of the bilaterally neurons are located in the amphid pore (ASE, ASG, ASH, ASI, ASJ, ASK, ADF and ADL) or are embedded in the sheath cell (AWA, AWB and AWC) (Figure I.14.B) (Hall and Russell, 1991).

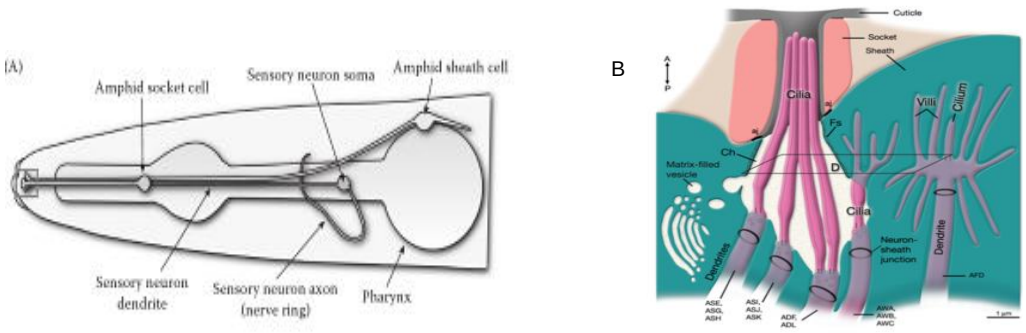

Fig.I.14: The structure of amphid organ (A) the soma of the amphid sensory neurons are arranged around the pharynx, the axons synapse with interneurons in the nerve ring, dendrites extend anteriorly. For simplicity, only neuron is shown. (B) Detailed structure of the amphid sensory opening where the sensory ending of the neurons are embedded either in sheath or socket cells. (Reproduced from Wormatlas.org and Perkins et al., 1986)

I.8.2.2 Ciliary cell biology

Cilia are microtubule based hair like cytoplasmic extensions with motile and a range of sensory functions, which are critical for developmental and physiological functions. They fall into two broad categories: motile and immotile. Primary cilia are typically immotile and consist of nine peripheral doublet microtubules, while motile cilia in addition contain a central pair of singlet microtubules (9+2 arrangement) to which they are connected by the radial spoke proteins. Immotile primary cilia are characterised by the absence of the central pair of singlet microtubules (9+0 arrangement) (Beales et al., 2011). Primary cilia are main responsible for chemosensory and osmosensory functions as discussed later in the thesis. The ciliary axoneme develops from and is anchored to a specialised centriole called the basal body, which acts as a microtubule organising centre (MTOC) for its ciliary counterpart. The ciliary axoneme consists of nine doublet microtubules that originate at the triplet microtubules of the basal body centriole and extend the length of the cilium. (Beales at al., 2011) (Fig I.15).

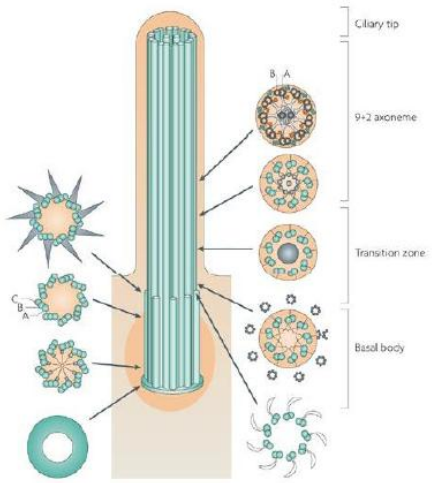

Fig.I.15: Schematic diagram depicting longitudinal section through a cilium. At the proximal cytoplasmic end of the cilium lies the basal body with microtubule triplets. Transition zone lies distal to this where the microtubules are arranged in doublets. The axoneme comprises the majority of the cilium´s length (Fliegauf et al., 2007).

I.8.2.3 Amphid cilium in *C. elegans*

Sensory cilia are immotile, microtubule rich extensions specialized as receptors for diverse sensory modalities present at the termini of some sensory neuron dendrites.

They contain receptor molecules and various signal transduction components which are the primary sites of transduction at which environmental stimuli are converted into receptor potentials. The amphid cilia is structurally divided into a distal segment, middle segment, transition zone, neuron/sheath junction and the main dendrite (Fig I.16, A, B).

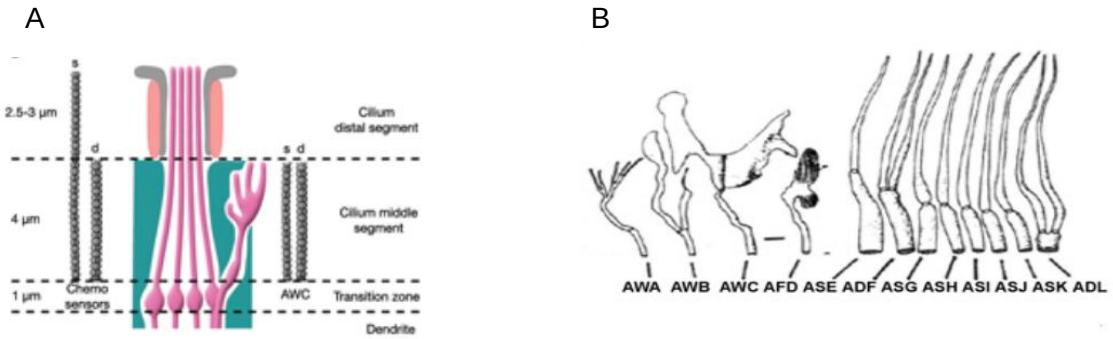

Fig.I.16: (A) Schematic structure of amphid cilia. Each cilium is 7.5 µm long in an adult hermaphrodite and consists of three segments: the proximal, middle and distal segment. (B) Detailed cilial structure of the 12 amphid neurons (Unmodified from Wormbook).

I.8.2.4 Odorant receptors

Odorant receptors in *C. elegans* and other animals are G-protein coupled seven transmembrane (str) proteins. Worms generally have a large number of these domain proteins expressed in the sensory neurons that function as chemoreceptors. One of these genes, *str-1* is expressed in AWB neuron pair (as mentioned above), whereas the *str-2* gene is expressed in one of the two AWC olfactory neurons (Bargmann et al., 1997 and 1995). There are also other families of seven transmembrane-domain receptors that are also expressed in chemosensory neurons (*sra, srb, srd, sre,* and *srg* genes). These putative receptors are mainly useful for investigating cell function and morphology. Importantly, a single neuron can express multiple receptor genes, including receptors from different gene families. The expression and regulation of several different odorant receptor genes allow each individual neuron to sense and discriminate among several odorants. And also an individual neuron has been shown to detect either attractant or repellent but not both, suggesting there are differences between these cell types (Bargmann et al., 1997).

OBJECTIVES

Objectives:

The main interest of the Neurometabolic Disease Laboratory is to unravel the molecular mechanisms underlying X-ALD, in order to develop rational therapeutic strategies. Using *C. elegans* as the model organism this dissertation aim to decipher the cause of mitochondrial dysfunction and role of mitochondrial ROS causing axonal damages and locomotor disabilities, also affecting chemosensation, and to evaluate therapeutic potential of mitochondrial boosters in X-ALD.

These are the specific objectives of each study in relation to the global aim of this dissertation:

1. To investigate the real influence of mitochondrial ROS in the neurological phenotypes observed in our *C. elegans* model of X-ALD.
2. To investigate the functionality of the amphid organ (containing most of the glia-like cells) in our *C. elegans* model of X-ALD.
3. To investigate whether the specific anti-oxidants are able to rescue the observed phenotypes in our *C. elegans* model of X-ALD.
4. To corroborate the use of *C. elegans* as a good *bona fide* model for the investigation of peroxisomal diseases.

RESULTS

R. Results (Chapter I):

R.1 Basic peroxisomal related phenotypes observed in *pmp-4* mutant worms

Peroxisomal β-oxidation processes long chain fatty acids (C_{15}-C_{20}) or VLCFAs (very long chain fatty acids, >C_{20}) including straight and methyl branched chains to produce SCFAs, components of daumone, an aromatic compound necessary to induce the dauer stage (Joo et al.,2009). Two enzymes, DHS-28 (human homolog, bi- functional protein) and DAF-22 (human homolog, thiolase) actively participate in this daumone biosynthesis pathway. *C. elegans* mutants defective for these enzymes show inability to form dauers, reduction in growth rate, body size, brood size and lifespan, and massive accumulation of fatty acids inside the mutant worm body (Paik et al., 2009). PMP4 being a peroxisomal β-oxidation protein we investigated whether its absence reproduced the same phenotypes.

R.1.1 Dauer formation is strongly reduced

Impaired peroxisomal β-oxidation in worms has effects on dauer induction (Paik et al., 2009); it was therefore investigated whether the lack of PMP-4 peroxisomal transporter had similar consequences. After a prolonged starvation (for 7 days at 20^0C), the percentage of dauer induction in *pmp-4* mutant animals is significantly reduced as compared to wild type (> 80%). *daf-22* and *dhs-28* mutant animals were used as controls and as expected they failed to produce any dauer under similar starve condition at 20^0C (Fig R.1.1).

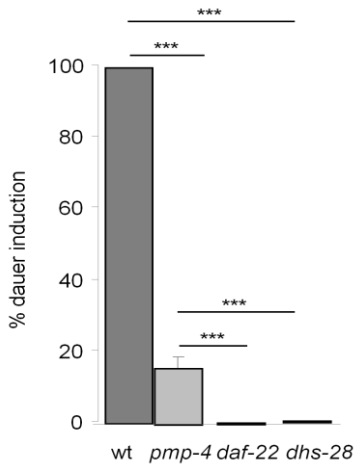

Fig R.1.1: Dauer assay *pmp-4* mutant worms generated a higher number of dauers compared to *daf-22* and *dhs-28* mutant worms but significantly reduced to wild type animals. 10 L4 hermaphrodites were placed in a small agar plate with 50µl of OP-50 and left to starve. After approximately, one week the number of dauers was counted per plate and genotype. The same experiment was repeated three times, using 10 plates per genotype. *** $P < 0.001$ compared with wild type. *P* values were derived from *t* test.

R.1.2 Reduced growth and lifespan

Impaired peroxisomal β-oxidation in worms has effects on post embryonic development and life span (Paik et al., 2009); it was therefore investigated whether the lack of PMP-4 peroxisomal transporter had similar consequences. The developmental stage of mutant and wild type animals was scored 72h after eggs were laid. *pmp-4* mutant worms have a reduced growth rate as compared to wild type but not that severe compared to other peroxisomal mutants (*daf-22* and *dhs-28).* After 72h where 85% wild types have developed into adult, only 65% of *pmp-4* has reached this developmental stage and only 20% of *daf-22* and *dhs-28* mutant animals were adult at the same time period (Fig R.1.2.A). *pmp-4* also displayed a reduced lifespan with median survival at 14 days compared with 15 days for wild type at 25^{0}C (Fig R.1.2.B), although no difference was observed at 20^{0}C (data not shown). During lifespan assays, mutant animals stopped moving around the plate sooner than wild type, indicating an accelerated age-associated decline in movement.

A

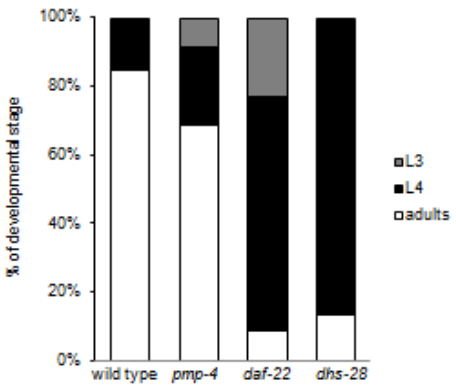

B

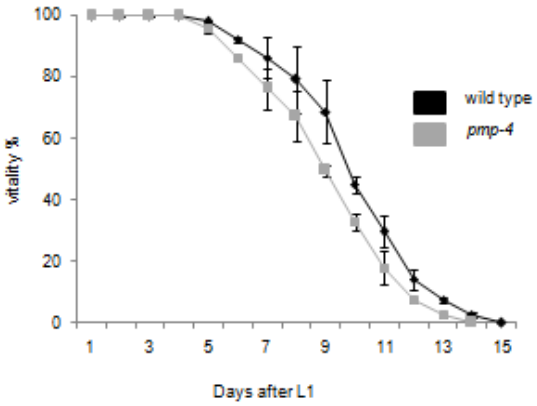

Fig R.1.2: Developmental and lifespan assay (A) *pmp-4* mutant animals developed at a slower rate compared to wild type animals but faster than animals mutated in *daf-22* and *dhs-28* genes. Worms were grown from egg synchronized stage in NGM agar plates with food and after 72 hours they were counted at the stage they have developed. One hundred animals per strain

per experiment were assayed in a total of three independent experiments. (B) *pmp-4(ok396)* animals have a median survival of one day less compared to wild type at 25^0C. Data points represent the percentage of age-synchronized animals found alive each day post-synchronization. Data from three independent assays are presented.

R.1.3 Defects in egg laying and breeding

Impaired peroxisomal β-oxidation in worms has effects on egg laying and breeding as well (Paik et al., 2009); it was therefore investigated whether the lack of PMP-4 peroxisomal transporter had similar consequences. On food, age synchronized young adult *pmp-4* animals laid significantly lesser eggs than wild type at various time intervals. The average number of eggs by a young healthy one day adult is approximately 40 in case of wild type, which decreases 35 in case of *pmp-4* mutant animals. This difference in the number of eggs laid increases further for the second overnight (Fig R.1.3A). Brood size assays confirmed that egg laying is affected; *pmp-4* animals laid fewer eggs over a lifetime for 4 days than wild type worms. Mostly in the second day, where approximately 100 broods were observed in a plate of wild type only approximately 80 broods were observed in case of *pmp-4(ok396)* animals (Fig R.1.3B).

A B

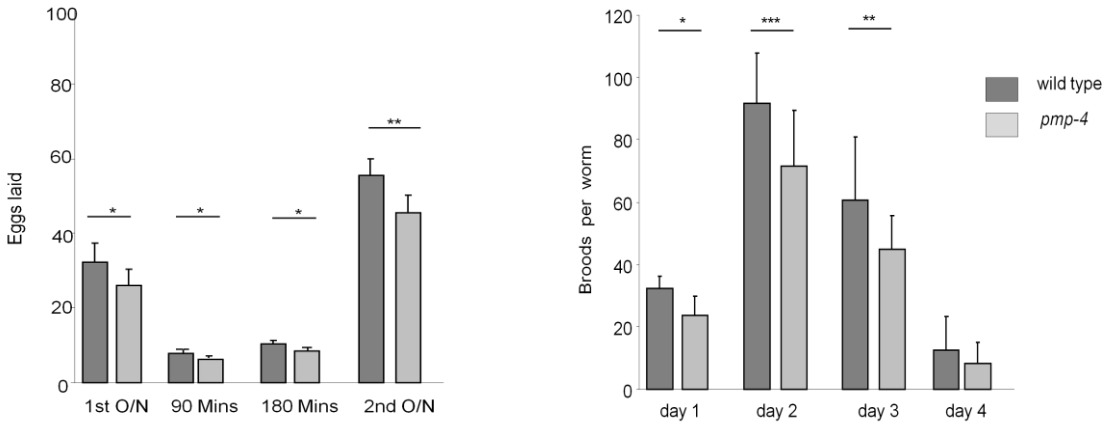

Fig R.1.3: Characterization of *pmp-4* egg laying behavior (A) Overnight at 20^0C, age-synchronized young adult *pmp-4* animals laid lesser number of eggs as wild type on food. About 25 animals were assayed per strain over five independent experiments. ***P < 0.001, unpaired t-test. (B) The total brood size of *pmp-4* animals was reduced throughout four consecutive days. Thirty animals were assayed per strain over five independent experiments. *** P < 0.001, unpaired t-test. Means ± SEM are plotted for all figures.

R.2 *pmp-4* absence reproduces X-ALD oxidative stress and mitochondrial impairment

R.2.1 *pmp-4* mutants display increased oxidative stress

Oxidative damage is a main etiopathogenic factor in the X-ALD mouse models (Fourcade et al., 2009) and characterizes the human X-ALD disease (Galino et al., 2011; Lopez-Erauskin et al., 2011). In X-ALD an increase of oxidative stress markers can be detected in mouse models (spinal cords) and in human (peripheral mononuclear cells or fibroblast) (Fourcade et al., 2008; Fourcade et al., 2010; Galino et al., 2011). We investigated whether oxidative stress was also a hallmark in *pmp-4(ok396)* animals. First, as oxidative damage is directly correlated with ROS production, the ROS formation was measured by detecting the oxidation induced by the fluorescence emitted by the dye carboxy-H2 DCFDA as described before in *C. elegans* (Shi et al., 2012; Yang et al., 2013; Yang and Hekimi, 2010). Levels of the dye were significantly increased in *pmp-4* mutant animals and ROS levels were restored by introducing wild type PMP-4 in mutant animals (Fig R.2.1.G-H) thus suggesting an essential role of PMP-4 in maintaining ROS homeostasis and also with the anti-oxidants (CoQ and MitoQ) (Fig R.2.1.B-F). Second, using the dye mitoSOX, which specifically labels mitochondrial superoxide (Smith et al., 2014; Yang and Hekimi, 2010), we found that *pmp-4* mutants displayed elevated superoxide levels (Fig R.2.1.I-K), thus indicating that the most of the ROS induced by the *pmp-4(ok396)* mutation are superoxides generated in the mitochondria.

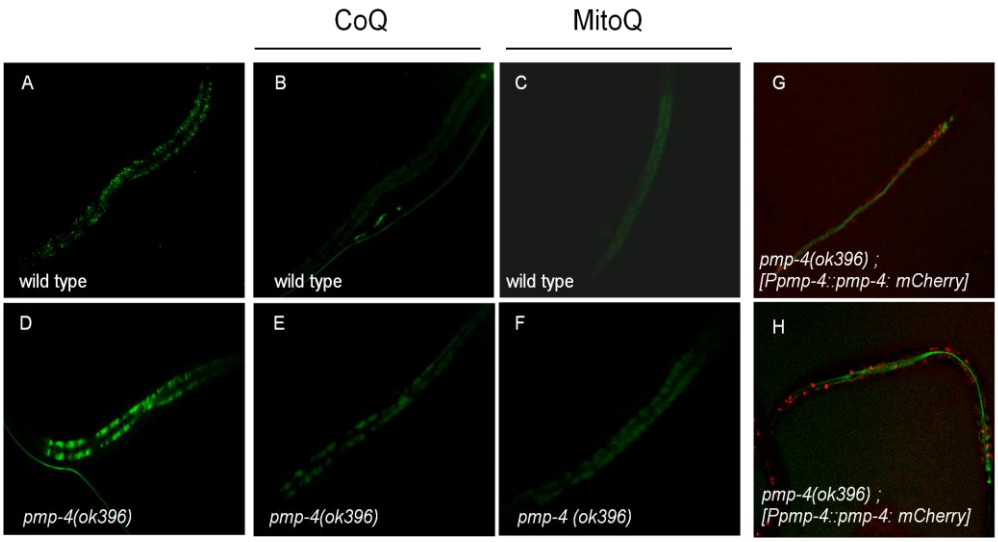

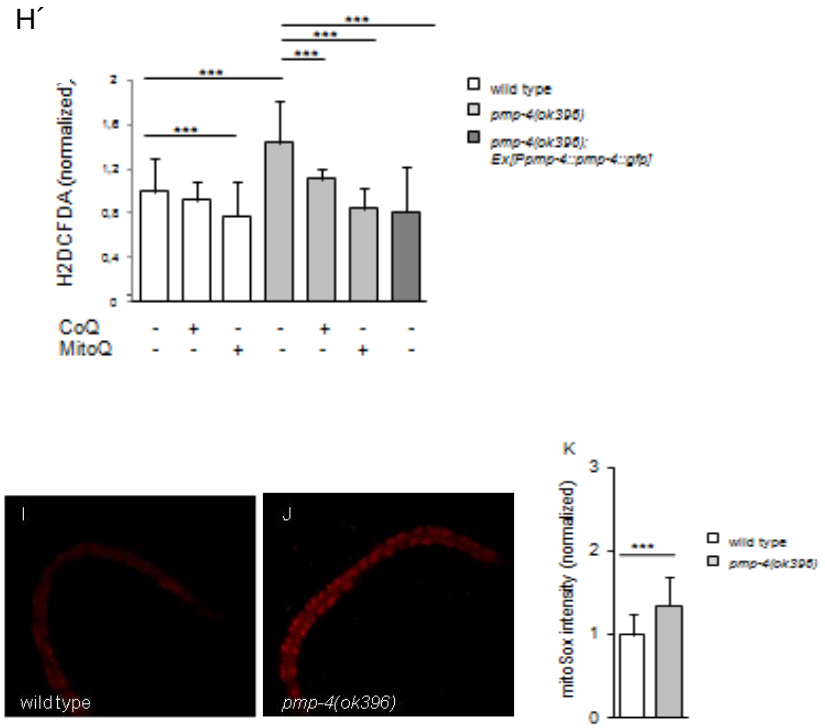

Fig R.2.1: ROS levels (A-H´) Global ROS levels. Top: representative images of H2DCDFA staining in live animals of the indicated genotype. Bottom: quantification of the fluorescent signal; values are expressed as fold increase respect to wild-type, and are given as means ± SD, n=3. *** P < 0.001; ANOVA followed by Tukey HSD post hoc. (I-K) Mitochondrial ROS levels Left: representative images of MitoSOX staining in live animals of the indicated genotype. Right: quantification of the fluorescent signal; values are expressed as fold increase respect to wild-type, and are given as means ± SD, n=30. *** P < 0.001; Student´s t-test.

R.2.2 mitochondria in *pmp-4* mutant animals were more susceptible to external ROS

Mitochondria in X-ALD patients are susceptible to ROS (Fourcade et al., 2008). To investigate the involvement of the mitochondrial complexes in the ROS induction in our *C. elegans* model of X-ALD we have used different electron transport inhibitors specific for each complex to explore the ROS contribution of each complex. Paraquat, PQ (1, 1'-dimethyl-4,4'-bipyridinium dichloride) has been described an inhibitor of the mitochondrial complex I (Betarbet et al., 2000; Castello et al., 2007; Cocheme and Murphy, 2008) and it is widely used as a redox cycler to stimulate superoxide production in mitochondria (Cochemé, 2009). After 72 hours of incubation with PQ the lethality after 72 hours was analyzed under the microscope (Feng et al., 2001; Ray et al., 2014; Runkel et al., 2013). *pmp-4* mutant worms showed a higher sensitivity to PQ

in comparison to wild type animals. Wild type PMP-4 rescued PQ-induced lethality in *pmp-4* mutant animals, thus confirming that the gene *pmp-4* is important in the sensitivity to ROS due to superoxide generation (Fig R.2.2.a). Impaired metabolism caused by a defect in one mitochondrial respiratory chain (MRC) complex is often associated with altered levels of the other MRC complexes (Grad and Lemire, 2004; Heddi et al., 1999; Ray et al., 2014). To investigate the sensitiveness of other mitochondrial complexes against external inhibitors we used Antimycin-A which specifically inhibits mitochondrial complex III and sodium azide which inhibits complex IV. We found mitochondrial complex III and complex IV more severely affected in *pmp-4(ok396)* worms compared to wild type animals (Fig R.2.2.c,d) but both wild type and *pmp-4* mutant animals are similarly affected by the complex II inhibitors, as demonstrated by the non-altered sensitivity *vs* the complex II inhibitor TTFA (Fig R.2.2.b).

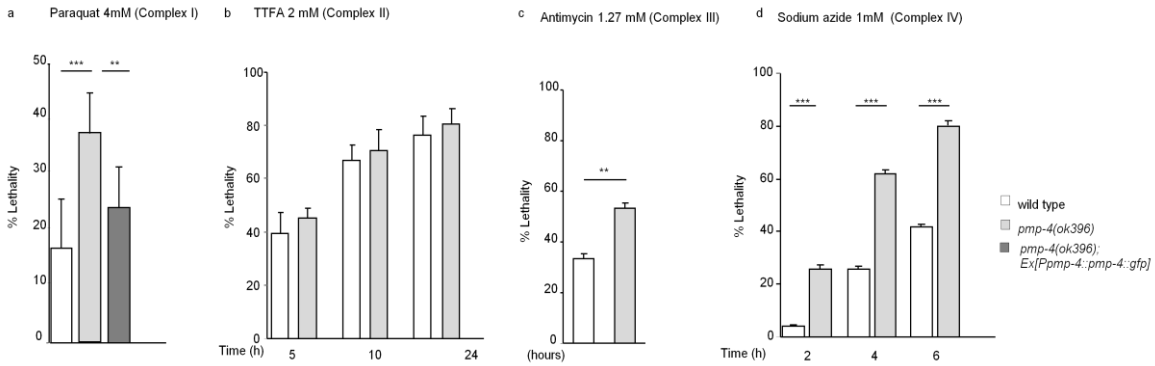

Fig R.2.2: Lethality assay with mitochondrial inhibitors (a) Worms were incubated on agar plates with 4mM paraquat and their lethality was checked after 72hours. (b) Worms were incubated on agar plates with 2mM TTFA and their lethality was checked at different time intervals. (c) Worms were incubated on agar plates with 1.27mM Antimycin-A and their lethality was checked after 72 hours. (d) Worms were incubated on agar plates with 1mm sodium azide and lethality was checked after every 2 hours. All the experiments were repeated 3 times and with using 50 worms per genotype. *** $P < 0.001$, unpaired t-test. Means ± SEM are plotted for all figures.

R.2.2.1 optimizing the sub lethal dose of paraquat

The sub lethal dose of PQ was established to explore the effect of external ROS on the main X.ALD phenotypes such as axonal degeneration and locomotion. Synchronized eggs were placed on paraquat plates containing different concentration from 0.2mM to 1mM and after 72 hours they were studied at which developmental stage they reached

(Ahn et al., 2008). At all concentrations tested *pmp-4* mutants developed slower than wild type animals and mostly the difference was observed at 0.2 mM concentration of paraquat. Consequently, this PQ concentration was chosen as the optimum sub lethal concentration (Fig R.2.2.1).

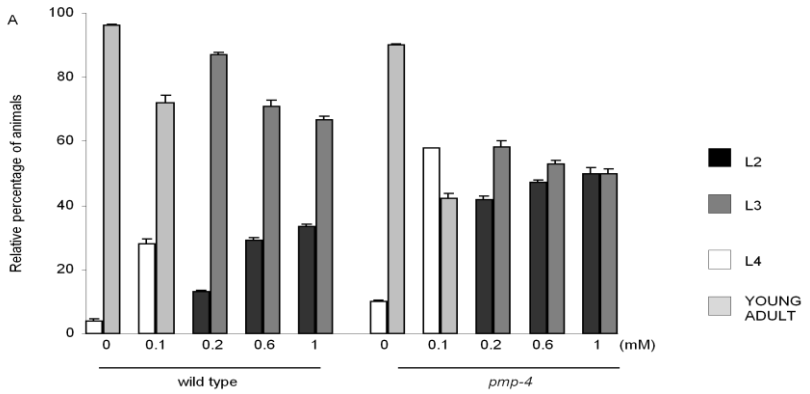

Fig R.2.2.1: Larval developmental assay in presence of paraquat Ten eggs per plate in a total of 10 plates were grown on plates containing paraquat. The developmental stage of each worm on each plate was recorded after 72 hours. The same experiment was repeated 3 times.

To corroborate the specific effect of PMP-4 in PQ sensitiveness the sub lethal dose of 0.2 mM was also examined in eggs of transgenic worm containing wild type of PMP4. At this specific concentration, after 72 hours 60% of *pmp-4* worms reach L3 stage whereas 80% of the transgenic worms reach L3 stage like wild type. Hence confirming that gene *pmp-4* essential in the regulation of ROS homeostasis due to superoxide generation (Fig R.2.2.1.1)

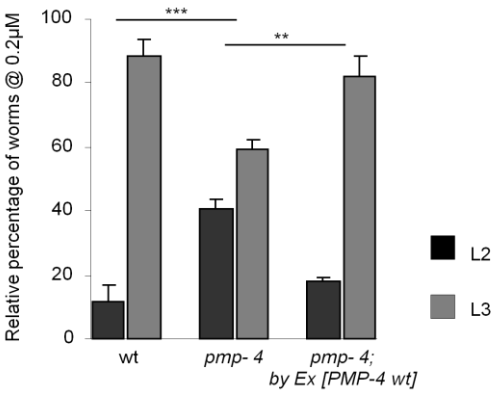

Fig R.2.2.1.1: Larval developmental assay at 0.2 mM Paraquat Ten eggs per plate in a total of 10 plates were grown on plates containing paraquat. The developmental stage of each worm

on each plate was recorded after 72 hours. The experiment was repeated 3 times. *** $P < 0.001$, One-way Anova. Means ± SEM are plotted for all figures.

R.2.2.2 Mitochondria targeted anti-oxidant rescued the ROS increase in *pmp-4 (ok396)* animals

Mitochondria are the main source of ROS and mitochondrial ROS were purposed as a main ethiopathogenic factor in the development of X-ALD (Gallino et al., 2011; Lopez-Erauskin et al., 2013). To investigate the main source of ROS induced by the *pmp-4(ok396)* mutation nematodes were treated separately with two antioxidants CoQ and MitoQ. MitoQ (mitoquinone mesylate:10-(4,5-dimethoxy-2-methyl-3,6-dioxo-1,4 cycloheexadienlyl) decyltriphenyl- phosphonium methane sulfonate) is considered a mitochondria targeted treatment in comparison to a general antioxidant drug such as CoQ or Coenzyme Q_{10} (CoQ, ubiquinone) (Giordano et al., 2013; James et al., 2010) MitoQ is a modified form of CoQ and one of the best characterized mitochondria-targeted antioxidants (Kelso et al., 2001; McManus et al., 2011; Tauskela, 2007). To find out the optimum concentration for these anti-oxidants, the PQ experiments were repeated as explained in the previous section, but with adding 1000 µg/ml of CoQ in the paraquat plates and then the same with different concentrations of MitoQ (0.1-10 µg/ml) (Fig R.2.2.2A,B).

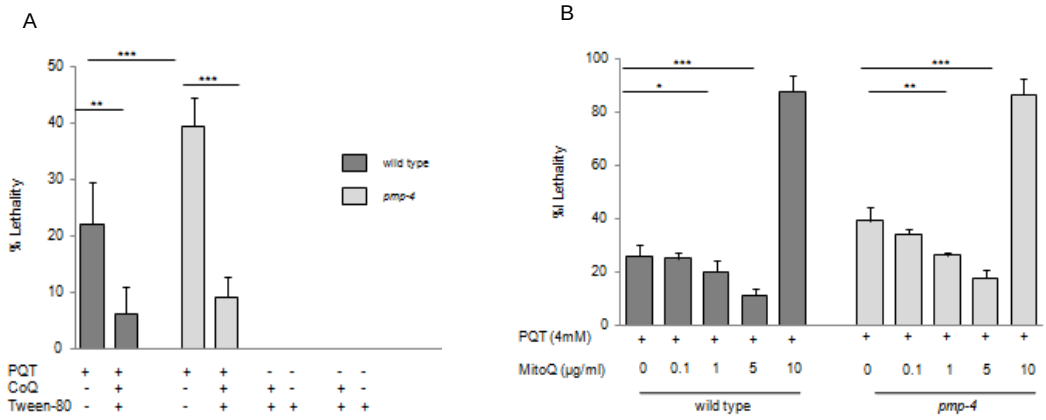

Fig 2.2.2 A, B: Lethality assay with anti-oxidants (A) worms were incubated on agar plates with 4 mM paraquat and 1000 µg/ml CoQ, their lethality was checked after 72hours. Detergent Tween 80 alone has no effect on worms lethality (B) worms were incubated on agar plates with 4 mM paraquat and different concentrations of MitoQ, their lethality was checked after 72 hours.

The lethality was restored to basal levels in CoQ and MitoQ treated *pmp-4* worms and in wild type animals, MitoQ at a greater extent especially at 5 µg/ml concentration. After these set of experiments we conclude that mitochondria are the main source of ROS also in *C. elegans* (Brown, 1992; Izyumov et al., 2010) and reviewed in (Marchi et al., 2012).

R.2.3 MitoQ rescued lipid accumulation in *pmp-4 (ok396)* mutant animals

The biochemical characteristic of X-ALD is lipid accumulation generated by the abnormal metabolism of VLCFA (Igarashi, 1976; Moser, 1997). In *C. elegans* the majority of lipids are stored in fat storage organelles called lipid droplets (LD) mainly located in the gut and in the hypodermis (Mak, 2011). In our laboratory, we previously demonstrated the increased presence of LD in our *C. elegans* model of X-ALD (A. Coppa dissertation, 2015). To explore the ROS derived mitochondrial influence the presence of lipid droplets was investigated and quantified in the presence/absence of both antioxidants, CoQ and MitoQ separately. Both, the diameter (> 5µm) and also the presence of the lipid granules were significantly increased in mutant worms compared to wild type animals (Fig R.2.3 A, a-b). After treating the animals with antioxidants, the length and the amount of lipid droplets were decreased in the *pmp-4* mutant animals, thus confirming the role of mitochondrial ROS in the modulation of LD metabolism (Fig R.2.3 A, c-f and Fig R.2.3.B).

A

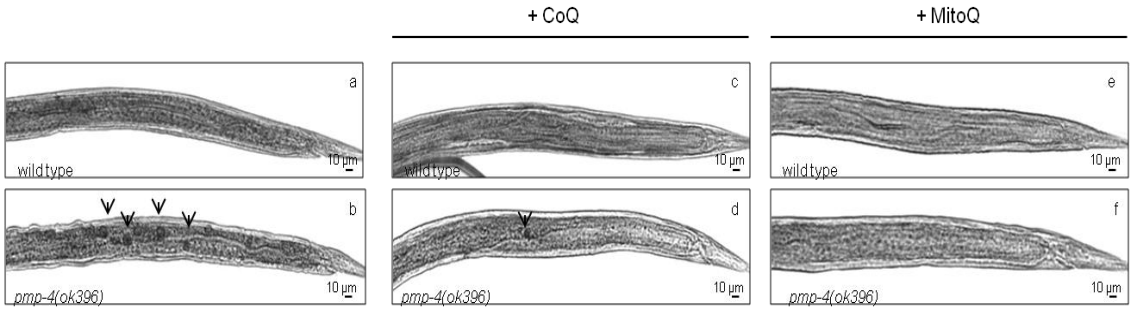

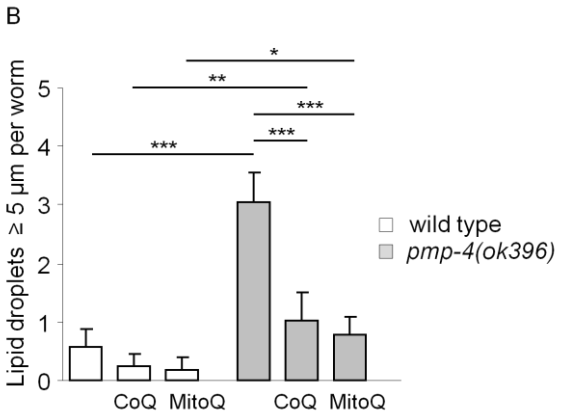

Fig R.2.3: Lipid accumulation (A, a-f) Sudan black. Representative images of Sudan Black stained L4 worms. For each animal the posterior part (from the vulva to the tail) is shown. Scale bars, 10µm. (B) Quantification of lipid droplets per worm. In each photo we have counted the number of Sudan Black stained structures with a diameter ≥ 5µm. N = 35±5. Significant differences were revealed by ANOVA followed by Tukey HSD post hoc. (*** $P < 0.001$ referred to *pmp-4(ok396)* strain respect to the other genotype).

R.2.4 *pmp-4* mutants displayed neurological abnormalities

R.2.4.1 *pmp-4* mutants displayed locomotion abnormalities

The most common phenotype related to human X-ALD is adrenomyeloneuropathy (AMN), an axonopathy in spinal cord, resulting in spastic paraparesis and defective peripheral nerve conduction, without myelin involvement (Ferrer et al., 2010; Moser, 2001; Powers et al., 2000). The X-ALD mouse phenotype resembles very much to AMN, with axonal degeneration in spinal cords, without brain involvement (Pujol et al., 2004; Pujol et al., 2002). To analyze whether the lack of *pmp-4* cause a motor neuron related phenotype, the motility of *pmp-4* mutant and wild type animals was evaluated. Thrashing assays were performed in M9 buffer on L4 and seven consecutive day's post-L4 (Sattelle et al., 2008). Thrashing and locomotion assays are simple robust methods for assessing neuromuscular function (Horwich et al., 2009) and for studying degeneration of motor neurons leading to muscle wasting. *C. elegans* swim (thrash) back and forth at a regular rate when placed in liquid medium and crawl when placed in solid agar medium (Wormbook). *pmp-4* null mutants show a dramatic and progressive decline in thrashing and locomotion rates at L4 stage (Fig R.2.4.1.A) that continues till L4 plus seven more days (Fig R.2.4.1.B). Similar to wild type, *pmp-4* animals showed a gradual reduction in thrashing rate over time; but the difference between them

increases as the worm ages. Likewise, *pmp-4* did consistently move at a significantly reduce rate compared with wild type animals at both times tested on NGM agar plates with *E. coli,* indicating a robust motility defect (Fig R.2.4.1C,D). This motor impairment could derive from defects of muscle cells or motor neurons. To explore the structure of muscle cells, F-actin was labelled with a fluorescent form of phalloidin, a bicyclic peptide belonging to a family of toxins isolated from the deadly *Amanita phalloides* mushroom and commonly used in imaging applications (Cooke et al., 2009). Comparing the structure and the microfilament organization of muscles cells in N2 wild type and in *pmp-4* strains, no obvious differences were observed (Fig R.2.4.1E).

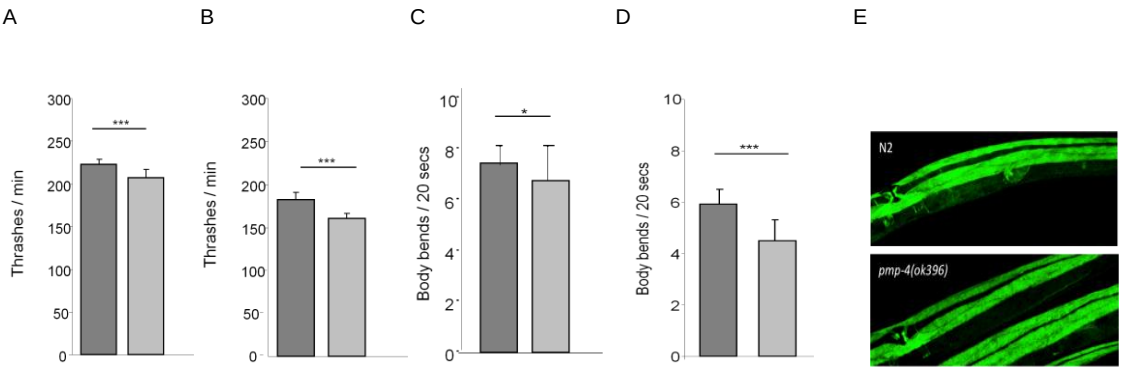

Fig R.2.4.1: *pmp-4* thrashing and locomotion assays: (A-B) Thrashing rates of wild type and *pmp-4* after 2 minutes in M9 at L4 and 7 days post larval L4 stage counted manually. (C-D) Body bends of wild type and pmp-4 for 20 seconds at L4 and L4 plus 7 days. *pmp-4* mutant animals showed gradual decline in motility as they age more. At least 20 animals per strain per time point were assayed over three independent experiments. *** $P < 0.001$, unpaired t-test. Means ± SEM are plotted for all figures. (E) Phalloidin staining. Representative images of phalloidin stained worms, N2 and *pmp-4* are shown. No obvious differences, between the two strains, are detected in muscle morphology. In all the graphs, the darker grey bar represents wild type values whereas the lighter grey bar is for *pmp-4* values.

R.2.4.2 Worm microtracker also provides evidence for *pmp-4 (ok396)* mutants delayed locomotion

To determine whether the *pmp-4* thrashing defect could be used as the basis of an *in vivo*, automated chemical library screen, thrashing rates of wild type and *pmp-4* animals were measured using an Infrared locomotor tracking system also known as ¨Worm Microtracker¨ (Simonetta et al., 2007). Synchronized L4 stage animals were assayed at 30 minutes in liquid suspension. Similar to the results of the manual assay, the automated assay was able to detect a significant difference between wild type and

pmp-4 animals; the mutants consistently thrashed at a slower rate in solution (Fig R.2.4.2).

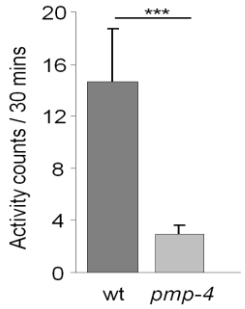

Fig R.2.4.2: Thrashing assay tracking system - the thrashing activity recording system counts infrared photo beam interruptions in a fixed time lapse. 5 worms per well was placed with 50µl of M9, in a total of 10 wells per genotype. The activity was measured for each worm and the average ± S.E.M. of 50 worms was graphed for each genotype. Activity was seen to be decreased in *pmp-4* animals.

R.2.4.3 *pmp-4* mutants thrashing defects are rescued with antioxidants

Thrashing assays were performed blindly in M9 at L4 (Fig R.2.4.3.A) and 7 days post L4 (Fig R.2.4.3.B) as described (Francis et al., 2005; Kraemer et al., 2003) and as mentioned in the previous section. The thrashing abnormalities were restored by the antioxidant CoQ, but more efficiently by the mitochondrial targeted MitoQ, thus suggesting mitochondrial ROS as causative for the locomotion abnormalities (Fig R.2.4.3).

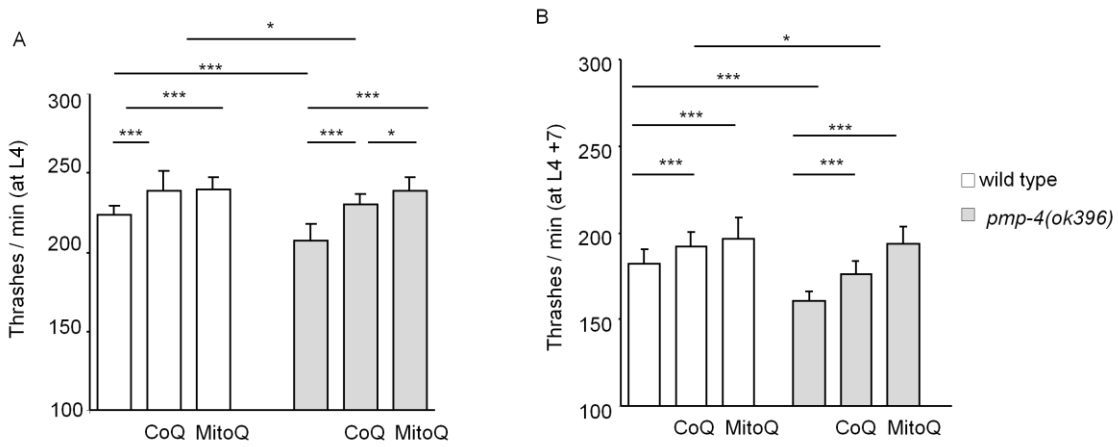

Fig R.2.4.3: *pmp-4* mutants thrashing defects at L4 and at L4+7 days stage are rescued with antioxidants A. The *pmp-4(ok396)* mutation confers abnormal locomotion at L4 stage of development. The thrashing behavior was analyzed at L4 in wild type and *pmp-4(ok396)* nematodes with and without the presence of the indicated drugs CoQ and MitoQ. The thrashes per minute were recorded after 72hours for 3 minutes under bright field microscopy and analyzed using the ImageJ software. At L4 stage *pmp-4* mutant worms were more defective in thrashing compared to wild type animals but both genotypes were rescued by the two mitochondrial antioxidants B. The *pmp-4(ok396)* mutation confers severe abnormal locomotion at L4 +7 stage of development. Same experiment was performed as explained before only with the older stage of worms. (Two-way ANOVA Bonferroni's post hoc. Data are mean ± SD ***p<0.001)).

R.2.4.4 Antioxidant treatment halted axonal abnormalities in *C. elegans* model of X-ALD

Because worms lacking *pmp-4* exhibited motor defects we examined the structural integrity of GABAergic D-type motor neurons and their processes in *pmp-4 (ok396)* animals by using the *Punc-25:: GFP* reporter. Worms expressing this reporter showed GFP labeling distributed along the axons and the GABAergic cell bodies of the ventral cord (Cinar et al., 2005). The strain *Punc-25::GFP* allows analyzing for defects in axonal outgrowth or navigation in individual neurons with neurites in both nerve cords as well as interconnecting commissural axons (Brandt et al., 2009) and has been widely used to investigate neurodegeneration in the nematode (Guthrie et al., 2009; Kraemer et al., 2003; Lim et al., 2012; Rawson et al., 2014). Wild type worms expressing the *Punc-25::GFP* reporter show both the dorsal and ventral nerve cords continuous and contain the normal complement of 19 inhibitory motor neurons (13 VD and 6 DD GABAergic neurons (Lim et al., 2012).

Animals *Punc-25::gfp; pmp-4(ok396)* were generated and the percentage of axonal defects was quantified by analyzing the number of commissural abnormalities detected per animal (Earls et al., 2010; Firnhaber and Hammarlund, 2013), added to the number of gaps per animal present in the dorsal and in the ventral nerve cord, indicative of either incomplete neurite outgrowth during development or a potential degeneration of neuritis (Fig R.2.4.4 A) (Brandt et al., 2009). This is the applied formula used to quantify axonal damage: % of axonal damage = [((number of commissural abnormalities + number of gaps/animal))/number of axons detected) x100]. Whereas no neuronal loss was observed at any time point investigated in wild type worms, loss

of *pmp-4* increased the axonal damage earlier at L4 (Fig R.2.4.4 B-C) and at L4 + 7 days of development (Fig R.2.4.4 E-F). Interestingly, in the aged worms (L4 + 7) after treatment with the two antioxidants CoQ (Fig R.3.4.4 G-H) and MitoQ (Fig R.3.4.4 I-J), axonal damage was reduced in wild type and in *pmp-4* mutant animals. Quantification of the axonal damages at their respective stages per genotype and treatment are represented at Fig R.2.4.4 D and K.

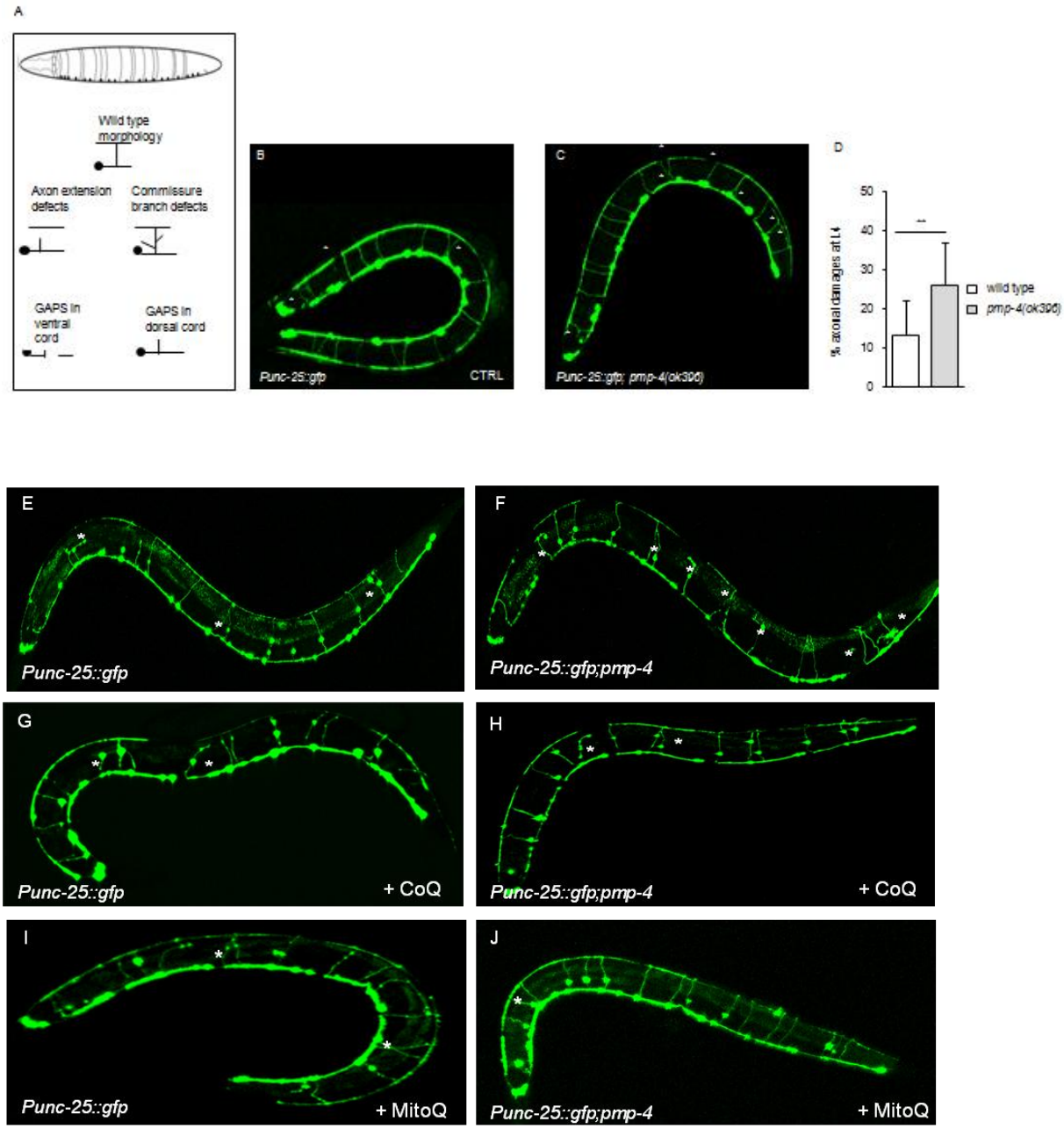

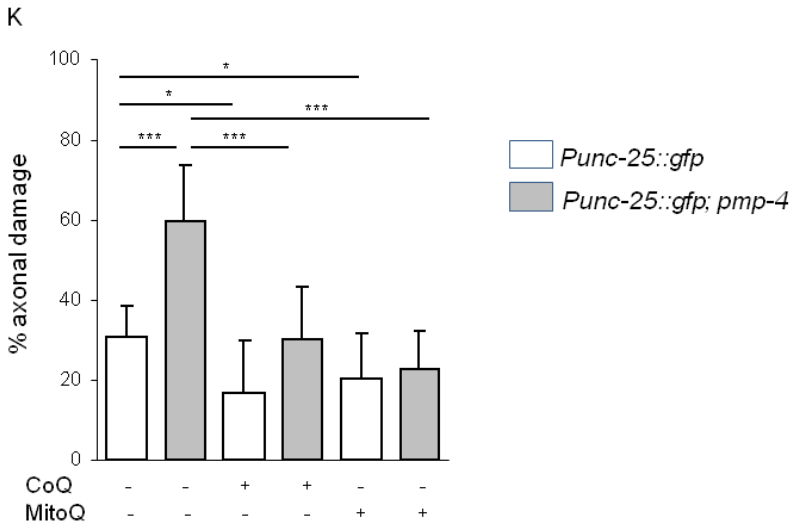

Fig R.2.4.4: Confocal fluorescence microscopy of GFP-labeled GABAergic neurons in living worms at L4 and at L4+7 (A) Schematic diagram showing the defects that are typically observed in *pmp-4* mutant animals. (B-J) GABA neuron cell bodies processes in the ventral nerve cord and dorsally projecting commissures labeled with *unc-25:: GFP*. All worms are oriented with anterior end left and ventral side down. Commissural abnormalities and gaps in the dorsal and ventral cord are the considered axonal abnormalities and are labeled with the white asterisks. Objective is 20X. (D and K) Quantitative analyses of the axonal defects. The percentage of axonal damage was calculated as stated in the methodology. Between 50 and 80 animals were analyzed per genotype and condition (One-way ANOVA Tukey's post hoc. Data are mean ± SD ***p<0.001)).

R.2.4.5 Antioxidant treatment halted mechanosensory abnormalities in *C. elegans* model of X-ALD

To ascertain the specificity of the axonal damage, *pmp-4 (ok396)* worms were crossed with the mechanosensory strain *Pmec-7:: gfp.* Main abnormalities detected in *pmp-4* mutants compared to wild type animals were PLM over extension and ALM outgrowth defects. These sensory neuron defects were significantly increased in *pmp-4* mutant animals compared to wild type in aged worms (L4 + 7) and both CoQ and MitoQ rescued axonal abnormalities in the pmp-4 background (Fig R.2.4.5). Therefore mitochondrial ROS affected axonal integrity in both motor and mechanosensory neurons and axonal morphology might be susceptible to mitochondrial ROS.

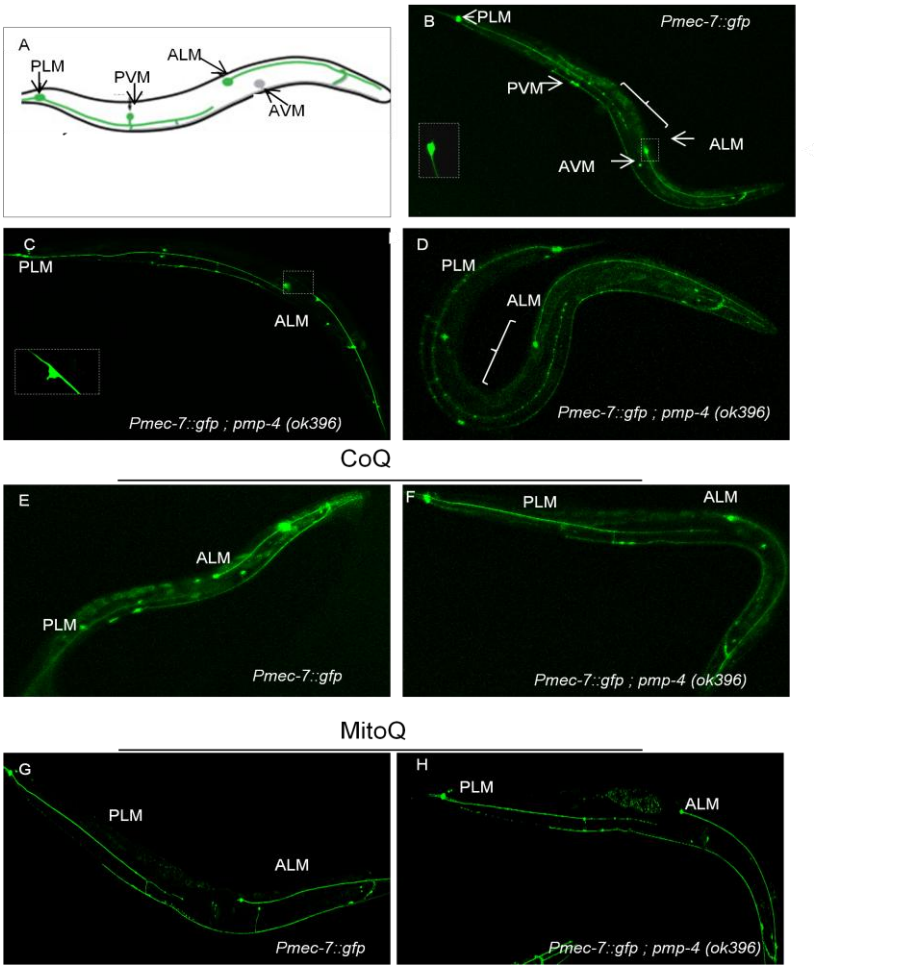

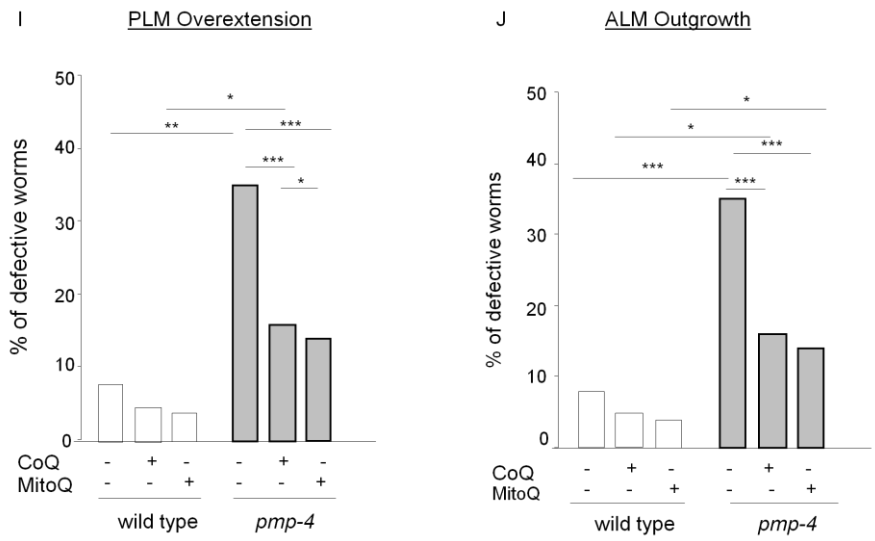

Fig R.2.4.5: Mitochondrial ROS depending defects occur in *C. elegans* touch receptor neurons A. Diagram of *C. elegans* paired ALM and PLM touch receptor neurons (lateral view).

Only neurons on the right are shown. B-D. Representative Confocal GFP images of wild-type and *pmp-4* ALM and PLM cells. GFP is from *Pmec-4:: gfp*. Anterior is to the right and ventral side down. B. Wild type animal without abnormalities in the mechanosensory neurons. The square in the corner represents an enlargement of the ALM neuron without irregular extensions. C. Shows irregular ALM outgrowth in the ALM cell body of *pmp-4(ok396)* animals. The defect is expanded in the attached dashed square. D. Irregular extension of the PLM process overlapping ALM axon in *pmp-4* animals. E-J. Mechanosensory abnormal processes are rescued with the antioxidants CoQ and MitoQ in wild type and in *pmp-4* mutant animals. I-J. Quantification of the PLM overextension and the ALM outgrowth in wild-type and mutant adult animals. Error bars are SDs of proportions. *P < 0.05, **P < 0.01, and ***P < 0.001 (Fisher's exact test or two-proportion test).

R.3 Axonal sensitivity towards mitochondrial ROS

R.3.1. Axons in *pmp-4* mutant animals are more sensitive to exogenous mitochondrial ROS

To investigate the influence of mitochondrial ROS in the axonal maintenance and function, worms from the same GABAergic strain *Punc-25:: gfp* with and without the *pmp-4(ok396)* mutation were treated in parallel with the pro oxidant PQ at sublethal dose (0.2 mM). The morphology of the axons was analyzed by confocal microscopy and quantified as described in the previous section (R.2.4.4). After 72 hours of PQ treatment, both wild type and *pmp-4* mutant animals showed increased thrashing defects and axonal abnormalities. However the absence of pmp-4 increased both these phenotypes in the presence of PQ (Fig R.3.1,D).We previously showed mitochondria as the main source of ROS in this nematode model of X-ALD (Fig R.2.1). Consequently, we hypothesize that by lowering the ROS levels specifically in the mitochondria with MitoQ, axonal integrity in PQ treated animals might be restored. Indeed, the mitochondrial targeted MitoQ restored locomotion (Fig R.3.1.G) to basal levels and axonal abnormalities (Fig R.3.1.H) in both wild type and in *pmp-4(ok396)* PQ treated animals, thus corroborating our hypothesis of the axonal sensitivity to mitochondrial ROS.

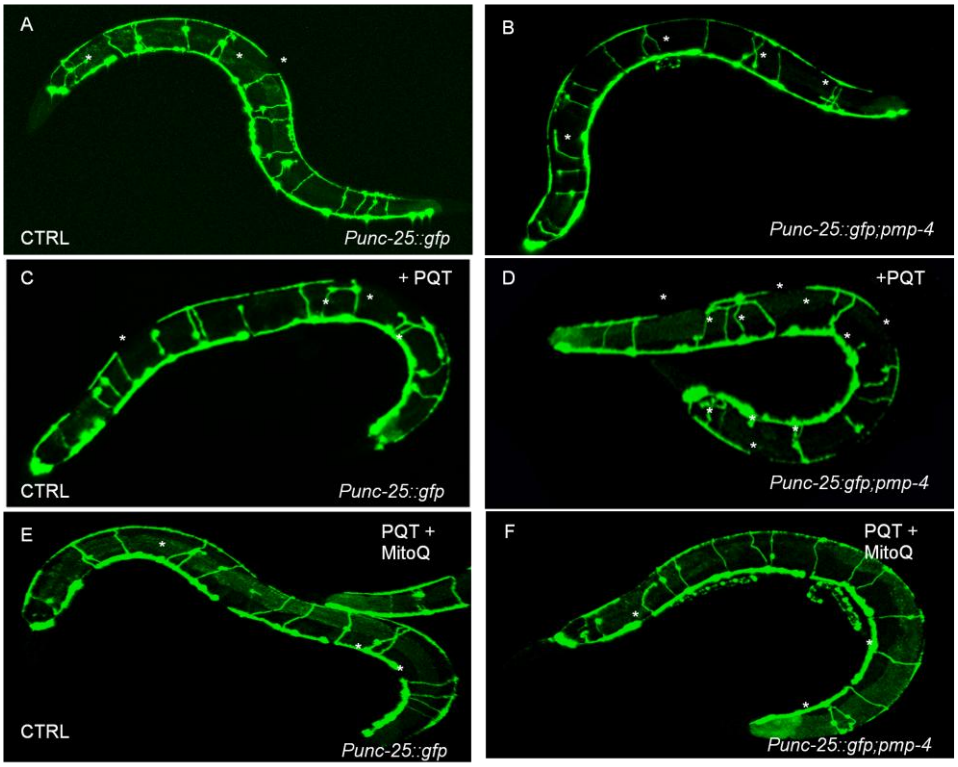

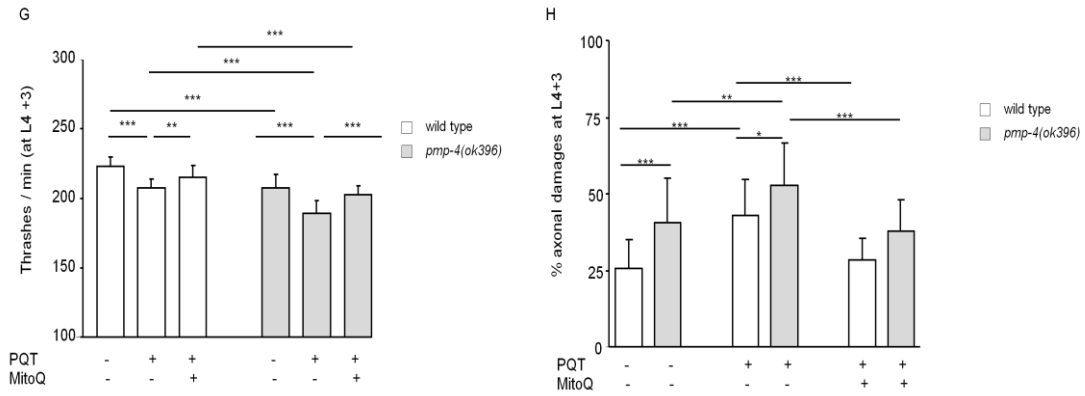

R.3.1: Behavior and axons in *pmp-4* mutant animals are more sensitive to external ROS

A-F. Paraquat treatment increased axonal abnormalities. Confocal fluorescence microscopy of GFP-labeled GABAergic neurons in living worms treated during 72h with the pro oxidant drug paraquat at the sublethal dose of 200 µM. All worms are oriented with anterior end left and ventral side down. White asterisks are labeling the considered abnormalities. Objective is 20X Wild type (A) and *pmp-4* mutant (B) GABA neuron cell bodies processes in the ventral nerve cord and dorsally projecting commissures labeled with *unc-25:: GFP*. At 3 days post L4 the number of axonal abnormalities is increased in *pmp-4* animals compared to wild type. C and D. Paraquat increased the number of axonal abnormalities wild type and in *pmp-4* animals. E and

F. MitoQ 7.3 µM restored the morphology of the axons in the two genotypes tested but the effect of MitoQ is better achieved in *pmp-4* worms. G. Locomotion behavior is affected more severely by external ROS in *pmp-4* mutant animals. The thrashing behavior was analyzed at stage L4+3 of development in wild type and in *pmp-4(ok396)* nematodes with and without paraquat and/or MitoQ as indicated. The thrashes per minute were recorded after 72h for 3 minutes under bright field microscopy and analyzed using the ImageJ software. MitoQ treatment rescued the thrashing behavioral defects in both genotypes. Data are mean ± SD. ***P<0.001 with ANOVA statistical analyses. H. Quantitative analyses of the axonal damage. Between 30 and 50 animals were analyzed per genotype and condition. Data are mean ± SD. ***P<0.001 and **P<0.01 with 2 way ANOVA statistical analyses.

R.3.2 The absence of Mitochondrial complex I generated axonal abnormalities

To confirm the results obtained with the antioxidant drugs and to genetically corroborate the influence of mitochondrial ROS in axonal integrity, the mitochondrial gene *nuo-1* was knocked down by RNAi knockdown. *nuo-1* is the nematode gene homolog to the human NDUFB4/B15 subunit of complex I required for oxidative phosphorylation (Tsang, 2001)). *nuo-1* RNAi animals recapitulated the axonal defects present in the GABA neurons of PQ treated animals (Fig R.3.2.) thus confirming genetically the hypothesis of mitochondrial ROS damaging axons.

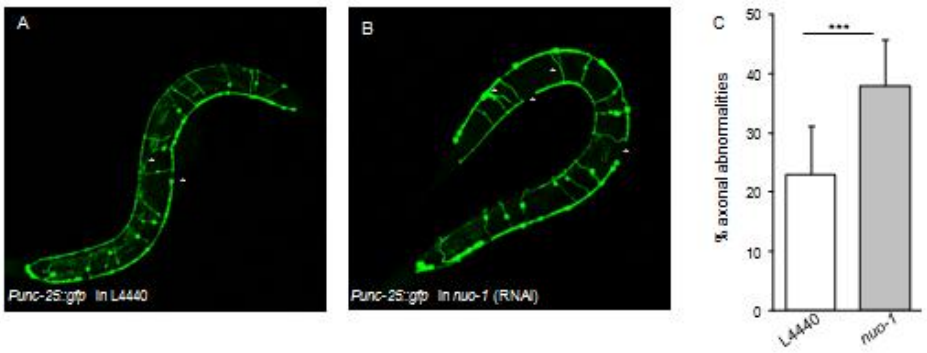

Fig R.3.2: Knock down of *nuo-1* induced axonal damage. RNAi knockdown of complex I component *nuo-1* resulted in increased axonal abnormalities. *C. elegans* strain *Punc-25:: GFP* incubated with RNAi against *nuo-1* was analyzed at day 7 and the same strain was incubated with empty vector bacteria (L4440) as a control for RNAi feeding. A-B is representative Confocal pictures of control and *nuo-1* RNAi incubated strains respectively whereas C is the quantitative analysis. Data were analyzed as the mean ± S.D. (*** P< 0.001; one-way ANOVA; n=30 worms).

R. Results (Chapter II):

Mitochondrial ROS regulation of the AWB chemosensory cilia in the *C. elegans* model of X-ALD

The nervous system in the *C. elegans* consists of 302 neurons and 50 glial-like cells associated with the sensory organ. Myelin sheaths as such are not formed in the worm, however glial-like cells ensheath neurons forming channels through which dendrites are threaded (Shaham et al., 2008). Since these glial-like cells are mainly adjacent to the chemosensory neurons, concreted in the amphid organ, we used this chemosensory amphid organ as readout for detecting damages concretely related to these cells and neurons. To investigate the functionality of the amphid organ we used three approaches. First, the dye, 1,1´- Dioctadecyl-3,3,3',3'- Tetramethylindo carbocyanine Percholrate (DiI) used to visualize the amphid organ, containing the glial-like cells and their related neuron and also to detect any alterations in them. Second, we used reporter strains that would allow us to visualize these glia-like cells and their related neurons. Third, we used volatile odorants to investigate whether the chemosensory neurons are functionally active or not (Sengupta et al., 2013). Collectively, our results suggest that *C. elegans´* chemosensation might provide a novel setting for exploring peroxisomal disease related disorders.

R.4 *pmp-4* mutants exhibit cell type-specific dye-filling defect owing to its ciliary dysfunction

R.4.1 AWB neuron in *pmp-4* mutants fail to take up the lipophilic dye, DiI

With the aim of characterizing different aspects of chemosensation related to the peroxisomal dysfunction, the general structure of amphid neurons was first analyzed through Dye-Filling (DiI) staining as described in (Sengupta et al., 2013; Olivier Mason, 2013). Six pairs of neurons in the head amphid sensory organs fill with the lipophilic dye DiI in wild-type animals (Fig. R.4.1B, C). We found that inactivation of PMP-4 at L4 stage of development caused AWB structural disruption resulting in failure of dye uptake, but had no effect on the structure of other DiI sensitive neurons (Fig R.4.1).

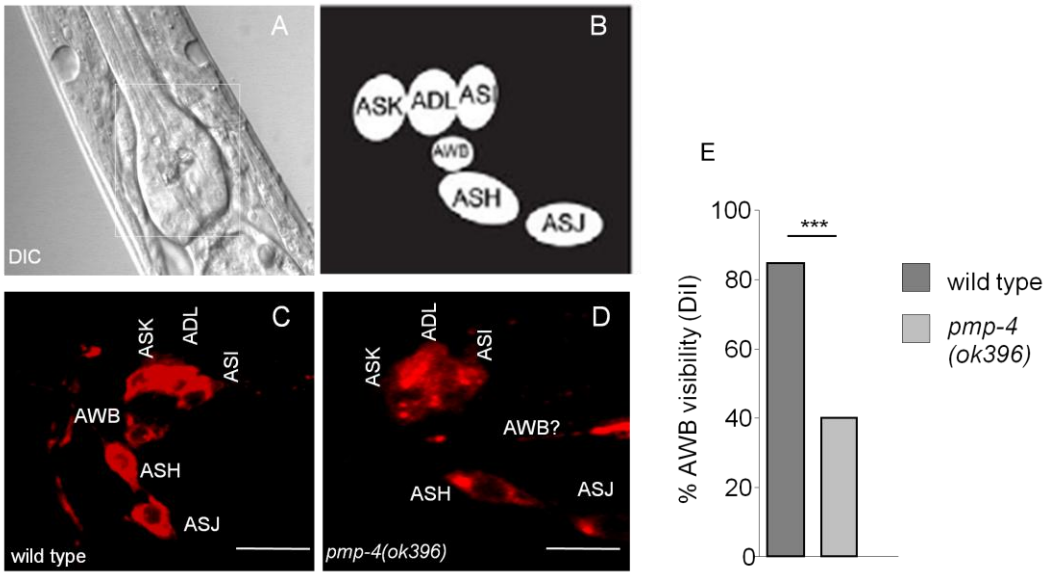

Fig R.4.1: ***C. elegans pmp-4*** **mutants exhibit cell-specific defects in uptake of lipophilic dye. (A)** Representative DIC-Nomarski picture of the head portion of an L4 worm. Only the anterior part, containing the DiI sensitive neurons, is depicted. Dorsal is up and anterior is left. The location of DiI stained neurons is delimited by the white square. (B) Schematic interpretation of DiI uptake in head amphid organ sensory neurons in wild-type is shown. (C) Wild type animal in which all neurons capturing the DiI are visible and named. (D) DiI staining of the peroxisomal β-oxidation mutant *pmp-4(ok396)*. All neurons except AWB fail to take up the dye. Side views showing one of each neuron pair; anterior is left. Animals were grown at 20°C. Scale bars: 10 µm. Objectives 63X. (E) Quantification of DiI uptake by AWB neuron in wild type and *pmp-4* mutants at the L4 stage. n=50 animals each, Fisher's test *** p<0.001.

R.4.2 *pmp-4(ok396)* mutation afects AWB cilia morphology

DiI dye-filling defect are frequently associated with defects in cilia or dendrite morphology (Olivier Mason, 2013; Ou et al., 2007; Williams et al., 2008). To determine whether the observed dye-filing phenotype in the *pmp-4* mutant animals reflected defects in the generation or maintenance of the neuronal morphology, we studied the AWB cilia morphology by using the reporter strain, *str-1p:: gfp,* which specifically expresses in the AWB chemosensory neurons ´cilia and cell body (Mukhopadhyay et al., 2007; Troemel et al., 1997) (Fig R.4.2 A,A'). Generally all AWB cilia in wild type animals possess the characteristic Y-shaped structure containing two branches of different lengths (Fig R.4.2 B, B'), the distal ends of which exhibit an irregular morphology and exhibit some animal to animal variability in the lengths of each cilial

branch, depending upon which temperature they are grown and in which conditions (presence or absence of food) (Mukhopadhyay et al., 2007). Mutants with defects in cilia or dendrite morphology frequently exhibit dye-filling defects in some or all dye-filling neurons (Sengupta el al., 2013). Accordingly, to observe any defect in AWB cilia in the *pmp-4* mutant animal, we genetically crossed them with the reporter strain, *str-1p::gfp.* We observed that the branch lengths of AWB channel cilia were weakly but significantly affected in *pmp-4* mutant animals in comparison to controls thus suggesting an underlying correlation between failures of DiI uptake with the regulation of cilia length (Fig. 4.4.1.A-B). Both cilia branches in *pmp-4* mutants were slightly shorter than in wild-type animals (Fig. 4.4.1.C-D).

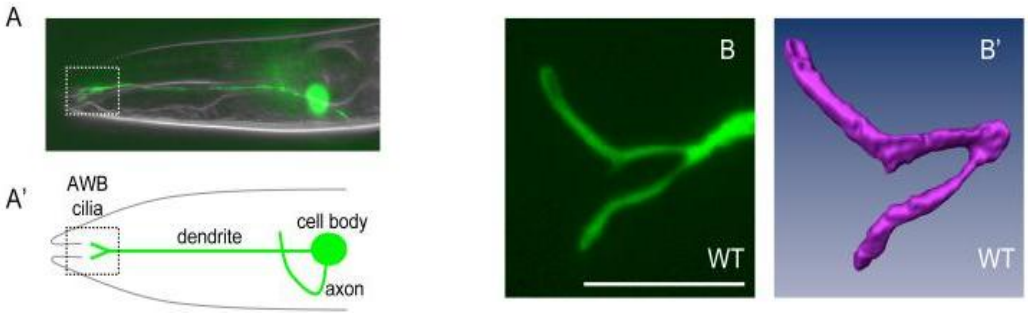

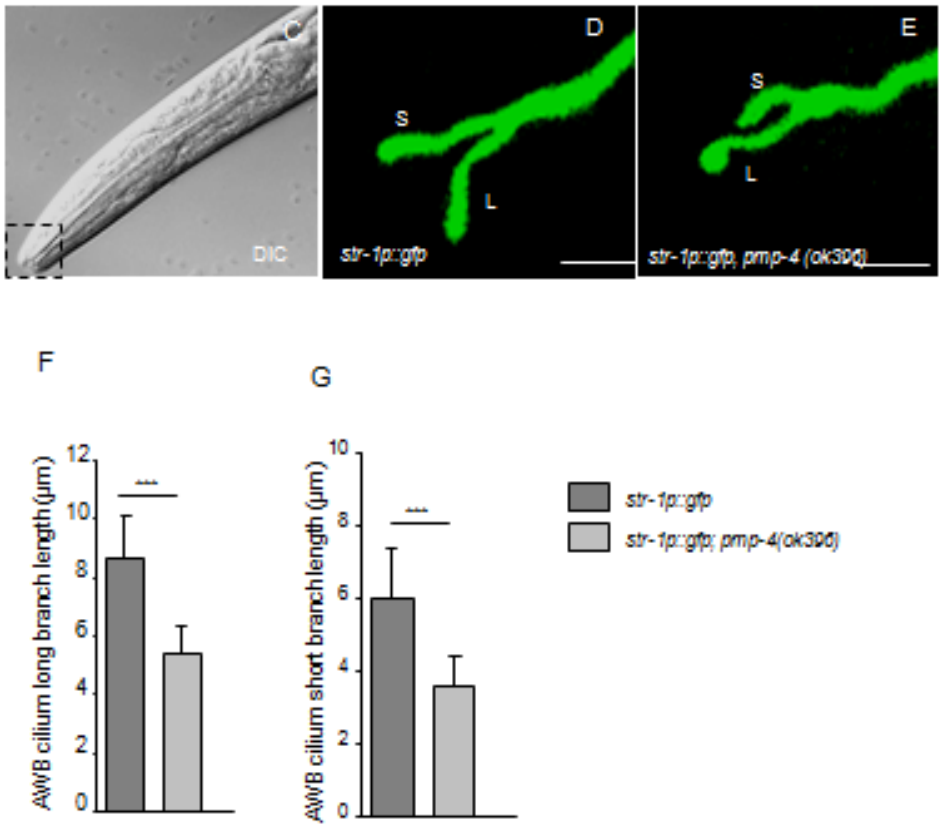

Fig R.4.2: *pmp-4* mutants exhibit AWB cilia morphological defects. (A, A´) refers to the location of cell body, processes and the cilia of the AWB neuron in an adult wild type animal. The AWB neuron is visualized via GFP expression driven by the AWB-specific *str-1* promoter. Only one of the bilateral AWB neuron pair is visible in the shown lateral view. (B, B´) The cilia of an AWB neuron visualized via *str-1p:: gfp* transgene expression in wild-type (WT) adults grown under standard conditions (Sengupta et al., 2009). C: Representative DIC-Nomarski picture of an L4 worm. Dorsal is up and anterior is left. The dashed line square is limiting the portion of the head containing the AWB cilia. D-E: Representative confocal fluorescent pictures of the AWB cilia labeled by the AWB specific reporter *str-1p::gfp* of the indicated genotypes. F-G: Quantification of the lengths of the long and short branches of the AWB cilia in the indicated genotype. N= 30 cilia analyzed per genotype. Student´s T-test with *** p<0.001, **p<0.01, *p<0.05. 63X objective. Letter S indicates short branch whereas letter L denotes Long Branch. Scale: 7.5 µm.

R.4.3 PMP-4 is essential to maintain AWB cell morphology and function

The dye-filling defects of *pmp-4* mutants (as shown in Fig R.4.1) together with the AWB cilia branch length defects (as shown in Fig R.4.2) were rescued via germline-based transformation of PMP-4 wild type (Fig R.4.3.D and H respectively). Therefore PMP-4 is essential to maintain AWB morphology and function.

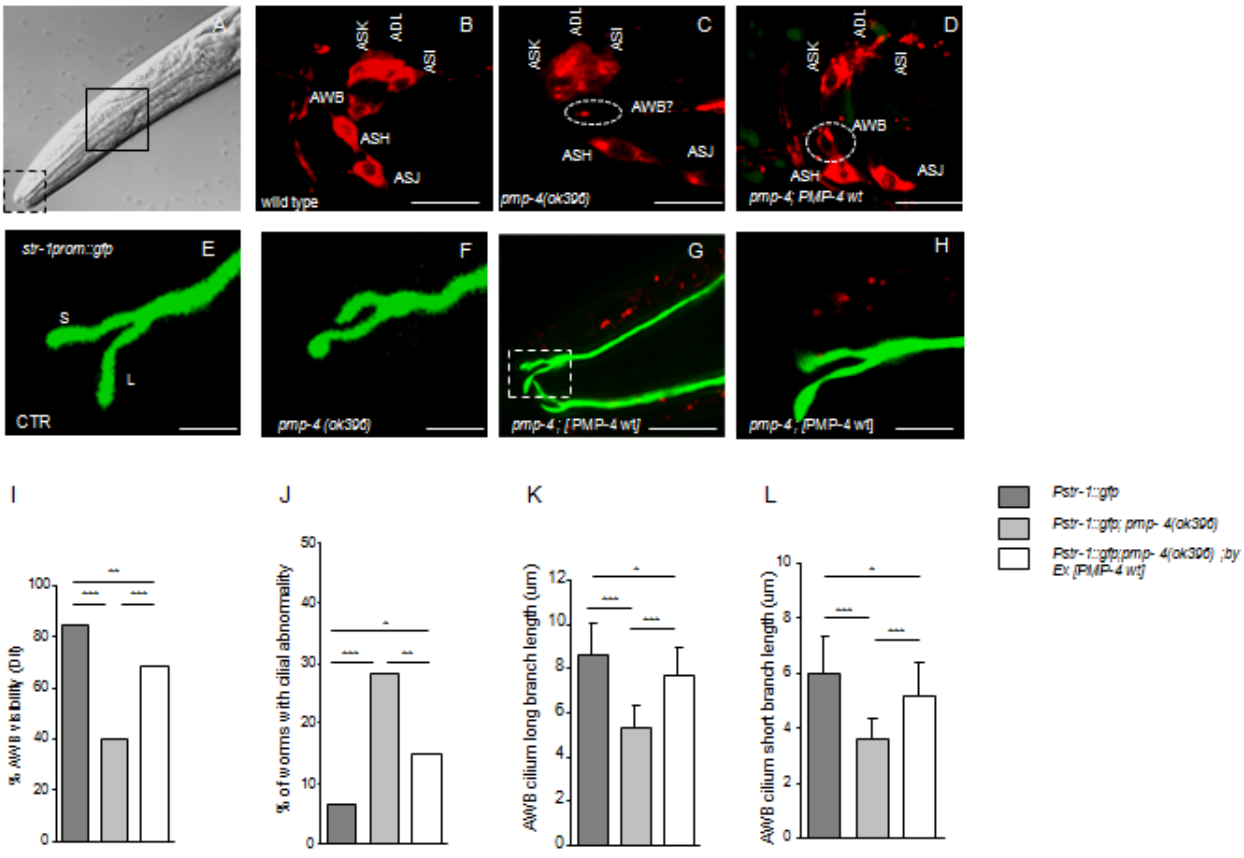

Fig R.4.3: The peroxisomal transporter PMP-4 is essential to maintain AWB morphology and function in *C. elegans* A: Representative DIC-Nomarski picture of an L4 worm. Only the anterior part, containing the DiI sensitive neurons, is depicted. Dorsal is up and anterior is left. The location of DiI stained neurons is delimited by the black square whereas the dashed line square is limiting the portion of the head containing the AWB cilia. B: Wild type animal in which all neurons capturing the DiI are visible and named. C: DiI staining of the peroxisomal β-oxidation mutant *pmp-4(ok396)*. D: DiI staining is rescued by PMP-4 wild type in the *pmp-4(ok396)* background (*pmp-4 (ok396); by Ex[Ppmp-4::pmp-4::gfp]*).The white dashed circle in C and D is indicating the absence/ presence of AWB staining respectively. Scale bar is 10 µm E-H: Representative confocal fluorescent pictures of the AWB cilia labeled by the AWB specific reporter *Str-1Prom::gfp* of the indicated genotypes. E: Long and short branches of the AWB cilia in the *Str-1Prom::gfp* strain used as a control. F: mutated *pmp-4* induces abnormalities in the

cilia length. G: The AWB reporter strain *Str-1Prom::gfp* was crossed with the rescue strain *pmp-4(ok396); Ppmp-4::pmp-4::mCherry.* The AWB cilia are labeled in green whereas the punctuate pattern is indicative of PMP-4. H: is an expansion of the region delimited by the white square in G to better appreciate the recovery of the cilia length by the wild type PMP-4. Scale E, F and H: 2 µm. Scale Bar in G: 7.5 µm I: Quantification of the number of worms in which the AWB neuron is visible by the DiI. J: Quantification of the number of animals defective in the cilia length expressed in percentages. I and J Fisher's test *** $p<0.001$, **$p<0.01$; n = 25 animals per genotype. K-L: Quantification of the branch cilia length, long and short, respectively. N= 25 cilia analyzed per genotype. One way ANOVA, Tukey's *post hoc* *** $p<0.001$, **$p<0.01$, *$p<0.05$. 63X objective.

R.4.4 the morphology of the glia-like cells associated to AWB remained unaltered by the presence of the *pmp-4(ok396)* mutation

Glia is regarded as the neuronal support cells as they provide essential nutritive and growth signals for neurons (Shaham et al., 2008). To examine how is the glial shape and morphology in our *pmp-4* mutant worms we used developmental imaging and genetics to study it. The presence of matrix filled vesicles in the sheath glia of the cilia mutants has been previously described (Lyman-Gingerich et al., 2014). So to observe only the sheath glial cells of *pmp-4* mutant animals, whether they contain vacuoles or not we used a reporter strain, containing *F16F9.3pro:: mCherry* (kindly provided to us by Dr. Maxwell Heiman) which is specifically expressed in the sheath glia surrounding the AWB amphid neurons (Fig R.4.4C). To investigate any alteration in the *pmp-4* mutants sheath glia like cells we made a genetic cross with the reporter strain mentioned above with *pmp-4(ok396)* animals. We didn't observe any difference in terms of morphology between wild type and *pmp-4(ok396)* L4 animals (Fig R.4.4.I) thus discarding a defect in AWB associated sheath glia like cells.

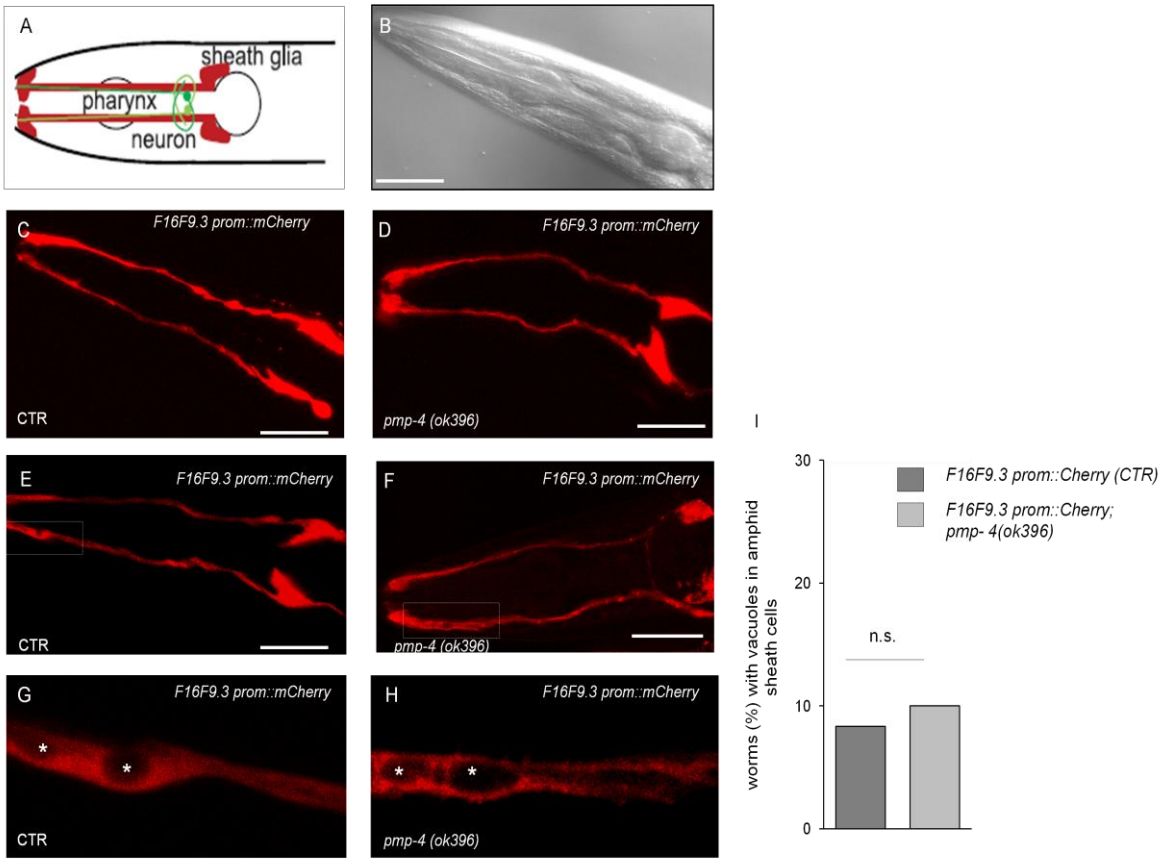

Fig R.4.4: The amphid sheath glia cell surrounding the AWB neuron is not influenced by the *pmp-4(ok396)* mutation. A: Cartoon illustrating how sheath glia shown in red surrounds the amphid neuron shown in green. B: Representative DIC picture of a wild type L4 worm depicting the amphid region. C-D: The reporter *F16F9.3Prom::mCherry* expressed in the amphid sheath cells at the indicated genotypes. The *pmp-4(ok396)* mutation is not affecting the morphology of the AWB ensheathing cells. E-F: In some cases the sheath cells have round areas in where F16F9.3 is absent. G-H: Enlarged views of boxed areas in E and F respectively in which vacuoles lacking expression are labeled with white asterisks. Dorsal is up and anterior is left in all representative pictures. I: Quantification of the number of vacuoles expressed in percentages. The percentage of animals with vacuoles in the amphid sheath cells doesn't differ between wild-type and mutant animals at the L4 stage. Approximate 30 animals were tested in two independent experiments. Scale bar in B-F is 20 µm. Objective is 63X Expanded 2X.

R.5 Intra peroxisomal β-oxidation mutants exhibit similar cell type-specific dye-filling defect owing to its ciliary dysfunction

PMP-4 is the membrane transporter for the degradation of VLCFA by the peroxisomal β-oxidation in the nematode. *pmp-4(ok396)* mutant derived phenotypes such as lipid accumulation, developmental delay and egg laying abnormalities, were similar to those generated by mutations in the peroxisomal β oxidation enzymes such as *dhs-28/*bifunctional protein and *daf-22/*thiolase (Mak, 2010), located in the peroxisomal matrix. To explore the phenotypical similarities between mutant animals for the *pmp-4* transporter and the intra peroxisomal mutants, *daf-22(ok693)* and *dhs-28(tm2851)* in the context of AWB, *daf-22* and *dhs-28* mutant animals were stained similarly with the DiI dye. In parallel, the AWB cilia of the *daf-22* and *dhs-28* mutant animals were examined by using the same reporter strain *str-1Prom::gfp* as described before for *pmp-4* mutant animals. As observed in Fig R.5, *dhs-28*/Bi-functional dehydratase and *daf-22/*thiolase were also similarly affected in taking up the dye by the AWB neuron and also it has significantly shorter cilial branch lengths as compared to the wild type animals.

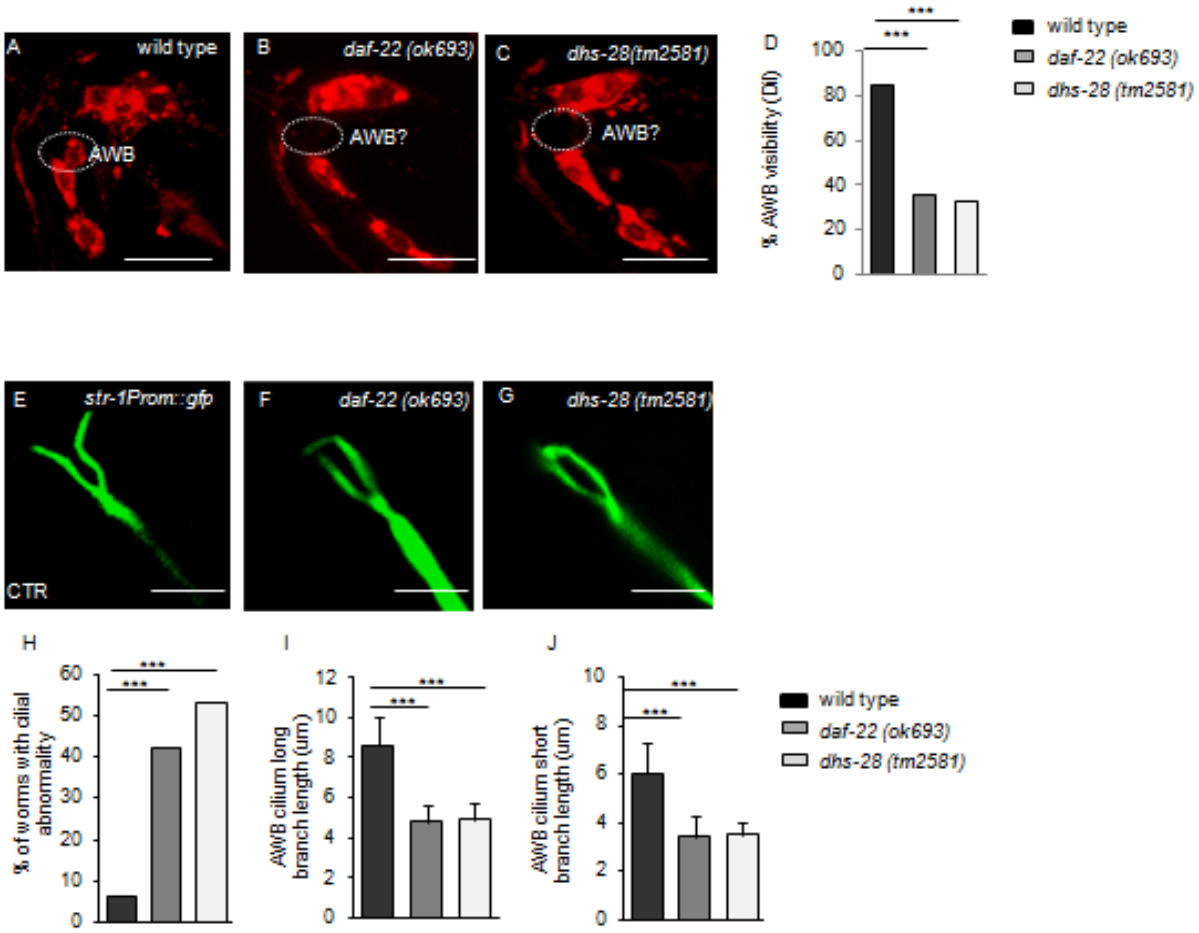

Fig R.5: Peroxisomal β-oxidation genes influence the AWB behavior and morphology. A-C: DiI staining of the wild type worms and the peroxisomal β-oxidation mutants of the indicated phenotypes. The white dashed circle is indicating the lack of AWB staining in peroxisomal mutants in comparison to wild type animals. Scale bar is 10 µm. D: Bar graph showing the percentage of AWB neuron visible after DiI staining of the corresponding genotypes (Fisher's test *** p<0.001, **p<0.01; n = 30 animals per genotype) F-G: AWB abnormal cilia in peroxisomal β-oxidation mutant animals. Representative confocal fluorescent pictures of the AWB cilia labeled with the specific AWB reporter *str-1Prom::gfp* of the indicated genotypes. All peroxisomal β-oxidation mutants are defective in the cilial branch lengths. Scale bar is 5 µm. H: Quantification of the number of animals defective in the cilial branch lengths expressed in percentages (Fisher's test *** p<0.001, **p<0.01; n = 50 animals per genotype). I-J: Length of the long and short branch respectively expressed in µm, of the indicated genotypes. N= 40 cilia analyzed per genotype. Error bars represent standard deviation (SD). One way ANOVA, Tukey's *post hoc* *** p<0.001, **p<0.01, *p<0.05).

R.6 The aversive associated AWB response is abnormal in peroxisomal β-oxidation mutants

AWB function during behavior is mediating repulsion against a subset of volatile odorants (Sagasti et al, 1999). The volatile compounds octanol together with 2-nonanol are detected by AWB neurons, latter odorant being more specific (Troemel et al. 1995; Chao et al. 2004). We used chemosensation behavior assay to explore whether AWB behavioral function is also influenced by mutations in peroxisomal β-oxidation. All β-oxidation mutant worms exposed to 2-nonanol either showed a strong impairment of their aversive function compared to wild type animals (42%, 57% and 71% for *pmp-4*, *daf-22* and *dhs-28* mutant animals respectively in comparison to wild types) (Fig R.6.B). Similar results but milder were obtained with exposure to 1-octanol (33%, 41% and 50% for *pmp-4*, *daf-22* and *dhs-28* mutant animals respectively in comparison to wild types) (Fig R.6.C). AWA attractant behavior is not influenced by the peroxisomal β-oxidation pathway since all mutant animals tested were attracted to diacetyl, specifically detected by the AWA neuron (Bargmann et al. 1993; Sengupta et al. 1996). Therefore the aversive response mediated by the AWB neuron is specifically modulated by the peroxisomal β-oxidation genes in *C. elegans* (Fig R.6.E).

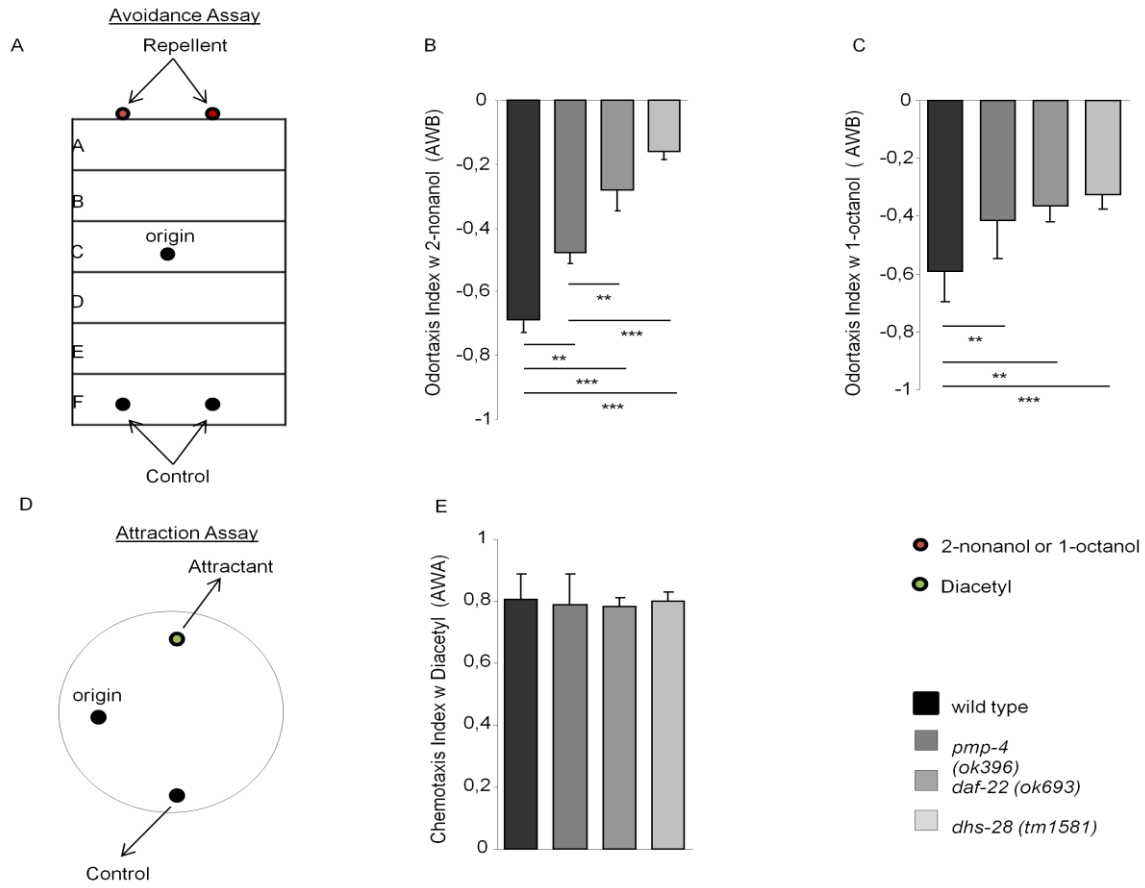

Fig R.6: The aversive associated AWB response is abnormal in peroxisomal β-oxidation mutant animals A-C: Odortaxis indexes. The odor taxis indexes against the aversive compounds 2-nonanol (B) and 1-octanol (C) are indicating AWB-associated odor sensation abnormalities in all peroxisomal β-oxidation mutants analyzed. *odr-4* and *odr-10* mutants were used as negative controls in case of Nonanol assay whereas *rgs-3* where used in case of Octanol assay. D: The AWA response is not affected by peroxisomal β-oxidation mutations. The volatile compound diacetyl was used to analyze the attractive behavior involving the AWA neuron. E: The attractive response was not affected in any of the peroxisomal β-oxidation mutants tested (one way ANOVA, Tukey's post hoc; *** $p<0.001$, ** $p<0.01$). Odortaxis indexes were calculated as described in the methodology section. Error bars represent standard deviation (SD). Figures A and D illustrate how the odor taxis experiments were performed as explained in the methods.

R.7 Mitochondrial ROS were not generated by mutations in intra-peroxisomal genes

As mentioned in the previous sections that the ROS was the main reason behind GABAergic and mechanosensory neurons' axonal degeneration (Fig R.2.4.4 and Fig R.2.4.5). Accordingly we sought to confirm this mechanism being part of the modulation of AWB cilial branch length defects. The ROS formation was measured by detecting the oxidation induced by the fluorescence emitted by the dye carboxy-H2 DCFDA as described before in *C. elegans* (Shi et al., 2012; Yang et al., 2013; Yang and Hekimi, 2010). In comparison to the wild type animals, levels of the dye were significantly increased in *pmp-4* mutant animals (Fig R.2.1) but also in the intra-peroxisomal mutant counterparts, but at lesser extent (Fig R.7, left column, untreated animals). As previously described, the ROS levels were restored to basal levels in CoQ and MitoQ treated *pmp-4* mutant worms and in wild type animals (Fig R.2.1). Interestingly, although the ROS levels were rescued in all the CoQ treated intra-peroxisomal mutants (Fig R.7, second column, left + CoQ), MitoQ treatment didn't rescue the amount of ROS generated intra-peroxisomally (Figure R.7, third column left, + MitoQ). Moreover, using the dye MitoSOX, which specifically labels mitochondrial superoxide (Smith et al., 2014; Yang and Hekimi, 2010), we found that only *pmp-4* mutants displayed elevated superoxide levels in comparison to the other intra-peroxisomal mutants and to the control wild types (Fig R.7, MitoSOX), thus indicating that the most of the ROS induced by intra-peroxisomal mutations are not mitochondria-generated, contrary to the observed with *pmp-4* mutant animals, in which the main source of ROS is mitochondria and no leakeage of intra-peroxisomal ROS.

.

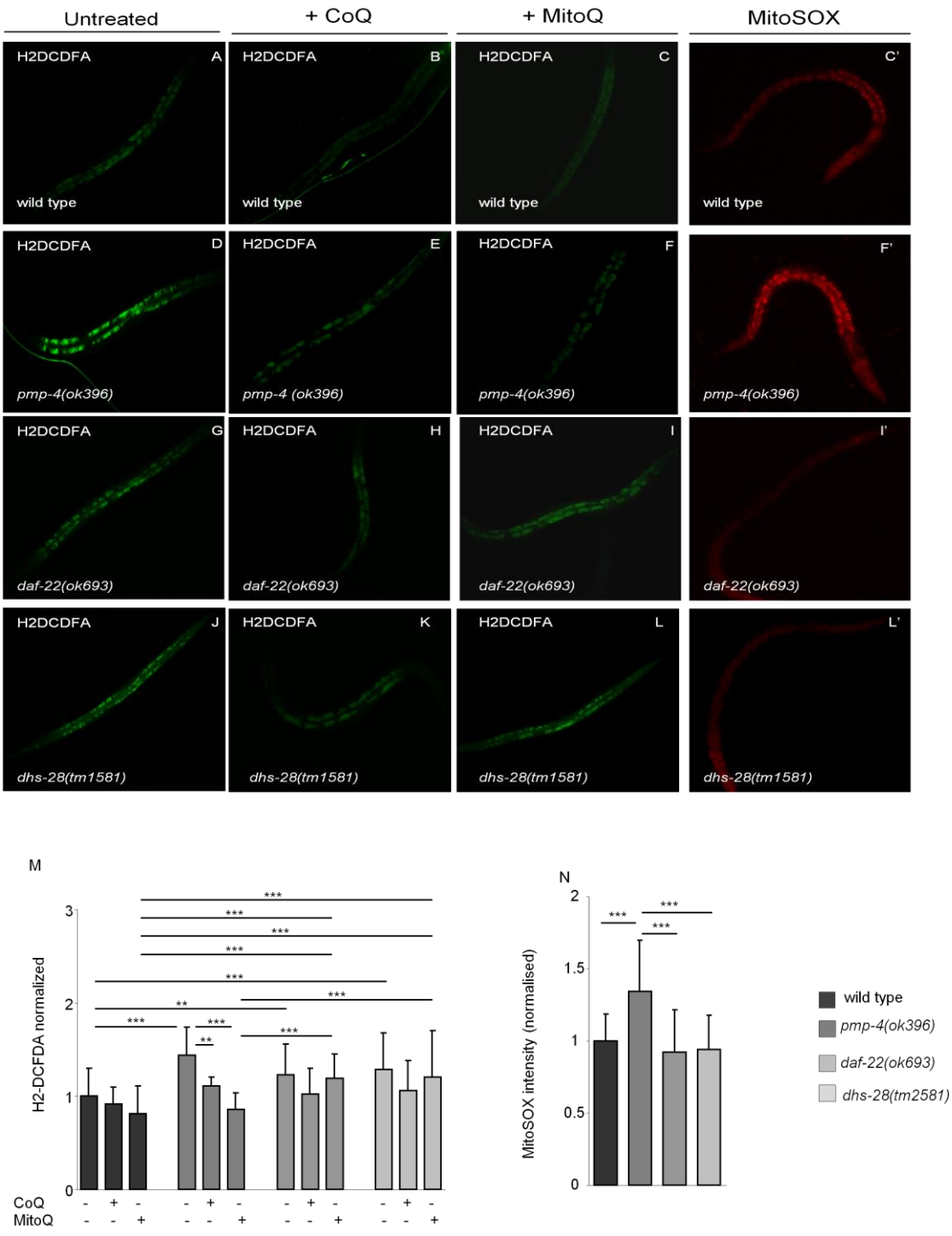

Fig R.7: The absence of the PMP-4 transporter, and not the intraperoxisomal enzymes, modulate the mitochondrial generation of ROS A,D,G,J: Untreated animals. Representative fluorescence images showing H2DCFDA staining indicative of ROS levels in living animals of the indicated genotypes. The intensity of the fluorescence is increased in all peroxisomal mutant animals. B, E, H, K: CoQ treatment. ROS levels are restored in all peroxisomal mutants analyzed. C, F, I, L: Mito Q treatment. The mitochondrial targeted drug MitoQ only rescued ROS

levels in *pmp-4(ok396)* mutant animals. C', F', I', L': The mitochondrial specific probe MitoSOX revealed increased in mitochondrial ROS only in *pmp-4(ok396)* mutant animals. M: Semi-quantitative analysis of the ROS levels measured by the fluorescent probe H2DCFDA and quantified as described in the methods (n = 50 animals per genotype. one way or two way ANOVA (without and with antioxidants), Tukey's post hoc; *** p<0.001, **p<0.01, * p<0.05). N. Quantitation of mitoSOX staining intensity, normalized to WT. N= 70 Statistics is One-Way Anova, post hoc Tukey's.

R.8 Mitochondrial stress reduces AWB neuron functionality

Given the strong generation of mitochondrial ROS in our *C. elegans* model of X-ALD together with the decreased AWB functionality, we hypothesized a mitochondrial ROS modulation also affecting AWB. To deeper investigate the effect of mitochondrial ROS in the AWB functionality, first wild type and *pmp-4* mutant animals were treated with the mitochondrial complex I inhibitor Paraquat (PQ) (200 µM) widely used as a redox cycler to stimulate superoxide production in mitochondria (Cochemé, 2009). PQ has been described an inhibitor of the mitochondrial complex I (Betarbet et al., 2000; Castello et al., 2007; Cocheme and Murphy, 2008). Treated animals were DiI stained as described before to evaluate the general chemo sensation function of the amphid organ. Surprisingly, only the AWB functionality was affected in wild type animals, whereas other neurons were also affected by the *pmp-4* mutation (Fig R.8: A'-B') and thus it seems to be the most sensitive neuron amongs the chemosensory neurons located in the amphid organ. To confirm the results obtained by exogenous ROS, the mitochondrial strains *nuo-1(ua1)* and *mev-1(kn1)* (representative mutants of complex I and complex II respectively) were similarly DiI stained. As shown in Figure R.8, all mitochondrial mutant animals were severely affected in comparison to their wild type counterparts (Fig R.8: C-E). In addition, the DiI abnormalities in the mitochondrial complex mutants were rescued when they were treated with the mitochondrial anti-oxidant MitoQ, thus confirming the role of mROS in the maintenance of AWB functionality but also other chemosensory neurons present in the amphid organ (Fig R.8: C'-E').

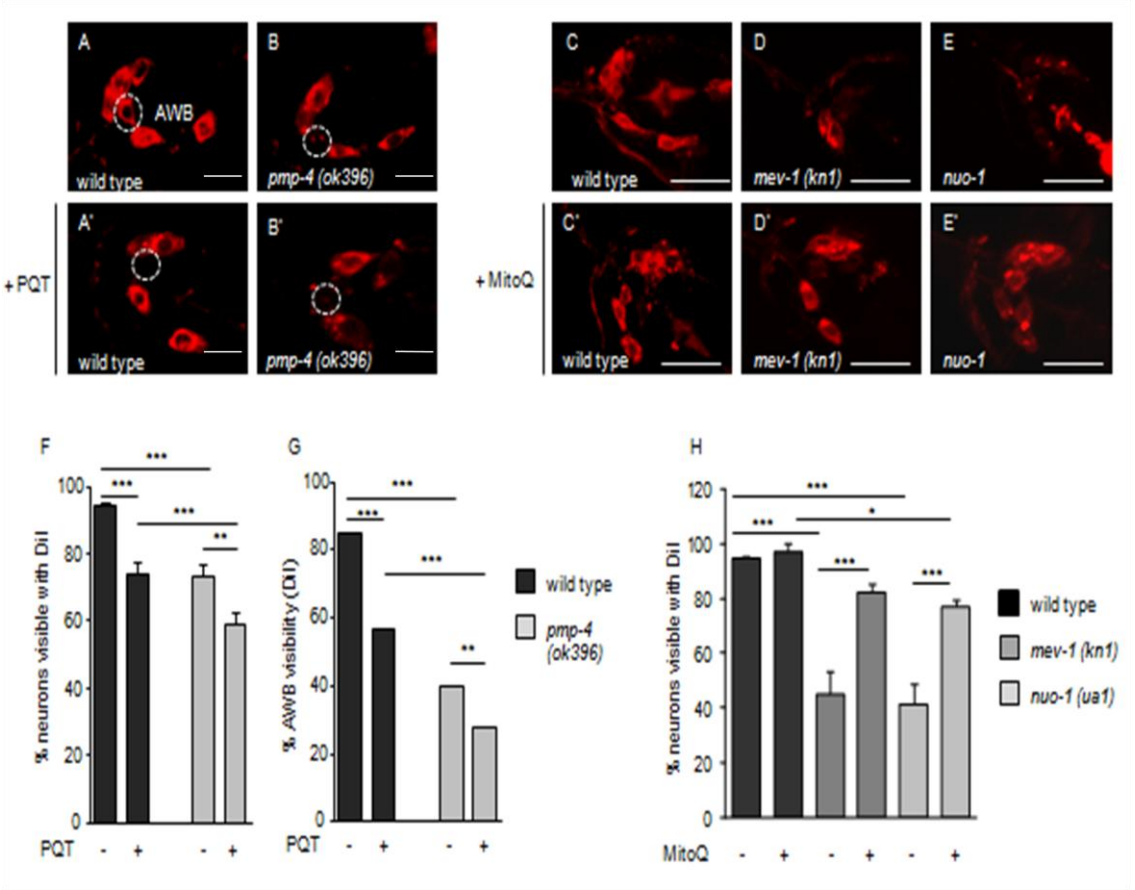

Fig R.8: The aversive behavior response is modulated by mitochondrial ROS A-B': wild type and *pmp-4(ok396)* animals were treated with the mitochondrial inhibitor Paraquat during 48 hours and the Dye filling capacity of the amphid organ was analyzed by DiI staining. A'-B': The AWB neuron is not DiI stained in any of the genotypes. C-E': Mutations in the mitochondrial ETC influences the AWB and the Dye filling capacity of the amphid organ. Mitochondrial mutant animals of the complex II and complex I, *mev-1(kn1)* and *nuo-1(ua1)* respectively, were defective in the dye filling capacity as showed by the DiI staining. C'-E': DiI staining abnormalities were rescued by the mitochondrial drug MitoQ. Scale bar is 10 µm. F: Bar graph representing the quantification of Dye filling defective neurons expressed in percentages without and with the presence of PQT G: Bar graph showing the percentage of worms in which the AWB neuron is not visible after DiI staining after PQT treatment. H: Bar graph representing the quantification of Dye filling defective neurons detected in the mitochondrial mutants *mev-1(kn1)* and *nuo-1(ua1)* and the corresponding rescue of the dye filling defect after MitoQ treatment. Number of animals is 30 per genotype and condition in all the experiments. F and G refer to figures A-B' and H refers to figures C-E'. Statistics in F and H is Two way ANOVA, Tukey's post hoc; whereas in G is F-Fishers. *** $p<0.001$, *$p<0.05$

R.8.1 AWB cilial morphology is disturbed by mitochondrial ROS

Similar results were obtained when using the AWB specific promoter *str-1Prom::gfp*. PQ treatment at 200 µM for 48 hours induced abnormalities in AWB cilia in both wild type and in *pmp-4* mutant animals which were reproduced by inhibiting RNAi complex I gene *nuo-1* (Fig R.8.1), henceforth proving that mitochondrial ROS is the main reason behind AWB´s disturbed cilial morphology.

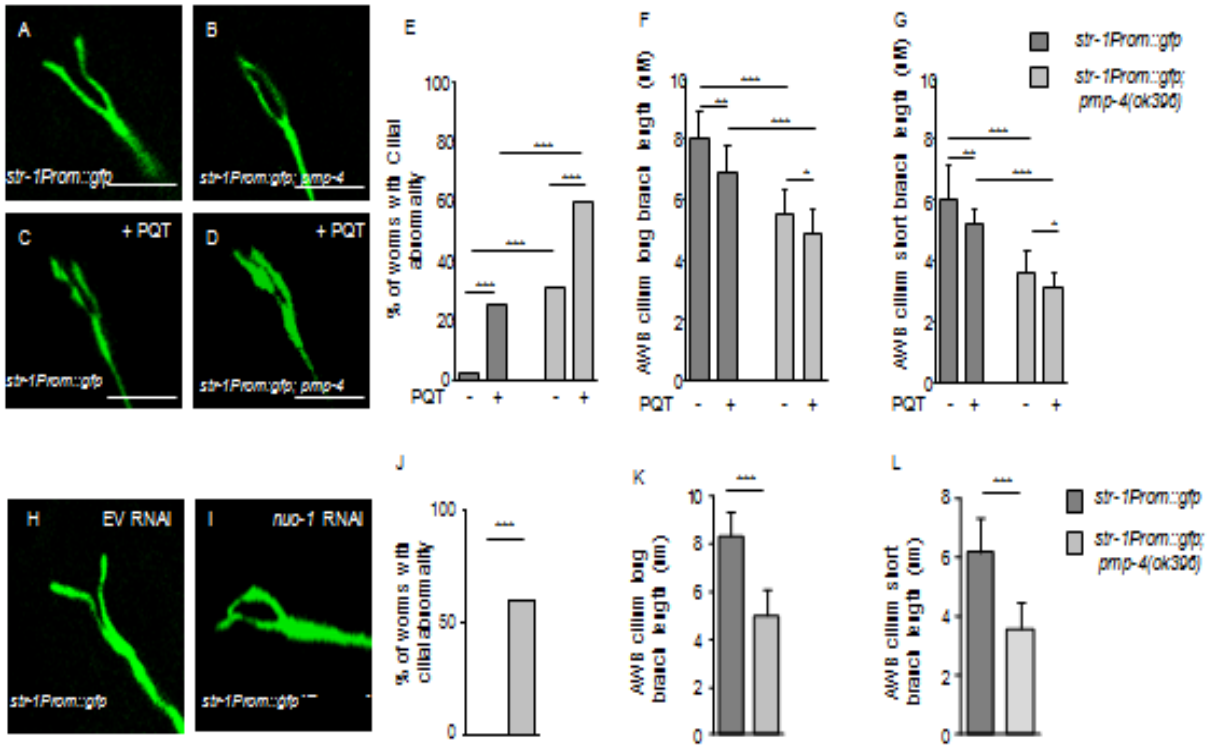

Fig R.8.1: Mitochondrial ROS disturb cilia morphology in AWB neurons A-G: Animals carrying the specific AWB reporter *str-1Prom::gfp* without and with the *pmp-4* mutation were treated with the mitochondrial inhibitor Paraquat (PQT) during 48 hours and the distal ends of the cilia were observed by confocal microscopy and measured by using the ImageJ software. A-D: Confocal pictures representative of the PQT influence at the indicated genotypes. E-G: Quantification of the cilia abnormalities as stated in the methodology. In F and G each bar represents the length of the short and long cilia respectively, expressed as average ± SD. H-L: RNAi knockdown of the ETC complex I component *nuo-1* resulted in increased cilia abnormalities. *C. elegans* strain *str-1Prom::gfp* incubated with RNAi against *nuo-1* was analyzed at L4 and the same strain was incubated with empty vector bacteria (EV) as a control for RNAi feeding. H-I are representative confocal pictures of control (EV) and *nuo-1* RNAi incubated strains respectively whereas J-L represent the quantitative analysis. Statistics for the

whole set of experiments is two-way ANOVA, post hoc Tukey's test in all experiments except in E and J, in which Fisher's test was applied. Data in F, G and K, L were analyzed as the mean ± S.D. Data in E and J represent the number of defective animals expressed in percentages. *** $p < 0.001$; ** $p < 0.01$ and * $p < 0.05$. For all this set of experiments n= 30 worms per animal and condition.

R.9 Mitochondrial ROS modulated AWB behavioral and morphological defect in *pmp-4* mutants but not in intra-peroxisomal mutants

The most affected neuron in PQ treated wild type animals and in the analyzed peroxisomal mutants is AWB. As widely described before, the most concomitant consequence of the *pmp-4/Abcd1/Abcd2* peroxisomal transporter disruption is the generation of mROS (Lopez Erauskin et al., 2013) thus pointing once more these radical species as main causative of AWB abnormalities. Nevertheless the generation of mROS by intra-peroxisomal disruptions remained unexplored thus opening the question of whether mROS were also causative of the amphid abnormalities detected in intra peroxisomal mutants and more generally, whether there exist a common mechanism of neurodegenration in peroxisomal diseases. To answer this question, the AWB functionality of the intra peroxisomal mutants *daf-22/thiolase* and *dhs-28/bi-functional* protein was extensively analyzed without and with the presence of antioxidants both, general and mitochondrial targeted.

Nematodes of the corresponding genotypes were treated separately with the two antioxidants CoQ (general antioxidant at 1000 µg/ml) and MitoQ (mitochondrial targeted at 5 µg/ml) and AWB the functionality and morphology was analyzed as widely described in the previous sections. AWB DiI staining and morphology was rescued in all CoQ treated animals. However, MitoQ treatment only rescued AWB abnormalities in *pmp-4* mutant animals (Fig R.9.1.A and R.9.1 A-J´). The AWB aversive behavior against 2-nonanol was rescued by MitoQ only in *pmp-4* mutant animals as well whereas CoQ rescued the AWB aversive behavior in all peroxisomal mutants tested (Fig R.9.B). Finally, MitoQ only rescued the AWB distal cilia morphology in *pmp-4* mutant animals but not in any of the intra peroxisomal mutants (Fig R.9.C-E and R.9.1.C-L´). Therefore the AWB abnormalities induced by alterations on the peroxisomal β-oxidation are not generated by the mitochondrial ROS, contrary to the

defects induced by the membrane located PMP-4, in which mitochondrial ROS are stated as a main ethiopatogenic cause of the X-ALD related phenotypes

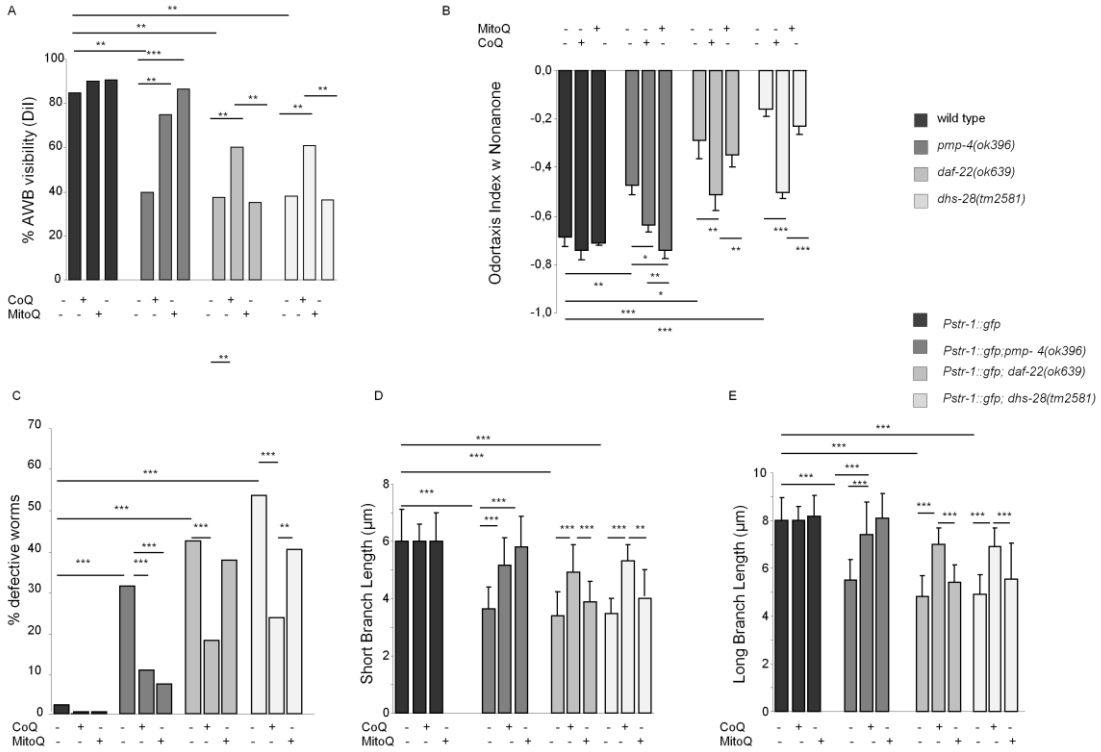

Fig R.9: MitoQ improves AWB neuron´s behavior and morphology in *pmp-4(ok396)* animals but fails in case of intra-peroxisomal mutants. Peroxisomal mutant animals together with their wild type counterparts were treated separately with the two antioxidants CoQ and MitoQ, and the capacity of the AWB behavior response was analyzed by the dye filling capacity or DiI staining (A), odor taxis index against nonanol (B) and by measuring the AWB cilial length (C-E). Shown are data from two or more experiments. Bar graphs in A and C represent the number of defective animals expressed in percentages and results were statistically analyzed by the Fisher's test. B, is the odortaxis index against nonanol and is represented as previously described and figures D-E represent the length of the AWB cilia, short and long branches respectively expressed in µm. Number of animals is between 30 and 50 per experiment and condition. Statistics in B, D, E is Two-way ANOVA Tukey's post hoc. *** p<0, 001; ** p<0, 01 and * p<0, 05

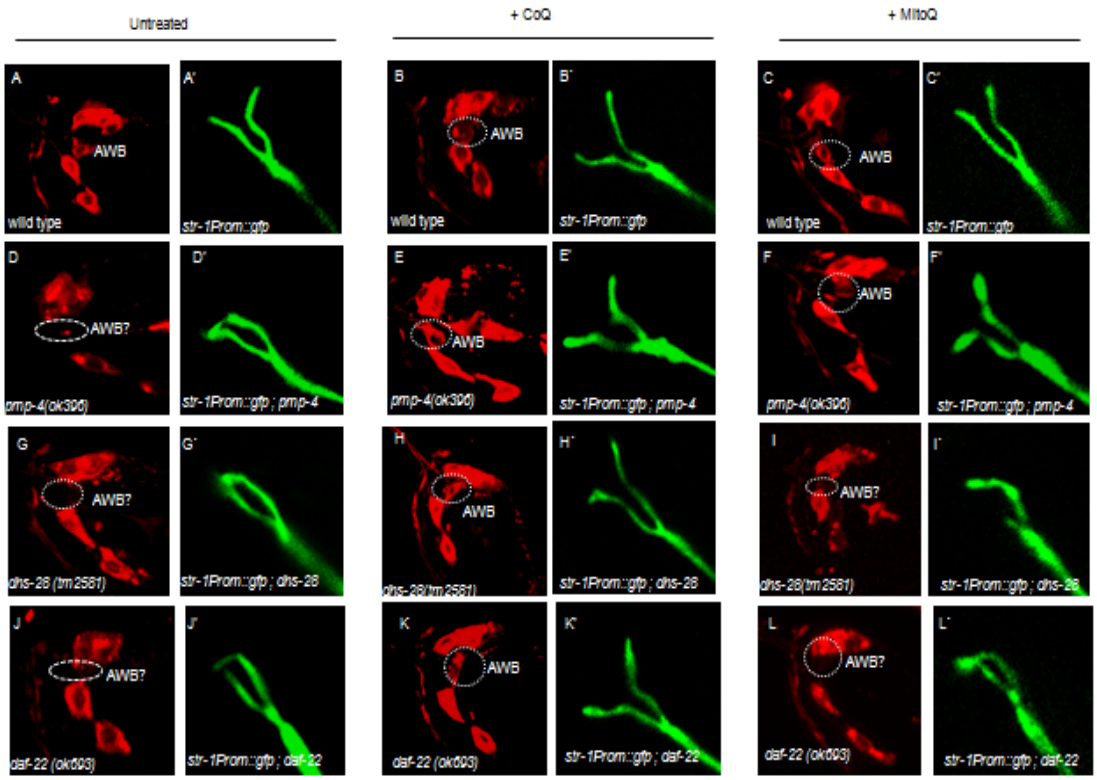

Fig R.9.1: The cross talk peroxisome – mitochondria is essential to modulate the AWB aversive behavior A, D, G, J: Confocal representative figures of the indicated genotypes showing DiI defects in all peroxisomal mutant animals tested. A', D', G', J': The same peroxisomal mutant animals are characterized by defects in cilial length. Only the distal parts of the cilia, in which the defects are described, are depicted. B, E, H, K: Treatment with the general antioxidant CoQ restored the DiI staining capacity in all the peroxisomal mutants tested. B', E', H', K': The cilial length is also restored in all peroxisomal mutants indicated after the CoQ treatment. C, F, I, L and C', F', I', L': The MitoQ treatment rescued both DiI staining and cilial length only in *pmp-4(ok396)* animals (F and F') and not in any of the intra-peroxisomal mutants indicated (I-I' and L-L'). Side views showing one of each neuron pair; anterior is left. N=30±5. Animals were grown at 20^0C. Scale bars: 10 µm.

R.10 Amphid associated functions are altered in peroxisomal β-oxidation mutants

AWB neuron is the most effected neuron in the amphid organ for the peroxisomal mutants (Fig R.4.2 and R.5). Apart from that the general functionality of the amphid organ is being affected. Six pairs of neurons in the head amphid sensory organs fill with the lipophilic dye DiI in wild-type animals. In the peroxisomal mutants, the AWB sensory neuron pairs in the amphid consistently failed to dye fill, and sometimes other neurons (like ASI, ASJ or ASH) exhibited weaker and variable dye filling in all the peroxisomal L4 animals observed (Fig R.10.A). Second, we used the food race assay (Baumeister et al., 2007), to demonstrate whether the worms are able to detect the odor of food with the help of amphid neurons. The peroxisomal mutants take longer time to detect and to reach the food than the wild type, with *dhs-28* mutant being the slowest (Fig R.10.B). Third, the osmosis assay, where we place the worms in high salt concentraion (500 mM) NGM plates and check their motility in due course of time (Calahorro et al., 2009). Where majority of wild types are motile till 8 minutes, the peroxisomal mutants lose their motility in less than 5 minutes (Fig R.10.C). Thus all these different chemo sensation assays prove that other sensory neurons apart from AWB can be affected and in general the amphid organ is defective in case of peroxisomal mutants with *dhs-28* being the most affected one.

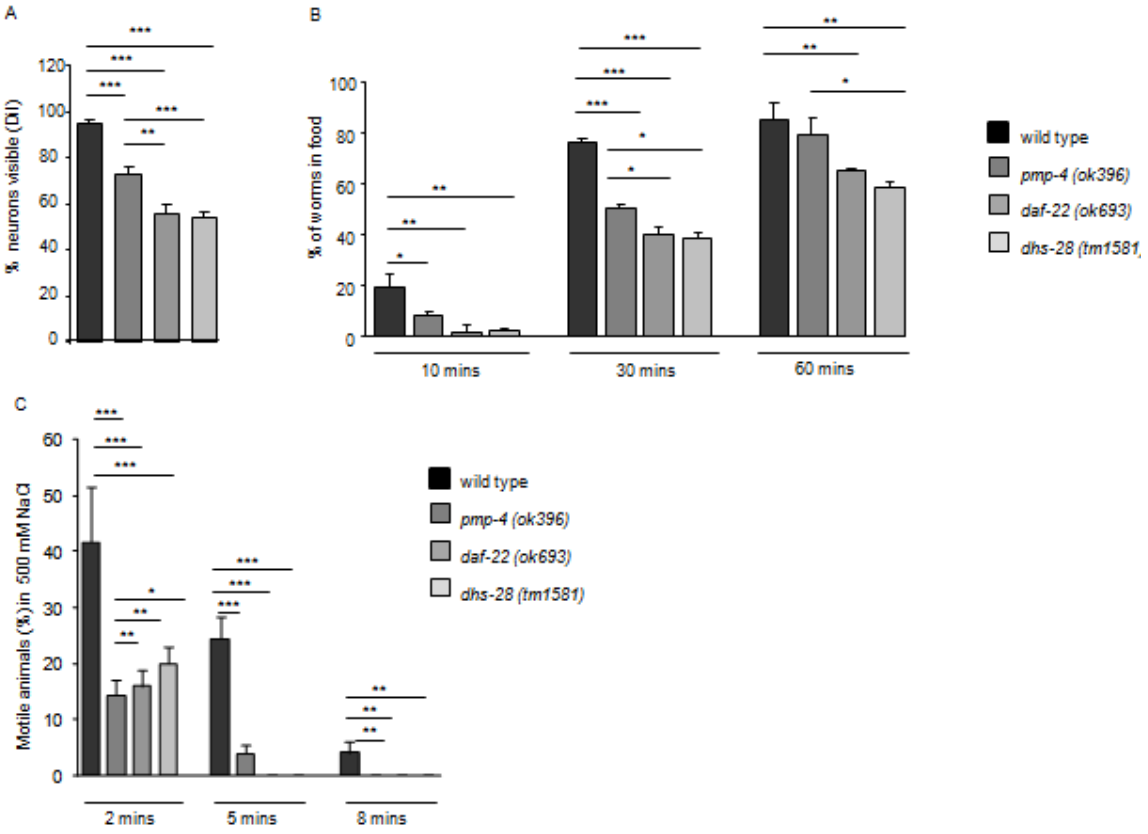

Fig R.10: Functionality of amphid organ in general is severely decreased in intra-peroxisomal β-oxidation mutants A: DiI staining. Bar graph showing the increase in dye filling abnormalities associated to peroxisomal β-oxidation mutants. N= 50. B: Food race assay. Bar graph showing the peroxisomal mutants takes longer time to reach the food. N= 100. C: Osmosis assay. Bar graph showing the peroxisomal mutants becomes immotile earlier than wild type. N= 50. Each experiment was repeated three times with Tukey's post hoc; *** $p<0.001$, **$p<0.01$, * $p<0.05$.

DISCUSSION

D. Discussion:

In the recent years big efforts have been made in the field of neurodegenerative diseases, X-linked adrenoleukodystrophy among them; in order to identify the molecular mechanisms leading to axonal damage. This thesis using *C. elegans* as the nematode model organism provides robust evidence that X-ALD, despite being a neurodegenerative disorder of peroxisomal origin, shows an impairment of mitochondrial complexes and mitochondrial dysfunction, which in its turn underlies axonal degeneration and thus can be considered as a mitochondrial disease. Moreover this work uncovers the therapeutic potential of cellular more specifically mitochondrial anti-oxidant for the treatment of this incurable disease.

In general, the *C. elegans* model provides an excellent tool to study this disease owing to its short life span, easy maintenance and availability of knockout strains. PMP4 is the homologue of human ABCD1, and is the common ancestor of ABCD1 (ALDP) and ABCD2 (ALDRP). *pmp-4 (ok396)* mutant associated phenotypes characterized in this thesis reproduces the main X-ALD phenotypes including the early onset of the main hallmarks. Thus this model has been a more advantageous tool in comparison to the existing mice models, *Abcd1*$^{-}$ and double *Abcd1*$^{-}$*/Abcd2*$^{-}$ mutant animals, in which the symptoms started at 22 and 12 months respectively (Pujol et al., 2002; Pujol et al., 2004). Apart from the X-ALD specific phenotypes, we have discovered that the peroxisomal mutant worms are not only defective in AWB chemosensory neuron cilia structural integrity but also in some cilia-mediated sensory behaviour suggesting that *C. elegans´* chemosensation might provide a novel setting for exploring peroxisomal disease related disorders.

D.1. *pmp-4(ok396)* mutant worms provide a new novel model for the investigation of human X-ALD

D.1.1. Oxidative stress and mitochondrial impairment

Main lines of evidence indicated that oxidative stress and mitochondrial impairment are important phenotypes characterizing the X-ALD disease in both humans and mice. After the initial characterisation of *pmp-4 (ok396)* mutant worms in our laboratory, we investigated whether the observed X-ALD phenotypes were reproduced in this

knockout *C. elegans* strain. With the combination of different dyes *in vivo* and the use of antioxidants, we demonstrated *in vivo* that *pmp-4* mutant animals displayed higher levels of ROS compared to wild types mainly originating from the mitochondria. This is in concomitant with the previous results obtained in X-ALD fibroblasts, in which high mitochondrial ROS levels were detected in cells when exposed to an excess of C26:0 (Lopez-Erauskin et al., 2013). Collectively all these data suggest that also in *C. elegans* and in mammals, the PMP4/ABCD1 deletion causes higher production of cellular ROS, mainly from mitochondrial, leading to oxidative stress.

In addition mitochondrial sensitivity to ROS in our *C. elegans* model of X-ALD were also demonstrated with the treatment of different mitochondrial complex inhibitors such as paraquat (for complex I), antimycin-A (for complex II), sodium azide (for complex IV). In all the cases *pmp-4 (ok396)* worms were highly sensitive as compared to wild types. Chemical inhibitors of the ETC can also produce symptoms reminiscent of neurodegenerative diseases (Miller et al., 2010). Genetic mutations linked to neurodegenerative diseases have been shown to disrupt the mitochondrial electron transport chain (ETC), the major pathway producing the cellular energy. Thus our data are in accordance with other major human neurodegenerative diseases including amyotrophic lateral sclerosis (ALS), Alzheimer´s disease (AD), Parkinson´s disease (PD) and Huntington´s disease (HD) in where mitochondrial dysfunction, selective neuronal vulnerability and progressive onset are the unifying features. Therefore our experimental model is highly useful for studying neurodegenerative diseases that are linked to oxidative stress and defective mitochondrial function.

D.1.2. Axonal damage in *C. elegans* model of X-ALD is rescued with antioxidants

It has been demonstrated in humans and mice (spinal cord, peripheral nerves or brain white matter) that X-ALD is a disease that affects axons (Galea et al., 2012). *pmp-4 (ok396)* mutant worms displayed a neurological phenotype as well, including morphological and behavioural defects in comparison to their wild type counterparts. Likewise at early stage of development, before the adulthood (L4) the percentage of axonal damages was higher in *pmp-4 (ok396)* worms. Axonal abnormalities increased severely as the worms aged (L4+7d) thus suggesting a degenerative process as cause of axonal defects. In our *C. elegans* model of X-ALD we demonstrated that axonal abnormalities are caused by cellular oxidative stress majorly coming from mitochondria. First we demonstrated the rescue of axonal abnormalities by the

lipophilic antioxidant Coenzyme Q (CoQ). CoQ being lipophilic, acts as an antioxidant in both mitochondrial and lipid membranes. Second, we evidence the effect of mitochondrial ROS on axonal morphology by rescuing the axonal abnormalities with MitoQ, acting specifically into mitochondria and separately, by knocking down the mitochondrial complex I *nuo-1,* thus confirming the role of mitochondrial ROS in the maintenance of axonal morphology suggested by (Earls et al., 2010) and previously postulated in the X-ALD existing models (Lopez-Erauskin et al., 2011). Collectively these data reveal that axonal damages are implication of cellular ROS more specifically mitochondrial ROS. Thus MitoQ provides an excellent therapeutic potential for oxidative stress-associated neurodegenerative disorders, particularly X-ALD.

D.2. Mitochondrial ROS regulation of the chemosensation in the *C. elegans* model of X-ALD

The nervous system of the *C. elegans* consists of 302 neurons and 50 glial-like cells associated with the sensory organ. The glial-like cells ensheath neurons forming channels through which dendrites are threaded (Shaham et al., 2008). Since these glial-like cells are mainly adjacent to the chemosensory neurons, concreted in the amphid organ, we used this chemosensory amphid organ as readout for detecting damages concretely related to these cells and neurons. We didn't observed morphological differences in glia-like cells, thus we investigated the functionality of the chemosensory neurons embedded in the amphid organ.

D.2.1 *pmp-4* mutation affects functions of AWB chemosensory neuron but the neuron-sheath cell interactions are unaffected

Our results suggest that PMP-4 regulate AWB sensory cilia morphology and function in *C. elegans.* This conclusion is based on several experimental evidences. First, AWB neuron of *pmp-4* mutants fails to take up the lipophilic dye, DiI. Second, cilial branch lengths of *pmp-4* mutants´ AWB neuron are significantly shorter than those of wild types. Third, introduction of wild type copy of PMP4 in *pmp-4 (ok396)* worms rescues both the observed phenotypes. These results are most consistent with the hypothesis that PMP-4 regulates AWB cilia. Finally, it is interesting to speculate on the cell-specific

nature of *pmp-4* mutant phenotypes. In majority cases, only AWB neuron fails to dye fill in *pmp-4* mutants. This cell type specificity might reflect distinct mechanisms by which axonal morphology and membrane growth are coordinated in different neuron types, as well as the distinct ultra structures and membrane compositions of functionality and morphologically distinct cilia (Sengupta et al., 2013; Pigino et al., 2012). Thus, multiple molecular mechanisms might be employed in a combinatorial manner, both in an individual neuron as well as across different neuron types, to regulate the dynamic remodelling of cilia morphology. Alternatively, the regulation of cilia structure might represent a diverged function for these proteins in invertebrates (Sengupta et al., 2013). Proper amphid glia formation has been shown to be required for cilia formation and function of some of the amphid neurons (Lyman-Gingerich et al., 2014). Nevertheless, we didn't find any significant difference between wild type and *pmp-4* mutant worms in the terms of matrix filled vesicles in the amphid sheath cells (Fig. R.4.4). Thus, at the larval stage 4 (L4) the mutant phenotypes observed in *pmp-4 (ok396)* animals are likely to be the result of AWB cilia dysfunction and not due to perturbation of cilia-sheath cell interactions. It should be interesting to check the glial cell morphology at older stages of worms as it has been reported that as the animal age, small vacuoles begin to build-up within the sheath cells of the wild type animals and it approaches 100% at 7 days post L4 stage (Lyman-Gingerich et al., 2014).

D.2.2 Intra-peroxisomal mutants show chemosensation defects via regulation of different kinds of cellular ROS

In nature, *C elegans* are soil-dwelling and depend on a relatively simple nervous system of 302 neurons to identify, integrate and respond to the complex array of chemicals present in order to find food and avoid toxins. Distinct subsets of neurons mediate responses to aversive and attractive odors: the AWA and AWC neurons detect attractive odors while the ASH, ADL, AWB and ASK neurons detect aversive odors (Lyman-Gingerich et al., 2014). The peroxisomal mutants don't respond normally like wild type animals to the volatile repulsive odorants 2-nonanol and 1-octanol with *dhs-28 (tm2581)* being the least responsive, but respond normally to the attractant, diacetyl. The different behavioural responses to the volatile odorants may be due to altered overall perception of specific chemicals or an inability to finely map changing concentrations of the chemicals over time (Lyman-Gingerich et al., 2014). Furthermore

the number of neurons stained with the dye DiI is comparatively much lesser in the peroxisomal mutant worms as compared to the wild types (Fig R.10.A). Thus it is highly possible that the observed chemosensory behaviour defects and the amphid dye-filing defects detected in these peroxisomal mutants might be interrelated (Doroquez et al., 2014). Interestingly both these defects have been rescued successfully by the general cellular anti-oxidant CoQ and even better with mitochondria-targeted anti-oxidant, MitoQ, this latter only in *pmp-4* mutant worms. Accordingly higher mitochondrial ROS might be the primary reason behind *pmp-4 (ok396)* worms AWB neuron dysfunctionality. Nevertheless in case of intra peroxisomal mutants although CoQ is able to rescue the observed defects, MitoQ fails in doing so. Consequently concluding there is no peroxisomal leakage of ROS that can affect the mitochondria of *daf-22 (ok693)* and *dhs-28 (tm2581)* animals. Our findings suggest that mitochondrial ROS are responsible for the amphid phenotypes observed in *pmp-4* mutants but not in the case of *daf-22* and *dhs-28* mutant animals. In future, further advances in cilia imaging techniques and examination of other chemosensory neurons´ cilia may allow the description not only of how these structures are formed, but how their morphologies shape and neuronal functions in peroxisomal mutant animals. Also it has been demonstrated that the relatively subtle ciliary defects from mutations affect specific sensory behaviors under defined environmental conditions and genetic backgrounds and have significant consequences for animal survival and fitness (Sengupta et al., 2013; Huang et al., 2011). So it should be interesting for our research to investigate whether this genetic mutations resulting in production of cellular ROS which in turn affects the chemosensory neurons involved in other aspects of worms behavior like social feeding, memory and learning, mating.

CONCLUSIONS

Conclusions:

Based on the objectives outlined before, the conclusions of the present dissertation can be listed as below:

1. The lack of PMP-4 in worms causes lipid accumulation, increased oxidative stress, mitochondria impairment, higher production of ROS, locomotor impairment and axonal degeneration in *C. elegans,* reproducing the main X-ALD phenotypes found in humans and mice, thus providing a new *in vivo* model to deeper investigate X-ALD. Importantly, drug and genetic screenings will be applied to this model to study in detail candidate drugs and genes fighting against this fatal disease.

2. The prevention of axonal damage upon treatments with anti-oxidants provides the proof of concept that cellular ROS, mainly mitochondrial, underlies axonal degeneration in X-ALD. Treatment with mitochondria targeted anti-oxidant neutralizes oxidative damage, prevents locomotor defects and axonal degeneration by decreasing mitochondrial ROS production. These results uncover a novel molecular mechanism of action of this anti-oxidant in the nervous system. It also paves the way for the use of mitochondrial booster / anti-oxidant in clinical trials with AMN or other axonopathies in which oxidative stress and mitochondrial dysfunction are contributing factors.

3. Peroxisomal mutants (*pmp-4(ok396)*, *daf-22(ok693)* and *dhs-28(tm2581*)) present chemosensation defects; specifically the AWB amphid neuron morphology is hampered and is dysfunctional resulting in the inability to take up lipophilic dyes and showing defects in volatile odor sensation. This new line of investigation for the first time has linked the peroxisomal genes with the chemosensation and providing different therapeutical approaches for treating peroxisomal diseases.

4. Mitochondrial ROS are the specific contributors to the modulation of the AWB neuron functionality regulated by *pmp-4*. Nevertheless, AWB chemosensation is modulated by other types of ROS in intra-peroxisomal mutants. Therefore suggesting that there is no ROS leakage from the peroxisome of the intra-peroxisomal mutants which can affect its mitochondria.

MATERIALS & METHODS

M. Materials and Methods:

M.1 Media and buffers

Strains are maintained on Nematode Growth Medium (NGM) agar plates seeded with a lawn of *E. coli* (Strain: OP50). *E. coli* OP50 is a uracil auxotroph whose growth is limited on NGM plates. *C. elegans* stocks can best be maintained between 15°C and 25°C, most typically at 20°C. M9 and S-basal buffers are used to harvest and to wash the populations. For transferring or picking of worms, a worm picker (width 0.2mm, length 1.5cm approximately) is made with a platinum wire placed in a glass Pasteur pipette and then fixed by melting the tip of the pipette in the flame of a Bunsen burner.

M.1.1 Preparation of NGM plates:

Bacto agar (g)	17
NaCl (g)	3
Bacto peptone (g)	2.5
dH_2O (ml)	977.5
(Autoclave)	
Kalium phosphate buffer 1M pH 6.0 (ml)	25
$CaCl_2$ (ml)	1
$MgSO_4$ (ml)	1
Cholesterol (5 mg/ml in Ethanol) (ml)	1

M.1.2 Kalium phosphate buffer 1M:

KH_2PO_4 (g)	108.3	
K_2HPO_4 (g)	35.6	
dH_2O (ml)	upto 1L	(Autoclave)

M.1.3 1X M9 buffer:

KH_2PO_4 (g)	3
Na_2HPO_4	6
NaCl	5

dH_2O (ml)	upto 1L	(Autoclave)
$MgSO_4$ (1M) (ml)	1	

M.1.4 S basal buffer:

KH_2PO_4 (g)	6	
K_2HPO_4	1	
NaCl	5.85	
dH_2O (ml)	upto 1L	(Autoclave)
Cholesterol (ml)	1	

M.1.5 Luria-Bertani (LB) medium:

NaCl (g)	10	
Tryptone (g)	10	
Yeast extract (g)	5	
dH_2O (ml)	upto 1L	(Autoclave)

M.1.6 Luria-Bertani (LB) agar:

NaCl (g)	10	
Tryptone (g)	10	
Yeast extract (g)	5	
Bacto agar (g)	5	
dH_2O (ml)	upto 1L	(Autoclave)

M.2 Worm strains and maintenance

Deletion strains are ordered from the *C. elegans* Genetics center (CGC, Minneapolis, USA) which provides knockout strains to scientists performing research using *C. elegans*. The strains that are used in the research are listed below:

Strain	Name	Source
wild-type	N2	CGC
pmp-4(ok396)	RB675	CGC
daf-22(ok693)	RB859	CGC
dhs-28(tm2581)	VS8	CGC
hjIs67 Is[Patgl-1::atgl-1::GFP ::(unc-54)3'UTR + Pmec-7::RFP]	VS20	CGC
juIs76 Is[Punc-25::GFP ::(unc-54)3'UTR + lin-15(+)]	CZ1200	CGC
muls32[Pmec-7::GFP + lin-15(+)];lin-15B(n765)X	CF702	CGC
kyIs104 [str-1p::GFP]	CX3553	CGC
mev-1(kn1)	TK22	CGC
nuo-1(ua1)	LB10	CGC
nsIs105 Is[Phlh-17::gfp::(unc-54)3'UTR]	OS1914	Shai Shaham (Rockefeller University, NY)
oyIs44 Is[odr-1pro: RFP, lin-15(+)]; nsEx1153 Is [F16F9.3pro::mCherry, itr-1pro:: CFP + rol-6(su1006)]	CHB28	Maxwell Heiman (Harvard Medical School, MA)

For the creation of new strains in lab, males were generated and employed for crossing. To achieve a successful mating, several males were placed with a single hermaphrodite on a small plate (35 mm diameter) seeded with a small drop of OP50 at the center.

M.2.1 Generation of males:

- Transfer L4 hermaphrodites to NGM plates seeded with OP50 (6 medium plates with 10 worms each)
- Heat shock at 32^0C for 5 hours
- Transfer those plates to 20^0C
- Some males should be found in the F1 progeny

M.2.2 Preparing synchronize *C. elegans* worms or cleaning contaminated *C. elegans* stock by household bleaching method:

- Use *C. elegans* plates that have many gravid hermaphrodites. Wash the plates with sterile water and the collect the liquid and worms in a sterile 15ml falcon.
- Centrifuge for 1min at 1300g to have a pellet of worms.
- Aspirate to 500µl and add water to total of 4ml.
- Mix 0.5ml 5N NaOH with 1ml bleach and add to the falcon with worms.
- Shake well and vortex for every 2mins for a total of 10mins.
- Centrifuge for 1 min and aspirate till 500µl. Add M9 till 5 ml and repeat this step for one more time.
- Transfer the eggs to another falcon and put M9 till 1ml.
- Rotate the falcon overnight at 20^0C for the eggs to hatch and then to get arrested at L1 stage.
- Next day transfer the L1 s to NGM plate with OP50.

M.2.3 Freezing of *C. elegans* stocks:

- Collect freshly starved L1-L2 animals in 0.6ml of S buffer.
- Add an equal volume of S buffer + 30% glycerin. Mix well.
- Aliquot 1 ml of this mixture into 1.8ml cryovials labeled with the strain name and the date of freezing.
- Place the cryovials into small Styrofoam box and keep the box at -80^0C.
- Following day, thaw one vial to check whether the worms survived the freezing.

M.2.4 Recovery of frozen *C. elegans* stocks:

- Remove a frozen vial from -80^{0}C freezer and allow it to thaw at room temperature until all ice has melted to liquid.
- Pour the contents of the vial into one large NGM plate seeded with OP50 and labeled with the strain name.
- Transfer the plate at 20^{0}C after the liquid has dried up.
- After 2 days, transfer the surviving worms into fresh seeded NGM plates and let them reproduce for one generation and score the progeny for correct phenotypes.

M.3 Genotyping of mutant alleles:

M.3.1 Worm lysate preparation

To confirm genotypes, genomic DNA is extracted using a standard protocol. In brief, I collected the worms to be genotyped in 25µl of lysis buffer (95 µL of PCR buffer + 5 µL of 20mg/mL proteinase K, Roche, Manheim, Germany) in small PCR tubes (0.2ml Cultek, Madrid, Spain). After checking that the worms are placed in the tube or not under stereo microscope, I placed the PCR tubes at -80^{0}C for 20 minutes. The tubes are then placed in a PCR machine and a program with the following parameters is run:

Step 1: 65°C 4hours

Step 2: 95°C 15minutes

Step 3: 4°C forever

The single freeze thaw cycle cracks the tough worm cuticle and the 2X Proteinase K buffer lyses the worms, digests the proteins therein. The incubation at 95°C inactivates Proteinase K. The samples are then used immediately or stored in -20^{0}C for future PCR analysis.

M.3.2 PCR Amplification

Polymerase chain reaction (PCR) is performed using 3µl of crude genomic DNA extract.

Primers used to amplify the deletion region in *pmp-4(ok396)* include:

ok396_left flank
5´- TCGGTAATCCCTTGTCTTCTC-3´
ok396_deletion
5´- ACTCCGAAGCCGATGAAATT-3´
ok396_right flank
5´- CGGAGGTCATCAGGTTTGTT-3´

The wild type band sizes that I was expecting for the *pmp-4* were 1000bp and 300bp and the mutant band size was 200bp.

M.3.2.1 Master Mix:

10X Reaction buffer (µl)	2.5
2.5mM dNTP (µl)	1
Taq Polymerase (50U/µl) (µl)	0.2
Primer fwd (µl)	1
Primer rev (µl)	1
Primer del (µl)	1
DNA template (µl)	3
dH_20 (µl)	15.3
Total volume (µl)	25

M.3.2.2 PCR parameters: Program Name: ok396

Step 1: 94^0C for 5mins (Initial Denaturation)

Step 2: 94^0C for 30secs (Denaturation)

Step 3: 55^0C for 60secs (Annealing)

Step 4: 72^0C for 1min (Elongation)

Step 5: 72^0C for 3mins (Final Elongation)

Step 6: GOTO step 2 30 cycles

Step 7: 72^0C for 15mins

Step 8: 10^0C Forever

Step 9: End

The PCR tubes are then stored in 4^0C for subsequent agarose gel run at 2%.

Primers used to amplify the deletion region in *daf-22 (ok693)* include:

5' ACAATCGGTGTGTCCGGCCC 3' (forward)

5' AGCCGGCTCCGATGACGGCT 3' (reverse)

5' ATGGCGGGAAATGGGTGATCA 3' (inner)

With these set of primers we obtain two bands in wt (1400bp and 400bp) and one band in the mutant (700bp).

Primers used to amplify the deletion region in *dhs-28(tm2581)* include:

5´ TGTATGTCACGAGTGGGGT 3´ (Out Rvs)

5´ GAATCGACTCGAGTGTACCG 3´ (Out Fwd)

With these set of primers we obtain one band of 1100bp in wt and one band of 300 bp in the mutant. For this PCR reaction with two primers, one primer will be deduced at a 1µl volume and thus increasing the volume of water to 16.3µl.

PCR reactions were performed according to the annealing temperature and the elongation time which depends upon the Tm (melting temperature) of the primers and the length of the amplicon respectively. The annealing temperature was 64^0C and 53^0C for *daf-22* and *dhs-28* PCR reactions respectively. And, the elongation time was 2mins and 1min for *daf-22* and *dhs-28* PCR reactions respectively.

M.4 RNA-mediated by interference (RNAi)

RNAi by feeding

RNAi feeding libraries: out of the two different RNAi libraries (Julie Ahringer and Marc Vidal) that exist and cover together 94% of the *C. elegans* genome, we used the former one. Ahringer group developed a library under the usage of genomic DNA fragments that were amplified by PCR. Fragments encoding the gene of interest were cloned into the vector L4440 and transformed into the bacterial strain HT115. This *E. coli* strain allows accumulation of large quantities of ds RNA in the cell as it lacks functional RNAase III. Also the ¨ORFeome¨library employs HT115 as bacterial host strain for the L4440 vector. So the expression of the insert is controlled by a promoter inducible by IPTG (Isopropyl β-D-1-thiogalactopyranoside) which must be added to the RNAi plates.

RNAi clones: from wormbase, position of the desired clone in the RNAi feeding library was spotted. Streaking of the intended clone was done on a LB-Ampicillin plate (50µg/ml) and incubated overnight at 37^0C. Next day, single colony PCR was done using primers flanking the multiple cloning sites of the inserts to confirm that the insert had the expected length or not. For final validation, mini prep of the bacterial DNA was performed using QIAprep Spin Miniprep Kit (Qiagen, Hilden, Germany) and sent for sequencing to StabVida, Caparica, Portugal.

RNAi plates preparation: standard 1litre NGM agar was prepared as mentioned before. After cooling down and addition of respective chemicals, following were added –

Ampicilin (50 mg/ml) (ml)	1
IPTG (3 mM) (ml)	1

The plates were generally poured 5 days before seeding to allow them to dry at room temperature. In between, single colonies of the respective RNAi clones were inoculated in 5ml LB medium containing 50µg/ml ampicilin and allowed to grow at 37^0C o/n. If the plates are ready, the culture were seeded on them and allowed to grow for 24h at RT. The seeded plates were used immediately or stored at 4^0C in dark for future use.

Worm preparation: worms were synchronized by bleaching protocol as mentioned before. Once the desired stage is reached, they were transferred to the RNAi plates for the actual experiment. It is critical to remove OP50 as residual non-RNAi bacterial which can interfere with the feeding results.

M.5 Phenotypic analysis assays

M.5.1 Egg-laying assays

L4 larvae were placed on plates with food and allowed to mature at 20°C overnight to become young adults. Hermaphrodites with one full row of eggs in their gonads (10-15 eggs) were used in all assays. 10 adults were move to medium plates that contained 200µl of OP50 as food. The worms were allowed to lay eggs at 20°C for 3 days. The number of eggs was counted after every 24 hours and the results are expressed as the mean number of eggs laid per animal (Thomas et al., 1995).

M.5.2 Brood size assays

L4 hermaphrodites were placed into the plates and grown for 24 hours. Thereafter, the mothers were transferred to new plates daily until the mother either stopped producing offspring or died (maximum 4 days). The progeny of the previous plate were counted the next day. The number of progeny from the various plates was added up to give the final brood size. The experiment was conducted at 20^0C (Schafer et al., 2004).

M.5.3 Life span analysis

10L4 worms were transferred to a small individual NGM plate with OP50 with a total 10 plates. Each day they were transferred to new plates to avoid mixing of populations until the mother stopped producing offspring. Simultaneously the mothers were counted and if dead are noted along with the worms that escaped from the plate. The experiment was conducted at three different temperatures of 15°C, 20°C and 25°C and until all the worms died (Matt et al., 2009).

M.5.4 Larval developmental assay

Synchronized mothers were egg laid on 4-5 prepared plates for no more than 3 hours. Then they were heat killed. Development of the eggs was monitored after 72 hours at 20°C. Stages of the worms that were observed in these plates were noted (Kunzler et al., 2010).

M.5.5 Dauer Assay

10 L4 staged worms per small plate were grown on food (50µl of OP50) at 20°C and were allowed to lay eggs continuously. Dauers in the case of wild type and *pmp-4* mutant animals were counted after 6 days, whereas in case of *daf-22* mutant animals it took 48 hours more for the plate to get starved. After the mentioned days, the plates were flooded with 1% SDS (Merck, Darmstadt, Germany) and scored after 30 min for the presence of dauers (live thrashing animals) (Thomas et al., 2010).

M.5.6 swimming (thrashing) assays

A drop of 2% agarose (ultraPURE® agarose, Invitrogen, Carlsbad, CA, USA) is poured over the glass slide and allowed to dry and then 20µl of M9 is poured on it. Age-synchronized animals (treated and untreated) were picked to that drop of M9 buffer and left for adaptation for 2mins. Every other thrash was counted for 30 s and then multiplied by four to obtain an estimate per minute. A single thrash was defined as a complete change in the direction of the body down the midline. Animals that were motionless for 10 s were discarded from the analysis (Horwich et al., 2009).

M.5.7 Locomotion (body bend) assays

Age-synchronized young adults were placed on unseeded NGM plates and allowed to acclimatize for 5–10 min. This short period is essential because well-fed wild-type *C. elegans* tend to show frequent directional switching immediately post-transferral. The number of body bends was counted for 30 s and multiplied by 2 to obtain an estimate per minute. A complete body bend was defined as the bending of the head region across the central-line of the animal, in which a full sinusoid was completed. For the quantification of body bends of worms on seeded plate same technique was applied with the exception that worms were plated on the centre of the OP50 lawn and then their movement was noted (Sattelle et al., 2009).

M.5.8 Measurement of locomotor activity using infrared locomotor tracking system

This assay replaces the manual assay with an alternative, less direct method of estimating thrashing frequency. L4 worms were transferred to a 96-well microplate containing 10µl of M9. The detection of activity is based on infrared microbeam interruptions. This microbeam crosses a microhole array within an acrylic filter, passes

through the worm receptacle and is finally sensed by a phototransistor. When worms move across the light beam, a transient fluctuation in the signal received by the phototransistor is generated; movement is detected by digital analysis of the phototransistor output (Golombek et al., 2009).

M.6 Oxidative Stress assays

The list of inhibitors that we used to treat the *C. elegans* for further understanding the relation between inhibition of electron transport at each complex and oxidative stress are listed below:

Complex Inhibited	Complex Inhibitor
I	PARAQUAT
II	3-NP & TTFA
III	ANTIMYCIN-A
IV	SODIUM AZIDE

M.6.1 Larval Lethality in the presence of paraquat

Paraquat was purchased from Sigma (St. Louis, USA) in powder form. To generate the concentration series of paraquat, a stock of 389 mM paraquat was made by adding 1 ml of distilled water. From this stock at the appropriate dilutions, were added to autoclaved and cooled NGM agar medium. The plates were allowed to dry overnight and were seeded with OP50 the next day. In between, L1 larvae were cultured on normal seeded NGM agar plates. After 45 hours at 20°C, when the animals reach L4 stage they are transferred to other seeded NGM agar plates that contained 4mm

concentration of paraquat. 72 hours later, survival was determined by counting the number of animals that were either moving or those that responded to mild touch with a platinum wire. Animals that crawled away from the plate, exploded, or contained internally hatched worms were excluded from the analysis (Schulze et al., 2013; Hekimi et al., 2010).

M.6.2 Larval Lethality in the presence of mitochondrial complex inhibitors (TTFA, 3-NP, Antimycin-A and Sodium Azide)

L4 stage animals are transferred to seeded NGM agar plates that contained various concentrations of mitochondrial complex inhibitors, 2mM for TTFA, 100mM for 3-NP, 1.27mM for Antimycin-A and 1mM for Sodium azide. At various time intervals survivability was determined by counting the number of animals that were either moving or those that responded to mild touch with a platinum wire (Tsuda et al., 2001; Hekimi et al., 2010).

M.6.3 Larval Development in the presence of paraquat and antimycin-a

Eggs were exposed to various concentrations of paraquat and antimycin-a on NGM plates. The development stage of each worm was recorded after every 72 hours and 96 hours. Each experiment was repeated 3 times at 20°C (Ahn et al., 2008).

M.6.4 Anti-oxidant supplementation

In our research we have supplemented the worms exogenously with two major anti-oxidants to fight against oxidative stress and damage. One is Conenzyme Q (CoQ), also known as ubiquinone (2, 3- dimethoxy-5methyl-6-multiprenyl-1, 4-benzoquinone), is present in most aerobic microorganisms and all animals as a component of the mitochondrial respiratory chain. It participates in electron transport chain by carrying electrons from flavoprotein dehydrogenase [NADH CoQ reductase (Complex I)] and succinate CoQ reductase (Complex II) to Co-QH_2-cytochrome c oxidoreductase (Complex III). Other artificially synthesized antioxidant that we used is MitoQ (mitoquinone mesylate: [10(4,5-dimethoxy-2-methyl-3,6-dioxo-1,4-cycloheexadien-yl)decyl triphenylphosphonium methanesulfonate] which specifically targets and concentrates in mitochondria. It is produced by covalently binding ubiquinone to a triphenylphosphonium (TPP^+) cation.

M.6.4.1 CoQ Assay

Hundred milligrams of CoQ_{10} (4247, Sigma-Aldrich, Madrid, Spain) was dissolved in 10ml of distilled water containing 0.06% of Tween 80 and 10ml (10 mg/ml) added to autoclaved and cooled to 60°C NGM agar medium (total 100ml). We confirmed that the lethality of C. elegans is insensitive to Tween 80 and CoQ_{10} at this concentration. For paraquat and CoQ10 combined plates, paraquat is supplemented at a final concentration of 4mM in the NGM agar containing 1mg/ml CoQ10. Similar lethality test was performed as described before (Furukawa et al., 2004).

M.6.4.2 MitoQ Assay

One milligrams of $MitoQ_{10}$ was dissolved in 1ml of distilled water and 250ul (1mg/ml) was added to autoclaved and cooled to 60^0C NGM agar medium (total 50ml). We confirmed that the lethality of C. elegans is insensitive to TPP+ and $MitoQ_{10}$ at this concentration. For paraquat and MitoQ10 combined plates, paraquat is supplemented at a final concentration of 4mM in the NGM agar containing 5µg/ml MitoQ10 (Smith et al., 2007; Halliwell et al., 2013). Similar lethality test was performed as described before.

M.7 Staining and microscopy

M.7.1 With H2-DCFA

2´7´-H2DCFDA (2', 7'-dichlorodihydrofluorescein diacetate; Sigma-Aldrich, Madrid, Spain) was diluted in DMSO (Sigma-Aldrich, Madrid, Spain) at high concentration (10mM) and frozen at -20^0C as a stock. Before staining stocks were diluted in M9 buffer at a 1:1000 dilution. L4 staged worms were transferred into staining solution and stained for 30mins at 20^0C in a mixer. Worms were mounted on a thick layer of half-dried agar pad on microscopic glass slides and then subjected to fluorescent microscopy. Pictures were taken by NIS software and the fluorescence of the intestinal region was analyzed by ImageJ software (Hekimi et al., 2010).

M.7.2 With MitoSOX

MitoSOX Red (Invitrogen, Eugene, Orgeon, USA) was diluted in DMSO at high concentration (10mM) and frozen at -20^{0}C as a stock. Before staining stocks were diluted in M9 buffer at a 1:1000 dilution. L4 staged worms were transferred into staining solution and stained overnight at 20^{0}C in a mixer. After this incubation worms were washed twice with M9 buffer and were mounted on a thick layer of half-dried agar pad on microscopic glass slides and then subjected to fluorescent microscopy. Pictures were taken by NIS software and the fluorescence was analyzed by ImageJ software (Estes et al., 2014).

M.7.3 With Sudan Black

Fat accumulation was analyzed by Sudan Black (Sigma-Aldrich, Madrid, Spain) fixative staining. Animals grown were washed with M9 buffer and fixed with 2% paraformaldehyde (Merck, Darmstadt, Germany). The worms were then subjected to three freeze–thaw cycles to disrupt the cuticles and incubated 5 minutes and 10 minutes on ice. After 3 washes with cold M9, worms were dehydrated through an ethanol series (25%, 50%, 70%) and 2–5 vol. of 3% Sudan Black B solution (Sigma-Aldrich, Madrid, Spain) were added to the worms, which were then incubated O/N. Worms were rehydrated through an ethanol series (70%, 50%, 25%) and finally with M9. Lipid droplets are detectable as big black granules under bright field microscope. Pictures were taken by NIS software using bright field and subsequently analyzed by ImageJ software. The numbers of lipid droplets greater than 5µm diameter in size were counted in each worm's body from the vulval region till the tail tip (Mak 2012).

M.7.4 With BODIPY- Cholesterol

BODIPY- Cholesterol (Avanti polar lipids, Alabaster, Alabama, USA) was dissolved in DMSO (Sigma, Madrid, Spain) to a concentration of 1 mg/mL for a concentration of 1.73mM and was stored at -20^{0}C. Stock solutions were freshly diluted in 1X PBS (Gibco, Madrid, Spain) to 2 µM and 0.25 ml of the diluted solution was applied to the surface of the Nematode Growth Media (NGM) plates (5 ml agar) seeded with *Escherichia coli* OP50. Plates were allowed to dry in a laminar flow hood and were used immediately. Animals from a synchronous egg lay were allowed to develop on these plates at 20^{0}C and then processed for imaging at confocal microscope (Zeiss SP5) at an excitation wavelength of 488nm (Ashrafi et al., 2014).

M.7.5 With Lysotracker

For LysoTracker staining, NGM agar plates were supplemented with LysoTracker Red (Invitrogen, Eugene, Orgeon, USA) at 2µM. L1 stage animals were grown on these plates for 45-48h at 20^0C without exposure to light. L4 stage larvae were then removed from these plates and directly observed with Confocal microscopy (Zeiss SP5) at an excitation wavelength of 543nm (Ruvkun et al., 2009).

M.7.6 With Lysotracker and BODIPY-Cholesterol

BODIPY-Cholesterol (Avanti polar lipids, Alabaster, Alabama, USA) was included at 2 µM (final concentration) in *E.coli* OP50 plates containing 2 µM Lysotracker Red (Invitrogen, Eugene, Orgeon, USA). L1 animals were allowed to feed on labelled *E. coli* for 2 days in the dark and imaged at L4 stage with Confocal microscopy (Zeiss SP5) (Ruvkun et al., 2009).

M.8 Neuronal aging assays

C. elegans strains were grown at 20^0C for at least two generations before the experiments. After synchronization, F1 hermaphrodite animals were maintained at 20^0C until the late L4 larval stage (characterized by the appearance of the “Christmas tree vulva”) then transferred to the final assay plates (50worms/plate) supplemented with indicated concentrations of Paraquat, CoQ or MitoQ, 0.2mm, 1000µg/ml and 5µg/ml, respectively. Similarly, control animals were transferred to normal agar plates at the same time. Animal age, throughout the paper, refers to the adult age measured in days, calculated by adding one day consecutively from the given animal went through L4 molt. Animals were transferred daily to avoid mix population and while transferring was considered dead when they stopped pharyngeal pumping and failed to respond to mild touch by platinum wire picker. On the actual day of experiment, the plates were washed and animals were anesthetized in 10mm sodium azide (Merck, Germany) on 6% agar pads and subsequently mounted on the confocal microscope (Zeiss SP5) for image analysis.

The GABaergic reporter strain CZ1200 *[Punc-25::GFP + lin-15(+)];lin-15B(n765)X,* and the mechanosensory strain CF702 *[Pmec-7::GFP + lin-15(+)*];*lin-15B(n765)X* was used for this assay. For the former strain, worms were scored for number of GABAergic

neurons, gaps in ventral cord and in dorsal cord and defects in axonal morphology. Defects in axonal morphology were assigned to one of the following four classes of increasing severity: intact commissure, broken commissure, ectopic growth cone, and hyperthrophic branching (Miller et al., 2010). In analysis of touch neurons *Pmec-7:: GFP* expressing animals scored positive for the presence of extra neuronal processes when a visible GFP-labeled branch was observed emanating from the posterior portion of ALM cell body. Similarly, ALM / PLM neuron pairs were scored as overlapping when the PLM neurite extended anterior to the ALM cell body (Gallegos, 2004; Kirszenblat, 2013; Chen, 2013).

M.9 Chemosensory assays

M.9.1 Food race assay

The food race assay, a modified chemosensory assay, was carried out at 20^0C. 50 µl fresh OP50 was dropped on one side of 5 cm NGM agar plates and incubated at 37^0C. Before the food race started the plates were incubated for 12 h at 20^0C. Synchronized one-day adult animals were washed off the plates with pre-chilled M9 buffer. After 2 quick washes worms were dropped in 20 µl M9 buffer on the NGM agar plates, on the opposite side of the bacteria (OP50). The time count started when the M9 buffer was soaked into the agar. After defined time periods, the percentage of the worms that reached the food was calculated (Baumeister et al., 2007).

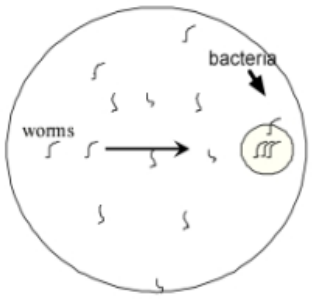

Fig M.1: Diagram illustrates the round medium size plate. The two dark spots at zone A, indicate where the repellent is placed. Worms are placed at one end of the plate opposite to the 50 µl drop of OP50 and were allowed to crawl for one hour.

M.9.2 Odor avoidance assays

Avoidance assays for 2-nonanol and 1- octanol (Sigma-Aldrich, Madrid, Spain) were performed on special square plates with grids (100x100x15mm, Ted Pella Inc, Madrid, Spain). The plates were divided into six sectors labeled A-F. One microliter each of odorants (10% and 100% respectively) and 1 M NaN3 were added in two spots in sector A, and 1 µl each of control diluent (absolute ethanol) and 1 M NaN3 were added in two spots in sector F. An avoidance index (AI) was calculated as [(number of animals in sectors A and B) − (number of animals in sectors E and F)]/ Total number of animals in all six sectors of the plate. Statistical differences were determined by student's t -tests.

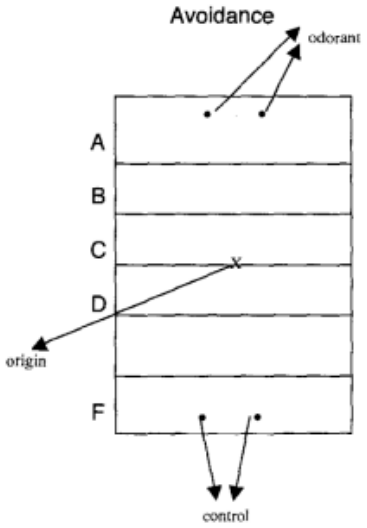

Fig M.2: Diagram illustrates the square plate with grids used specifically for avoidance assays. The two dark spots at zone A, indicate where the repellent is placed. Similarly, the two dark spots at zone F, indicate where the control is placed. The sign X indicates where the worms are placed.

In the chemotaxis attractant assay for diacetyl (Fisher Chemicals, Pittsburgh, USA), we used round medium size NGM plates, 60mm. The nematodes were washed thrice with S-Basal buffer and let them settle by gravity. Then they were aspirated from the bottom of the eppendorfs using a glass pipette and placed at the spot, origin. To avoid the effect of population density, approximately 30 nematodes were placed per plate. The nematodes were allowed to dry and clumped animals were separated from each other by gently touching them with a Kimwipe. Then they were allowed to move freely on the assay plate for 60min. 1.5µl of 0.01% diacetyl dissolved in absolute ethanol and 1.5µl of 1M sodium azide were spotted at the diacetyl location and also 1.5µl of absolute ethanol and 1.5µl of 1M sodium azide were spotted at the opposite control location, of

an assay plate shortly before the experiment. The number of nematodes at the diacetyl and control locations (circle of 1cm radius) was determined under a microscope during a 60-min assay. All the assays were performed in an experimental room maintained approximately at 20^0C (Kobayashi et al., 2013).

M.9.3 Dye Filling Assay

A stock dye solution containing 2mg/ml DiI (1,1- dioctadecyl-3,3,3,3-tetramethylindocarbocyanine perchlorate, Sigma-Aldrich, Madrid, Spain) in dimethyl formamide was stored at -20^0C in a tube wrapped in foil. Transfer well-fed worms from a plate into an eppendorf tube with 1ml M9, spin down worms at 2000-3000 rev/min, take out supernatant leaving worm pellet. Make a initial working solution of 5µl DiI solution from stock and 995µl of M9 (1:200 dilution). From this working, take out 10µl of solution and add into 1ml total of M9 containing worms. Tubes were shielded from light with aluminium foil and incubations carried out at room temperature on a slow shaker for overnight. Next day, spin and was worms with M9 twice before transferring them onto 6% agar pads with sodium azide to visualize fluorescence using appropriate filters under SP5 confocal microscope (Burglin et al., 2010).

M.9.4 Osmotic assays

Worms were placed on high-salt plates containing different concentrations of NaCl (300 mM, 400 mM and 500 mM) and scored for their motility over a period of 10min.

Osmotic stress survival assays were performed on the high – salt plates seeded with *Escherichia coli* (OP50). To score for viability, worms were collected from the salt plates using different recovery buffers (300 mM, 400 mM and 500 mM NaCl in M9), transferred to regular NGM plates (50 mM NaCl), and allowed them to recover overnight before scoring for viability.

Osmotic avoidance behaviour (OSM) was quantified as the percentage of worms that crossed a 2-cm ring of 4M NaCl or 8M fructose on an NGM agar plate, within 5 mins (Morimoto et al., 2004).

M.9.5 General Microscopy

For ciliary morphology, L4 animals grown at the appropriate temperature were mounted on 6% agarose pads set on microscope slides and anesthetized using 10 mM sodium azide (Merck, Germany) which is used to disable worm movement. Cilia were examined on SP5 confocal microscopes (Zeiss Axiovert) using a 63X objective to visualize the GFP expressed in the AWB neuron. Optical sections were collected and *z*-projected at maximum intensity unless noted otherwise. Cilia length and morphology measurements were performed using ImageJ software (National Institutes of Health). To measure cilia length (for both long and short branches), I used the segmented line tool to trace from the center of the AWB cilia to its tip and measured separately (Sengupta et al., 2013).

M.9.6 Reporter strain used for investigating AWB cilia and its related glia like cells morphology

In our research we have used reporter strain, *str-1p:: gfp,* which specifically expresses in the AWB chemosensory neurons ´cilia and cell body (Mukhopadhyay et al., 2007; Troemel et al., 1997) (Fig M.1 A,A'). Generally all AWB cilia in wild type animals possess the characteristic Y-shaped structure (Fig M.1.1 B,B'), but occasionally there is an animal to animal variability in the lengths of each cilial branch, depending upon which temperature they are grown and in which conditions (presence or absence of food) .

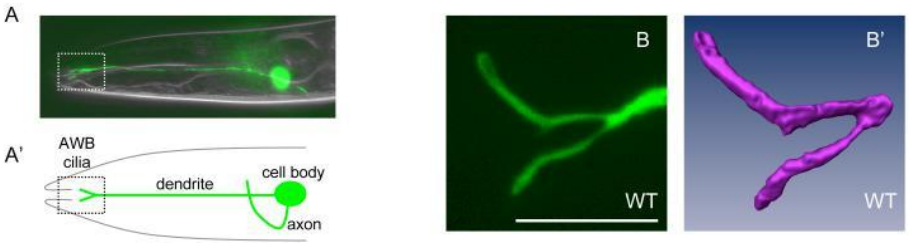

Fig M.3: Reporter strain to study AWB cilia morphology. (A, A´) refers to the location of cell body, processes and the cilia of the AWB neuron in an adult wild type animal. The AWB neuron is visualized via GFP expression driven by the AWB-specific *str-1* promoter. Only one of the bilateral AWB neuron pair is visible in the shown lateral view. (B, B´) The cilia of an AWB neuron

visualized via *str-1p:: gfp* transgene expression in wild-type (WT) adults grown under standard conditions (Sengupta et al., 2009)

Glia is regarded as the neuronal support cells as they provide essential nutritive and growth signals for neurons. To examine how neurons-glia interacts and how is the glial shape and morphology in our *pmp-4* mutant worms we used developmental imaging and genetics to study it. So to observe only the sheath glial cells of *pmp-4* mutant animals we used a reporter strain, containing *F16F9.3pro::mCherry* which is specifically expresses in the sheath glia surrounding the AWB amphid neurons in wild type worms (Fig M.2.A-B). This strain was kindly provided to us by Dr. Maxwell Heiman.

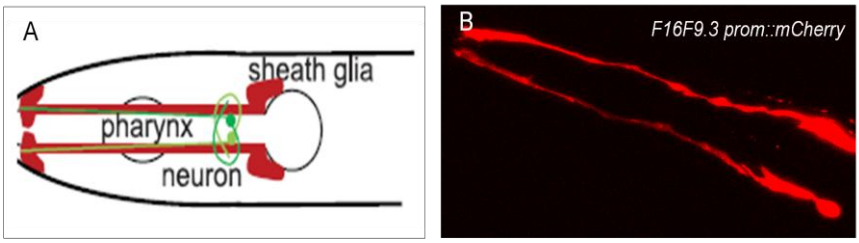

Fig M.4: The sheath glia surrounds the amphid neuron. (A) Cartoon illustrating how sheath glia shown in red surrounds the amphid neuron shown in green. (B) Confocal image of a wild type worm expressing *F16F9.3pro::mCherry* in the amphid sheath cells.

ABBREVIATIONS

List of abbreviations and acronyms

3NP:	3-nitropropionic acid
AA:	Antimycin A_3
Abcd1^{-}*:*	*Abcd1* null mice
Abcd1^{-}*/Abcd2*$^{-/-}$*:*	*Abcd1* and *Abcd2* null mice
ABCD1:	ATP-binding cassette, sub-family D(ALD), member 1
Abcd2$^{-/-}$*:*	*Abcd2* null mice
ACALD:	Adult cerebral adrenoleukodystrophy
Ace-CoA:	acetyl-Coenzyme A
Acyl-CoA:	acyl-Coenzyme A
AD:	Alzheimer´s disease
ALDP:	adrenoleukodystrophy protein
ALDRP:	adrenoleukodystrophy-related protein
ALM:	anterior lateral microtubule
AMN:	adrenomyeloneuropathy
ASH:	Amphid single-ciliated sensory neuron type H
ASJ:	Amphid single-ciliated sensory neuron type J
ATP:	Adenosine triphosphate
AWB:	amphid wing ¨B¨ cells
BSA:	Bovine Serum Albumin
C26:	Hexacosanoic acid
cAMN:	cerebral adrenomyeloneuropathy
CCALD:	Childhood Cerebral Adrenoleukodystropy
C. elegans:	*Caenorhabditis elegans*
cDNA:	complementary DNA
CGC:	*Caenorhabditis* Genetics Center
CoA:	Coenzyme A
CoQ:	Coenzyme Q
Daf:	Dauer formation
DIC:	Differential Interference Contrast
DiI:	1, 1'-Dioctadecyl-3,3,3',3'-Tetramethylindocarbocyanine Perchlorate

DNA:	Deoxyribonucleic acid
drp-1:	Dynamin related protein 1
dsRNA:	double stranded RNA
E.coli:	*Escherichia coli*
ELOVL:	elongation of very long chain fatty acids
ER:	Endoplasmic reticulum
ETC:	Electron Transport Chain
F1:	Filial generation 1
FA:	Fatty acids
FITC:	*Fluorescein Isothiocyanate*
GABA:	*gamma-aminobutyric acid*
GFP:	Green Fluorescent Protein
$HO^{\cdot}$:	Hydroxyl radical
H_2O_2:	Hydrogen peroxide
HSN:	Hermaphrodite specific neuron
HSP:	heat shock protein
IPTG:	isopropyl-β-D-1-thiogalactopyranoside
L1- L4:	Larval stages 1 to 4
LB:	Lysogeny broth
MRN:	mechanoreceptor neurons
mtDNA:	mitochondrial DNA
NA:	Nicotinic acid
NAD^{+}:	Nicotinamide adenine dinucleotide, oxidized form
NADH:	Nicotinamide adenine dinucleotide, reduced form
NMN:	Nicotinamide mononucleotide
NAM:	Nicotinamide
NGM:	Nematode growth media
NO:	Nitric oxide
NR:	Nicotinamide riboside
$O_2^{\cdot-}$:	superoxide anion
OXPHOS:	Oxidative phosphorylation
PARP-1:	Poly(ADP-Ribose) Polymerase-1
PARP:	Poly(ADP-Ribose) Polymerase
PBS:	Phosphate-buffered saline
PD:	Parkinson´s Disease

PGC:	Peroxisome proliferator-activated receptor-gamma coactivator
PLM:	posterior lateral microtubule
PMP:	Peroxisomal Membrane Protein
PQ:	paraquat dichloride
PUFA:	Polyunsaturated fatty acids
qPCR:	quantitative real time polymerase chain reaction
RNAi:	RNA-mediated interference Rna interference
ROS:	Reactive oxygen species
RT:	Room Temperature
SB:	sudan black
SDS:	Sodium Dodecyl Sulphate
SOD:	Superoxide dismutase
TCA:	tricarboxylic acid
TRN:	touch receptor neuron
TTFA:	Thenoyltrifluoroacetone
UNC:	UNCordinated
VLCFA:	very long chain fatty acids
VLCFA-CoA:	very long chain fatty acid thioesterification to coenzyme A
WT:	wild type
X-ALD:	X-linked Adrenoleukodystrophy

APPENDIX

A. Appendix

In the laboratory, we have successfully generated the new *C. elegans* model of X-ALD. As stated before *C. elegans* is a great model organism for molecular genetic research and for axonal studies, so we took its advantage in conducting other projects as well. This appendix section refers to the other projects of mine which involve *C. elegans* as the model organism and are direct consequences of the already created model by us.

Appendix 1

This appendix corresponds to the project investigating the role of PARP1 in *C. elegans* model of X-ALD.

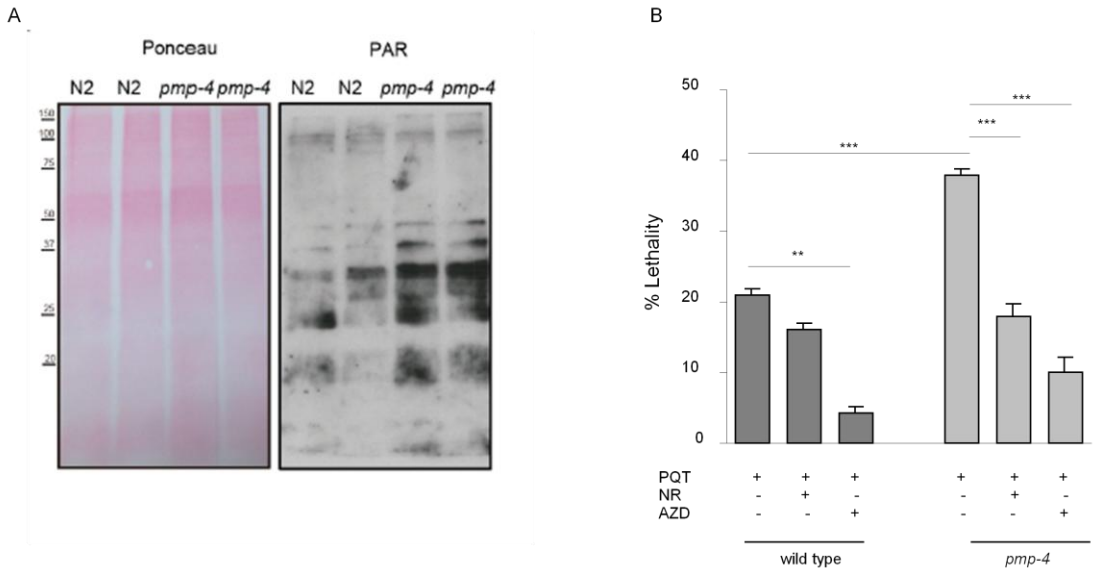

Fig A.1.1: PARP-1 activation in *pmp-4 (ok396)* worms, the *C. elegans* model of X-ALD. (A) Total parylation (PAR) levels were analyzed by Western Blot in aged (L4 + 7 days) N2 wild type and *pmp-4 (ok396)* worms. Ponceau staining is used as control. (B) NAD+ boosters rescue paraquat (PQ) ˉ induced lethality in *pmp-4 (ok396)* worms. Synchronized worms at L4 stage were incubated with PQ (4 mM) and NAD+ boosters (NR 500 µM) and PARPi (AZD2881) 100 nM) and the lethality was scored after 72 hours (N=50 per genotype and treatment). Values are expressed as mean ± SD (*P<05, **P<0.1 and ***P<0.001; two-way ANOVA followed by Bonferroni *post hoc* test).

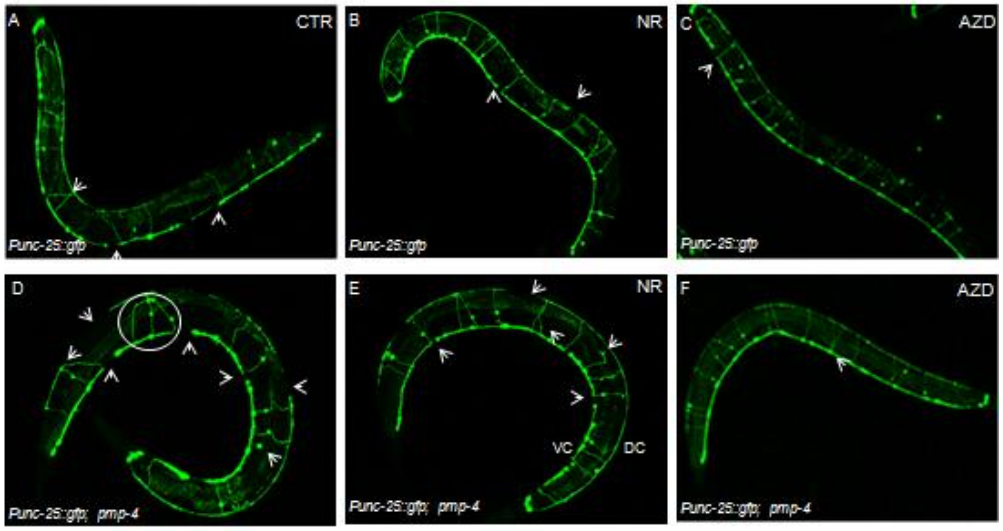

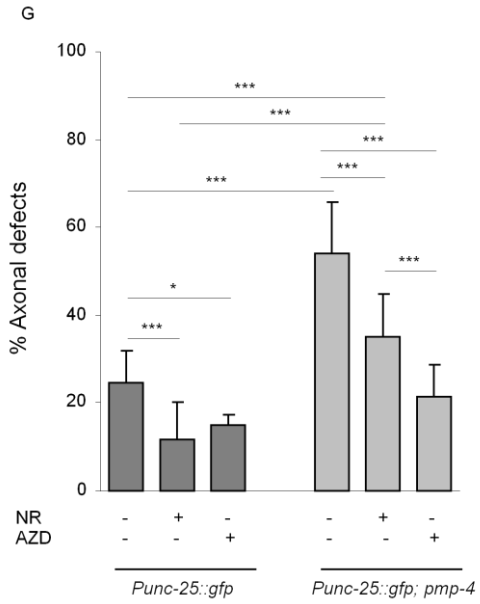

Fig A.1.2: NAD+ boosters rescue axonal damage in *pmp-4 (ok396)* worms. (A-F) Confocal microscopy of GFP-labeled GABAergic neurons (*Punc-25::gfp*), in living worm. Analyses of axonal damages was performed in N2 wild type and *pmp-4 (ok396)* worms treated either with NR (500 µM) or PARPi (AZD2881) 100 nM or untreated, starting at L4 post 7 days. White arrows are labeling the considered axonal abnormalities such as commissural defects and gaps in the ventral cord (VC) and dorsal cord (DC). Between 30 and 40 animals were analyzed per genotype and condition. Objective is 20X. (G) Quantification of axonal defects, represented as the sum of commissural abnormalities and gaps in VC and DC, divided by the total number of axons visible (*P<05, **P<0.1 and ***P<0.001; two-way ANOVA followed by Bonferroni *post hoc* test).

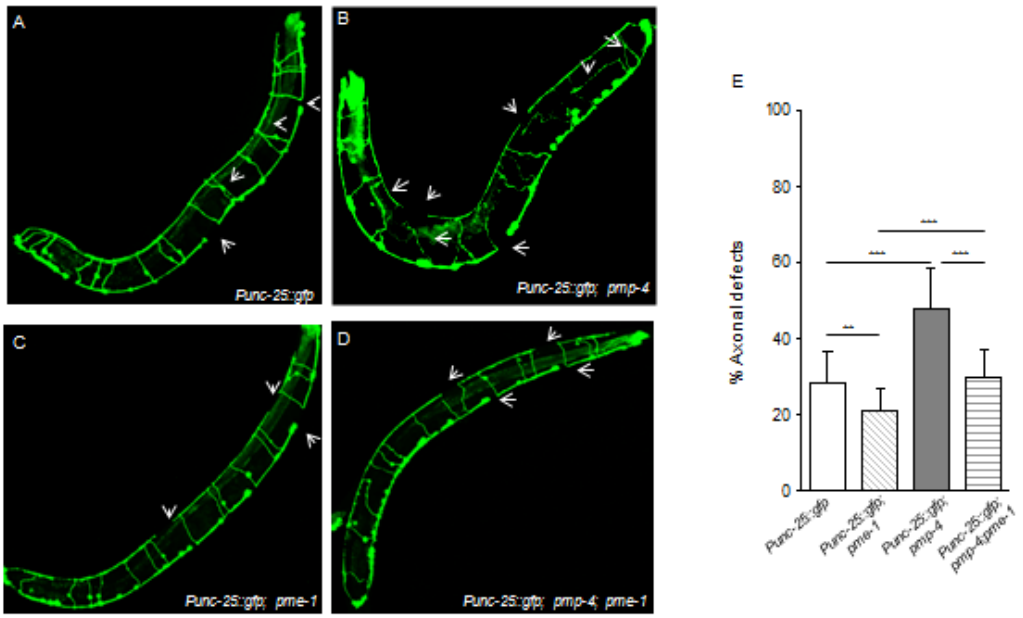

Fig A.1.3: Genetic mutation of PARP1 homolog, *pme-1* rescues axonal damage in *pmp-4 (ok396)* worms. (A-D) Confocal microscopy of GFP-labeled GABAergic neurons (*Punc-25::gfp*), in living worm. Analyses of axonal damages was performed in N2 wild type, *pmp-4 (ok396), pme-1 (ok988)* and *pme-1(ok988); pmp-4(ok396)*, starting at L4 post 7 days. White arrows are labeling the considered axonal abnormalities such as commissural defects and and gaps in the ventral cord (VC) and dorsal cord (DC). Between 30 and 40 animals were analyzed per genotype and condition. Objective is 20X. (E) Quantification of axonal defects, represented as the sum of commissural abnormalities and gaps in VC and DC, divided by the total number of axons visible (*P<05, **P<0.1 and ***P<0.001; one-way ANOVA followed by Tukey *post hoc* test).

Appendix 2

This appendix corresponds to ongoing project investigating the fasting mechanism in *C. elegans* model of X-ALD.

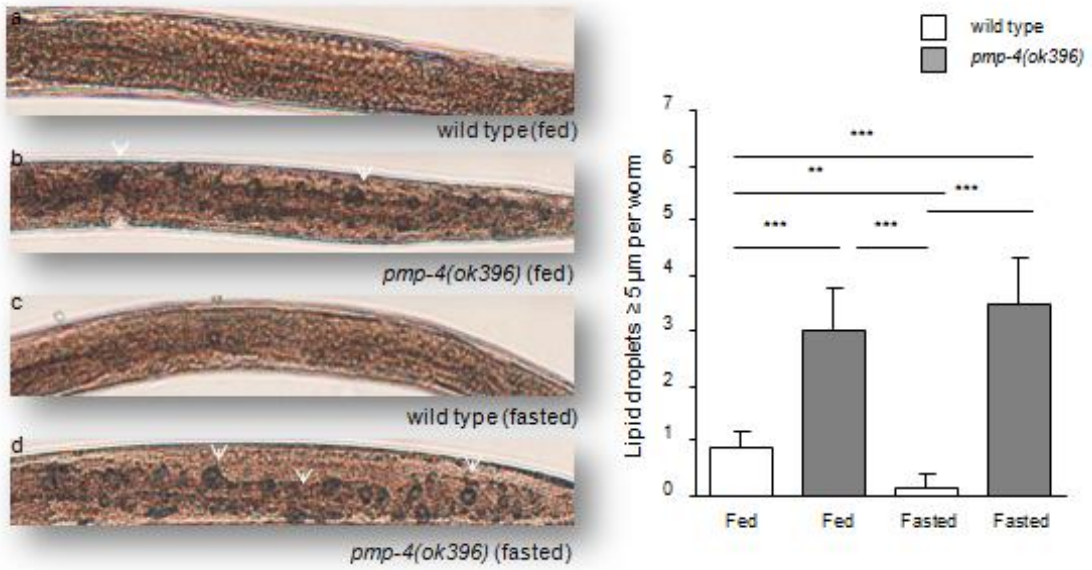

Fig A.2.1: Enlarged lipid droplets are resistant to fasting-induced lipolysis in *pmp-4 (ok396)* worms. Wild-type N2 and *pmp-4(ok396)* mutant animals at L4 stage were incubated in absence of food for 24 hours, and analysed by microscopy in comparison with fed worms. Representative DIC pictures of worms which were stained with sudan black (a-d). Scale bar: 20µm. (e) Quantification of lipid droplets per worm. In each photo we have counted the number of Sudan Black stained structures with a diameter ≥ 5µm. N = 35±5. Significant differences were revealed by ANOVA followed by Tukey HSD post hoc. (*** P < 0.001 referred to *pmp-4(ok396)* strain respect to the other genotype).

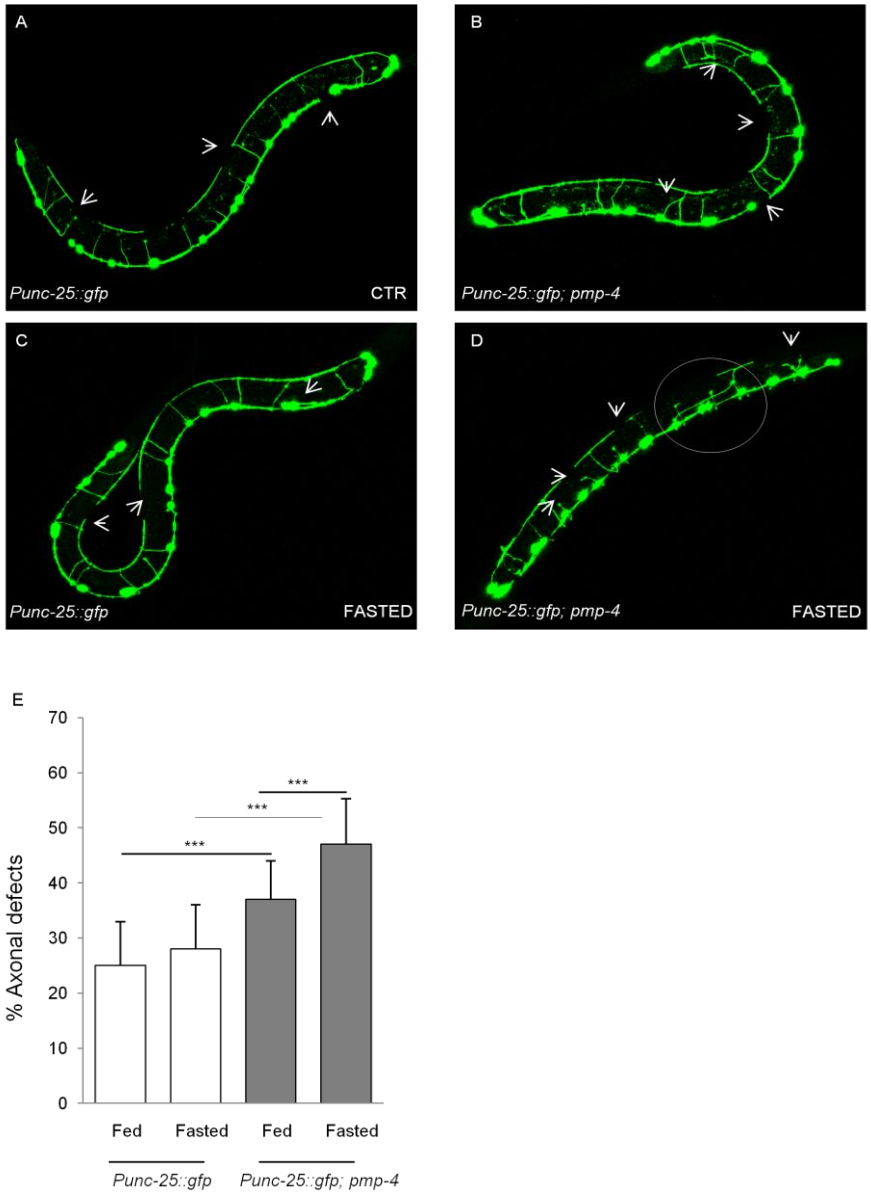

Fig A.2.2: Axonal defects increase in *pmp-4(ok396)* worms under fasting condition. (A-D) Fluorescent representative pictures of *Punc-25:: GFP* and *pmp-4(ok396); Punc-25:: GFP* worms at L4 stage, upon fed and fasted conditions, are shown. Asterisks indicate quantified axonal defects (E) Quantification of the axonal defects. The percentage of axonal defects were calculated as stated in the methodology (%axonal defects = [(comm. abnormalities + num. gaps)/num axons) x 100]). Between 30 and 40 animals were analyzed per genotype and condition (two-way ANOVA Tukey's *post hoc.* Data are mean ± SD ***p<0.001 and **p<0.01).

Appendix 3

This appendix corresponds to the project investigating the role of *drp-1* in *C. elegans* model of X-ALD.

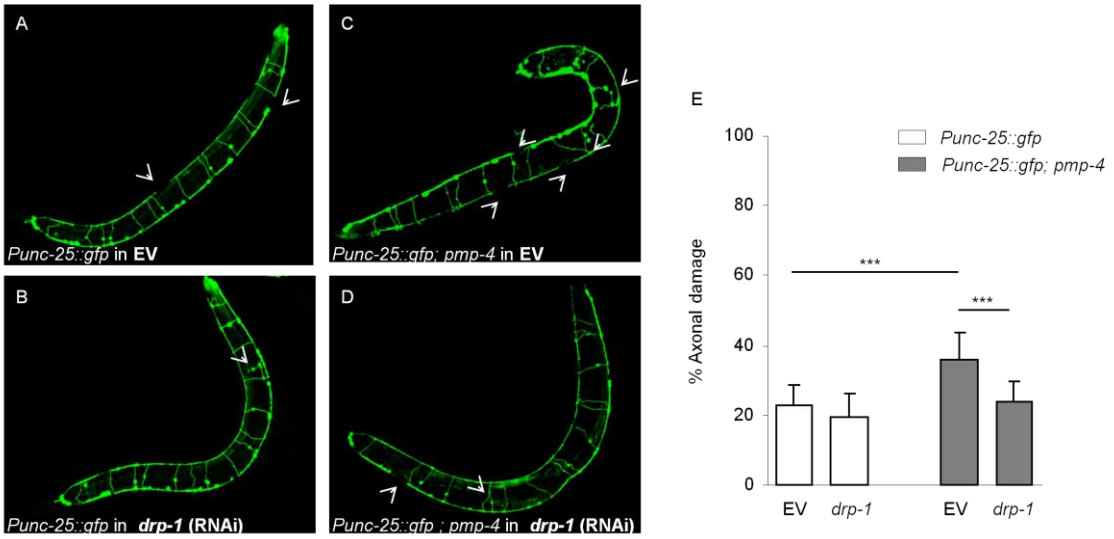

Fig A.3.1: Inactivating *drp-1* ameliorates axonal degeneration in a *C. elegans* model of X-ALD. Synchronized L1 worms at the indicated genotypes were treated with *RNAi* against *drp-1* or empty vector control (EV). At L4 stages worms were transferred onto plates with FUDR 5 µM. At 7 days of adulthood worms were analyzed for axonal abnormalities. (A-D) Fluorescent representative pictures of *Punc-25:: GFP* and *pmp-4(ok396); Punc-25:: GFP* worms at L4 + 7 days stage, upon *drp-1* RNAi treated and untreated, are shown. Asterisks indicate quantified axonal defects. (E) Quantification of the axonal defects. The percentage of axonal defects were calculated as stated in the methodology (%axonal defects = [(comm. abnormalities + num. gaps)/num axons) x 100]). Between 30 and 40 animals were analyzed per genotype and condition (two-way ANOVA Tukey's *post hoc.* Data are mean ± SD ***p<0.001 and **p<0.01).

REFERENCES

References:

A

Artal-Sanz, M., and Tavernarakis, N. (2010). Opposing function of mitochondrial prohibitin in aging. Aging (Albany NY) *2*, 1004-1011.

Ashrafi, K., Chang, F. Y., Watts, J. L., Fraser, A. G., Kamath, R. S., Ahringer, J., and Ruvkun, G. (2003). Genome-wide RNAi analysis of *Caenorhabditis elegans* fat regulatory genes. Nature *421*, 268-272.

B

Bentinger, M., Brismar, K., and Dallner, G. (2007). The antioxidant role of coenzyme Q. Mitochondrion *7 Suppl*, S41-50.

Bentinger, M., Tekle, M., and Dallner, G. (2010). Coenzyme Q--biosynthesis and functions. Biochem Biophys Res Commun *396*, 74-79.

Berger, J., Forss-Petter, S., and Eichler, F. S. (2014). Pathophysiology of X-linked adrenoleukodystrophy. Biochimie *98*, 135-142.

Berry, C., Vecchia, C.L., and Nicotera P. (2010). Paraquat and parkinson´s disease. Cell death and differentiation *17,* 1115-1125.

Betarbet, R., Sherer, T. B., MacKenzie, G., Garcia-Osuna, M., Panov, A. V., and Greenamyre, J. T. (2000). Chronic systemic pesticide exposure reproduces features of Parkinson's disease. Nat Neurosci *3*, 1301-1306.

Bezman, L., and Moser, H. W. (1998). Incidence of X-linked adrenoleukodystrophy and the relative frequency of its phenotypes. Am J Med Genet *76*, 415-419.

Bottelbergs, A., Verheijden, S., Hulshagen, L., Gutmann, D. H., Goebbels, S., Nave, K. A., Kassmann, C., and Baes, M. (2010). Axonal integrity in the absence of functional peroxisomes from projection neurons and astrocytes. Glia *58*, 1532-1543.

Brandt, R., Gergou, A., Wacker, I., Fath, T., and Hutter, H. (2009). A *Caenorhabditis elegans* model of tau hyperphosphorylation: induction of developmental defects by transgenic overexpression of Alzheimer's disease-like modified tau. Neurobiol Aging *30*, 22-33.

Braunreiter, K., Hamlin, S., and Lyman-Gingerich, J. (2014). Identification and characterization of a novel allele of *Caenorhabditis elegans bbs-7.* Plos One *9:* e113737.

Brown, G. C. (1992). Control of respiration and ATP synthesis in mammalian mitochondria and cells. Biochem J *284 (Pt 1)*, 1-13.

Butcher, R. A., Ragains, J. R., Li, W., Ruvkun, G., Clardy, J., and Mak, H. Y. (2009). Biosynthesis of the *Caenorhabditis elegans* dauer pheromone. Proc Natl Acad Sci U S A *106*, 1875-1879.

C

Castello, P. R., Drechsel, D. A., and Patel, M. (2007). Mitochondria are a major source of paraquat-induced reactive oxygen species production in the brain. J Biol Chem *282*, 14186-14193.

Cinar, H., Keles, S., and Jin, Y. (2005). Expression profiling of GABAergic motor neurons in *Caenorhabditis elegans*. Curr Biol *15*, 340-346.

Cocheme, H. M., and Murphy, M. P. (2008). Complex I is the major site of mitochondrial superoxide production by paraquat. J Biol Chem *283*, 1786-1798.

Chavez, V., Mohri-Shiomi, A., Maadani, A., Vega, L. A., and Garsin, D. A. (2007). Oxidative stress enzymes are required for DAF-16-mediated immunity due to generation of reactive oxygen species by *Caenorhabditis elegans*. Genetics *176*, 1567-1577.

Chen C.H., Chen Y.C., Jiang H.C., Chen C.K. and Pan C.L. (2013). Neuronal aging: learning from *C. elegans.* Journal Of Molecular Signaling *8,* 14.

D

Dalfo, E., Portero-Otin, M., Ayala, V., Martinez, A., Pamplona, R., and Ferrer, I. (2005). Evidence of oxidative stress in the neocortex in incidental Lewy body disease. J Neuropathol Exp Neurol *64*, 816-830.

Doroquez, D.B., Berciu, C., Anderson, J.R., Sengupta, P., and Nicastro, D. (2014). A high resolution morphogical and ultrastructural map of anterior sensory cilia and glia in *Caenorhabditis elegans.* eLife *10,* e01948.

E

Earls, L. R., Hacker, M. L., Watson, J. D., and Miller, D. M., 3rd (2010). Coenzyme Q protects *Caenorhabditis elegans* GABA neurons from calcium-dependent degeneration. Proc Natl Acad Sci U S A *107*, 14460-14465.

F

Fang, C., Bourdette, D., and Banker, G. (2012). Oxidative stress inhibits axonal transport: implications for neurodegenerative diseases. Mol Neurodegener *7*, 29.

Fang Ng, L., Gruber, J., Cheah, I., Kiat Goo, C., Fun Cheong, W., Shui, G., Ping Sit, K., Wenk, M. R., and Halliwell, B. (2014). The mitochondria-targeted antioxidant MitoQ extends life span and improves health span of a transgenic *Caenorhabditis elegans* model of Alzheimer disease. Free Radic Biol Med.

Feng, J., Bussiere, F., and Hekimi, S. (2001). Mitochondrial electron transport is a key determinant of life span in *Caenorhabditis elegans*. Dev Cell *1*, 633-644.

Ferrer, I., Aubourg, P., and Pujol, A. (2010). General aspects and neuropathology of X-linked adrenoleukodystrophy. Brain Pathol *20*, 817-830.

Fink, B. D., Herlein, J. A., Yorek, M. A., Fenner, A. M., Kerns, R. J., and Sivitz, W. I. (2012). Bioenergetic effects of mitochondrial-targeted coenzyme Q analogs in endothelial cells. J Pharmacol Exp Ther *342*, 709-719.

Firnhaber, C., and Hammarlund, M. (2013). Neuron-specific feeding RNAi in *C. elegans* and its use in a screen for essential genes required for GABA neuron function. PLoS Genet *9*, e1003921.

Fourcade, S., Lopez-Erauskin, J., Galino, J., Duval, C., Naudi, A., Jove, M., Kemp, S., Villarroya, F., Ferrer, I., Pamplona, R.*, et al.* (2008). Early oxidative damage underlying neurodegeneration in X-adrenoleukodystrophy. Hum Mol Genet *17*, 1762-1773.

Fourcade, S., Lopez-Erauskin, J., Ruiz, M., Ferrer, I., and Pujol, A. (2014). Mitochondrial dysfunction and oxidative damage cooperatively fuel axonal degeneration in X-linked adrenoleukodystrophy. Biochimie *98*, 143-149.

Fourcade, S., Ruiz, M., Camps, C., Schluter, A., Houten, S. M., Mooyer, P. A., Pampols, T., Dacremont, G., Wanders, R. J., Giros, M., and Pujol, A. (2009). A key role for the peroxisomal ABCD2 transporter in fatty acid homeostasis. Am J Physiol Endocrinol Metab *296*, E211-221.

Fourcade, S., Ruiz, M., Guilera, C., Hahnen, E., Brichta, L., Naudi, A., Portero-Otin, M., Dacremont, G., Cartier, N., Wanders, R.*, et al.* (2010). Valproic acid induces antioxidant effects in X-linked adrenoleukodystrophy. Hum Mol Genet *19*, 2005-2014.

Fujii, M., Matsumoto, Y., Tanaka, N., Miki, K., Suzuki, T., Ishii, N., and Ayusawa, D. (2004). Mutations in chemosensory cilia cause resistance to paraquat in nematode *Caenorhabditis elegans*. J Biol Chem *279*, 20277-20282.

G

Galino, J., Ruiz, M., Fourcade, S., Schluter, A., Lopez-Erauskin, J., Guilera, C., Jove, M., Naudi, A., Garcia-Arumi, E., Andreu, A. L.*, et al.* (2011). Oxidative damage compromises energy metabolism in the axonal degeneration mouse model of x-adrenoleukodystrophy. Antioxid Redox Signal *15*, 2095-2107.

Giordano, S., Darley-Usmar, V., and Zhang, J. (2013). Autophagy as an essential cellular antioxidant pathway in neurodegenerative disease. Redox Biol *2*, 82-90.

Gomez, F., Saiki, R., Chin, R., Srinivasan, C., and Clarke, C. F. (2012). Restoring de novo coenzyme Q biosynthesis in *Caenorhabditis elegans* coq-3 mutants yields profound rescue compared to exogenous coenzyme Q supplementation. Gene *506*, 106-116.

Gonzalez-Cabo, P., Bolinches-Amoros, A., Cabello, J., Ros, S., Moreno, S., Baylis, H. A., Palau, F., and Vazquez-Manrique, R. P. (2011). Disruption of the ATP-binding cassette B7 (ABTM-1/ABCB7) induces oxidative stress and premature cell death in *Caenorhabditis elegans*. J Biol Chem *286*, 21304-21314.

Gould, S. G., Keller, G. A., and Subramani, S. (1987). Identification of a peroxisomal targeting signal at the carboxy terminus of firefly luciferase. J Cell Biol *105*, 2923-2931.

Grad, L. I., and Lemire, B. D. (2004). Mitochondrial complex I mutations in *Caenorhabditis elegans* produce cytochrome c oxidase deficiency, oxidative stress and vitamin-responsive lactic acidosis. Hum Mol Genet *13*, 303-314.

Gray, E., Rice, C., Hares, K., Redondo, J., Kemp, K., Williams, M., Brown, A., Scolding, N., and Wilkins, A. (2014). Reductions in neuronal peroxisomes in multiple sclerosis grey matter. Mult Scler *20*, 651-659.

Greenberg, A. S., Egan, J. J., Wek, S. A., Garty, N. B., Blanchette-Mackie, E. J., and Londos, C. (1991). Perilipin, a major hormonally regulated adipocyte-specific phosphoprotein associated with the periphery of lipid storage droplets. J Biol Chem *266*, 11341-11346.

Gruber, J., Fong, S., Chen, C. B., Yoong, S., Pastorin, G., Schaffer, S., Cheah, I., and Halliwell, B. (2013). Mitochondria-targeted antioxidants and metabolic modulators as pharmacological interventions to slow ageing. Biotechnol Adv *31*, 563-592.
Guthrie, C. R., Schellenberg, G. D., and Kraemer, B. C. (2009). SUT-2 potentiates tau-induced neurotoxicity in *Caenorhabditis elegans*. Hum Mol Genet *18*, 1825-1838.

H

Harrington, A. J. Hamamichi, S., Caldwell, G. A., and Caldwell, K. A. (2010). *C elegans* as a model organism to investigate molecular pathways involved with Parkinson´s disease. Developmental dynamics *239,* 1282-1295.
Heddi, A., Stepien, G., Benke, P. J., and Wallace, D. C. (1999). Coordinate induction of energy gene expression in tissues of mitochondrial disease patients. J Biol Chem *274*, 22968-22976.
Heid, H. W., Moll, R., Schwetlick, I., Rackwitz, H. R., and Keenan, T. W. (1998). Adipophilin is a specific marker of lipid accumulation in diverse cell types and diseases. Cell Tissue Res *294*, 309-321.
Heiman, G.H., and Shaham, S. (2009). DEX-1 and DYF-7 establish sensory dendritic length by anchoring dendritic tips during cell migration. Cell *137,* 344-355.
Hilliard, M. A. (2009). Axonal degeneration and regeneration: a mechanistic tug-of-war. J Neurochem *108*, 23-32.

I

Ishiguro, H., Yasuda, K., Ishii, N., Ihara, K., Ohkubo, T., Hiyoshi, M., Ono, K., Senoo-Matsuda, N., Shinohara, O., Yosshii, F.*, et al.* (2001). Enhancement of oxidative damage to cultured cells and *Caenorhabditis elegans* by mitochondrial electron transport inhibitors. IUBMB Life *51*, 263-268.
Ishii, N., Senoo-Matsuda, N., Miyake, K., Yasuda, K., Ishii, T., Hartman, P. S., and Furukawa, S. (2004). Coenzyme Q10 can prolong *C. elegans* lifespan by lowering oxidative stress. Mech Ageing Dev *125*, 41-46.
Izyumov, D. S., Domnina, L. V., Nepryakhina, O. K., Avetisyan, A. V., Golyshev, S. A., Ivanova, O. Y., Korotetskaya, M. V., Lyamzaev, K. G., Pletjushkina, O. Y., Popova, E. N., and Chernyak, B. V. (2010). Mitochondria as source of reactive oxygen species

under oxidative stress. Study with novel mitochondria-targeted antioxidants--the "Skulachev-ion" derivatives. Biochemistry (Mosc) *75*, 123-129.

J

James, A. M., Cocheme, H. M., Murai, M., Miyoshi, H., and Murphy, M. P. (2010). Complementation of coenzyme Q-deficient yeast by coenzyme Q analogues requires the isoprenoid side chain. Febs J *277*, 2067-2082.

Jin, Y., Jorgensen, E., Hartweig, E., and Horvitz, H. R. (1999). The *Caenorhabditis elegans* gene *unc-25* encodes glumatic acid decarboxylase and is required for synaptic transmission but not synaptic development. The journal of neuroscience *19(2),* 539-548.

Joo, H. J., Kim, K. Y., Yim, Y. H., Jin, Y. X., Kim, H., Kim, M. Y., and Paik, Y. K. (2010). Contribution of the peroxisomal acox gene to the dynamic balance of daumone production in *Caenorhabditis elegans*. J Biol Chem *285*, 29319-29325.

Joo, H. J., Yim, Y. H., Jeong, P. Y., Jin, Y. X., Lee, J. E., Kim, H., Jeong, S. K., Chitwood, D. J., and Paik, Y. K. (2009). *Caenorhabditis elegans* utilizes dauer pheromone biosynthesis to dispose of toxic peroxisomal fatty acids for cellular homoeostasis. Biochem J *422*, 61-71.

K

Kassmann, C. M., Lappe-Siefke, C., Baes, M., Brugger, B., Mildner, A., Werner, H. B., Natt, O., Michaelis, T., Prinz, M., Frahm, J., and Nave, K. A. (2007). Axonal loss and neuroinflammation caused by peroxisome-deficient oligodendrocytes. Nat Genet *39*, 969-976.

Kassmann, C. M., Quintes, S., Rietdorf, J., Mobius, W., Sereda, M. W., Nientiedt, T., Saher, G., Baes, M., and Nave, K. A. (2011). A role for myelin-associated peroxisomes in maintaining paranodal loops and axonal integrity. FEBS Lett *585*, 2205-2211.

Kelso, G. F., Porteous, C. M., Coulter, C. V., Hughes, G., Porteous, W. K., Ledgerwood, E. C., Smith, R. A., and Murphy, M. P. (2001). Selective targeting of a redox-active ubiquinone to mitochondria within cells: antioxidant and antiapoptotic properties. J Biol Chem *276*, 4588-4596.

Kemp, S., Berger, J., and Aubourg, P. (2012). X-linked adrenoleukodystrophy: clinical, metabolic, genetic and pathophysiological aspects. Biochim Biophys Acta *1822*, 1465-1474.

Kemp, S., Pujol, A., Waterham, H. R., van Geel, B. M., Boehm, C. D., Raymond, G. V., Cutting, G. R., Wanders, R. J., and Moser, H. W. (2001). ABCD1 mutations and the X-linked adrenoleukodystrophy mutation database: role in diagnosis and clinical correlations. Hum Mutat *18*, 499-515.

Kennedy, L. M., Pham, S. C., and Grishok, A. (2013). Nonautonomous regulation of neuronal migration by insulin signaling, DAF-16/FOXO, and PAK-1. Cell Rep *4*, 996-1009.

Kirszenblat, L., Neumann, B., Coakley, S., and Hilliard, M. A. (2012). A dominant mutation in *mec-7/β-tubulin* affects axon development and regeneration in *Caenorhabditis elegans* neurons. MBoC *24.*

Kimura, K. D., Tissenbaum, H. A., Liu, Y., and Ruvkun, G. (1997). daf-2, an insulin receptor-like gene that regulates longevity and diapause in *Caenorhabditis elegans*. Science *277*, 942-946.

Kitay, B. M., McCormack, R., Wang, Y., Tsoulfas, P., and Zhai, R. G. (2013). Mislocalization of neuronal mitochondria reveals regulation of Wallerian degeneration and NMNAT/WLD(S)-mediated axon protection independent of axonal mitochondria. Hum Mol Genet *22*, 1601-1614.

Klapper, M., Ehmke, M., Palgunow, D., Bohme, M., Matthaus, C., Bergner, G., Dietzek, B., Popp, J., and Doring, F. (2011). Fluorescence-based fixative and vital staining of lipid droplets in *Caenorhabditis elegans* reveal fat stores using microscopy and flow cytometry approaches. J Lipid Res *52*, 1281-1293.

Koon, J. C., and Kubiseski, T. J. (2010). Developmental arrest of *Caenorhabditis elegans* BRAP-2 mutant exposed to oxidative stress is dependent on BRC-1. J Biol Chem *285*, 13437-13443.

Kraemer, B. C., Zhang, B., Leverenz, J. B., Thomas, J. H., Trojanowski, J. Q., and Schellenberg, G. D. (2003). Neurodegeneration and defective neurotransmission in a *Caenorhabditis elegans* model of tauopathy. Proc Natl Acad Sci U S A *100*, 9980-9985.

L

Lim, M. A., Selak, M. A., Xiang, Z., Krainc, D., Neve, R. L., Kraemer, B. C., Watts, J. L., and Kalb, R. G. (2012). Reduced activity of AMP-activated protein kinase protects against genetic models of motor neuron disease. J Neurosci *32*, 1123-1141.

Lombard-Platet, G., Savary, S., Sarde, C. O., Mandel, J. L., and Chimini, G. (1996). A close relative of the adrenoleukodystrophy (ALD) gene codes for a peroxisomal protein with a specific expression pattern. Proc Natl Acad Sci U S A *93*, 1265-1269.

Lopez-Erauskin, J., Fourcade, S., Galino, J., Ruiz, M., Schluter, A., Naudi, A., Jove, M., Portero-Otin, M., Pamplona, R., Ferrer, I., and Pujol, A. (2011). Antioxidants halt axonal degeneration in a mouse model of X-adrenoleukodystrophy. Ann Neurol *70*, 84-92.

Lopez-Erauskin, J., Galino, J., Bianchi, P., Fourcade, S., Andreu, A. L., Ferrer, I., Munoz-Pinedo, C., and Pujol, A. (2012). Oxidative stress modulates mitochondrial failure and cyclophilin D function in X-linked adrenoleukodystrophy. Brain *135*, 3584-3598.

Lopez-Erauskin, J., Galino, J., Ruiz, M., Cuezva, J. M., Fabregat, I., Cacabelos, D., Boada, J., Martinez, J., Ferrer, I., Pamplona, R.*, et al.* (2013). Impaired mitochondrial oxidative phosphorylation in the peroxisomal disease X-linked adrenoleukodystrophy. Hum Mol Genet *22*, 3296-3305.

M

Magwere, T., West, M., Riyahi, K., Murphy, M. P., Smith, R. A., and Partridge, L. (2006). The effects of exogenous antioxidants on lifespan and oxidative stress resistance in Drosophila melanogaster. Mech Ageing Dev *127*, 356-370.

Mak, H. Y. (2011). Lipid droplets as fat storage organelles in *Caenorhabditis elegans*: Thematic Review Series: Lipid Droplet Synthesis and Metabolism: from Yeast to Man. J Lipid Res *53*, 28-33.

Mak, H. Y. (2012). Lipid droplets as fat storage organelles in *Caenorhabditis elegans*: Thematic Review Series: Lipid Droplet Synthesis and Metabolism: from Yeast to Man. J Lipid Res *53*, 28-33.

Marchi, S., Giorgi, C., Suski, J. M., Agnoletto, C., Bononi, A., Bonora, M., De Marchi, E., Missiroli, S., Patergnani, S., Poletti, F.*, et al.* (2012). Mitochondria-ros crosstalk in the control of cell death and aging. J Signal Transduct *2012*, 329635.

Matyash, V., Liebisch, G., Kurzchalia, T. V., Shevchenko, A., and Schwudke, D. (2008). Lipid extraction by methyl-tert-butyl ether for high-throughput lipidomics. J Lipid Res *49*, 1137-1146.

McKay, R. M., McKay, J. P., Avery, L., and Graff, J. M. (2003). *C elegans*: a model for exploring the genetics of fat storage. Dev Cell *4*, 131-142.

McManus, M. J., Murphy, M. P., and Franklin, J. L. (2011). The mitochondria-targeted antioxidant MitoQ prevents loss of spatial memory retention and early neuropathology in a transgenic mouse model of Alzheimer's disease. J Neurosci *31*, 15703-15715.

McNew, J. A., and Goodman, J. M. (1994). An oligomeric protein is imported into peroxisomes in vivo. J Cell Biol *127*, 1245-1257.

Morgan, K. L., Estevez, A. O., Mueller, C. L., Cacho-Valadez, B., Miranda-Vizuete, A., Szewczyk, N. J., and Estevez, M. (2010). The glutaredoxin GLRX-21 functions to prevent selenium-induced oxidative stress in Caenorhabditis elegans. Toxicol Sci *118*, 530-543.

Moser, H., Smith, KD, Watkins, PA, Powers, J, Moser, AB (2001). X-linked adrenoleukodystrophy. In The Metabolic and Molecular Bases of Inherited disease, C. Scriver, ed. (New-York, McGraw-Hill), pp. 3257-3301.

Moser, H. W., Moser, A. B., Frayer, K. K., Chen, W., Schulman, J. D., O'Neill, B. P., and Kishimoto, Y. (1981). Adrenoleukodystrophy: increased plasma content of saturated very long chain fatty acids. Neurology *31*, 1241-1249.

Mosser, J., Douar, A. M., Sarde, C. O., Kioschis, P., Feil, R., Moser, H., Poustka, A. M., Mandel, J. L., and Aubourg, P. (1993). Putative X-linked adrenoleukodystrophy gene shares unexpected homology with ABC transporters. Nature *361*, 726-730.

Mukhopadhyay, S., Qin, Y.L.H., Lanjuin, A., Shaham, S. and Sengupta, P. (2007). Distinct IFT mechanisms contribute to the generation of ciliary structural diversity in *C. elegans.* The EMBO Journal *26,* 2966-2980.

Mukhopadhyay, S., Qin, Y.L.H., Shaham, S. and Sengupta, P. (2008).Sensory signaling-dependent remodeling of olfactory cilia architecture in *C. elelgans.* Dev Cell *14,* 762-774.

Murphy, M. P. (2001). Development of lipophilic cations as therapies for disorders due to mitochondrial dysfunction. Expert Opin Biol Ther *1*, 753-764.

Murphy, M. P., and Smith, R. A. (2007). Targeting antioxidants to mitochondria by conjugation to lipophilic cations. Annu Rev Pharmacol Toxicol *47*, 629-656.

N

Navas, P., Villalba, J. M., and de Cabo, R. (2007). The importance of plasma membrane coenzyme Q in aging and stress responses. Mitochondrion *7 Suppl*, S34-40.

Nix, P., Hammarlund, M., Hauth, L., Lachnit, M., Jorgensen, E. M., and Bastiani, M. (2014). Axon regeneration genes identified by RNAi screening in *C. elegans*. J Neurosci *34*, 629-645.

Nowicka, B., and Kruk, J. (2010). Occurrence, biosynthesis and function of isoprenoid quinones. Biochim Biophys Acta *1797*, 1587-1605.

O

O'Donnell, K. C., Vargas, M. E., and Sagasti, A. (2013). WldS and PGC-1alpha regulate mitochondrial transport and oxidation state after axonal injury. J Neurosci *33*, 14778-14790.

Oikonomou, G., and Shaham, S. (2011). The Glia of *Caenorhabditis elegans*. Glia *59*, 1253-1263.

Oikonomou G., Perens, E.A., Lu, Y., Watanabe, S., Jorgensen, E.M., and Shaham, S. (2011). Opposing activities of LIT-1/NLK and DAF-6/Patched-related direct sensory compartment morphogenesis in *C. elegans.* Plos Biology *9,* e1001121.

Olivier-Mason, A., Wojtyvniak, M., Bowie, R.V., Inna, V.N., Oliver, E.B., and Sengupta, P. (2013). Transmembrane protein OSTA-1 shapes sensory cilia morphology via regulation of intracellular membrane trafficking in *C. elegans.* Development *140*, 1560-1572.

Orsucci, D., Mancuso, M., Ienco, E. C., LoGerfo, A., and Siciliano, G. (2011). Targeting mitochondrial dysfunction and neurodegeneration by means of coenzyme Q10 and its analogues. Curr Med Chem *18*, 4053-4064.

P

Palgunow, D., Klapper, M., and Doring, F. (2012). Dietary restriction during development enlarges intestinal and hypodermal lipid droplets in *Caenorhabditis elegans.* PLoS One *7*, e46198.

Pamplona, R., Dalfo, E., Ayala, V., Bellmunt, M. J., Prat, J., Ferrer, I., and Portero-Otin, M. (2005). Proteins in human brain cortex are modified by oxidation, glycoxidation, and lipoxidation. Effects of Alzheimer disease and identification of lipoxidation targets. J Biol Chem *280*, 21522-21530.

Petriv, O. I., Pilgrim, D. B., Rachubinski, R. A., and Titorenko, V. I. (2002). RNA interference of peroxisome-related genes in *C. elegans*: a new model for human peroxisomal disorders. Physiol Genomics *10*, 79-91.

Powers, J. M., DeCiero, D. P., Ito, M., Moser, A. B., and Moser, H. W. (2000). Adrenomyeloneuropathy: a neuropathologic review featuring its noninflammatory myelopathy. J Neuropathol Exp Neurol *59*, 89-102.

Pujol, A., Ferrer, I., Camps, C., Metzger, E., Hindelang, C., Callizot, N., Ruiz, M., Pampols, T., Giros, M., and Mandel, J. L. (2004). Functional overlap between ABCD1 (ALD) and ABCD2 (ALDR) transporters: a therapeutic target for X-adrenoleukodystrophy. HumMolGenet *13*, 2997-3006.

Pujol, A., Hindelang, C., Callizot, N., Bartsch, U., Schachner, M., and Mandel, J. L. (2002). Late onset neurological phenotype of the X-ALD gene inactivation in mice: a mouse model for adrenomyeloneuropathy. Hum Mol Genet *11*, 499-505.

R

Rawson, R. L., Yam, L., Weimer, R. M., Bend, E. G., Hartwieg, E., Horvitz, H. R., Clark, S. G., and Jorgensen, E. M. (2014). Axons degenerate in the absence of mitochondria in *C. elegans.* Curr Biol *24*, 760-765.

Ray, A., Martinez, B. A., Berkowitz, L. A., Caldwell, G. A., and Caldwell, K. A. (2014). Mitochondrial dysfunction, oxidative stress, and neurodegeneration elicited by a bacterial metabolite in a *C. elegans* Parkinson's model. Cell Death Dis *5*, e984.

Riddle, D. L., Blumenthal, T., Meyer, B. J., and Priess, J. R. (1997). Introduction to *C. elegans.*

Robinson, C. E., Keshavarzian, A., Pasco, D. S., Frommel, T. O., Winship, D. H., and Holmes, E. W. (1999). Determination of protein carbonyl groups by immunoblotting. Anal Biochem *266*, 48-57.

Runkel, E. D., Liu, S., Baumeister, R., and Schulze, E. (2013). Surveillance-activated defenses block the ROS-induced mitochondrial unfolded protein response. PLoS Genet *9*, e1003346.

S

Sacksteder, K. A., Jones, J. M., South, S. T., Li, X., Liu, Y., and Gould, S. J. (2000). PEX19 binds multiple peroxisomal membrane proteins, is predominantly cytoplasmic, and is required for peroxisome membrane synthesis. JCell Biol *148*, 931-944.

Schackwitz, W.S., Takao, I., and Thomas, J.H. (1996). Chemosensory neurons function in parallel to mediate a pheromone response in *C. elegans.* Neuron *17,* 719-728.

Shonfeld, P., Kahlert, S., and Reiser G. (2004). In brain mitochondria the branched-chain fatty acid phytanic acid impairs energy transduction and sensitizes for permeability transition. Biochem *383,* 121-128.

Schluter, A., Espinosa, L., Fourcade, S., Galino, J., Lopez, E., Ilieva, E., Morato, L., Asheuer, M., Cook, T., McLaren, A.*, et al.* (2012). Functional genomic analysis unravels a metabolic-inflammatory interplay in adrenoleukodystrophy. Hum Mol Genet *21*, 1062-1077.

Schluter, A., Fourcade, S., Domenech-Estevez, E., Gabaldon, T., Huerta-Cepas, J., Berthommier, G., Ripp, R., Wanders, R. J., Poch, O., and Pujol, A. (2007). PeroxisomeDB: a database for the peroxisomal proteome, functional genomics and disease. Nucleic Acids Res *35*, D815-822.

Shai Shaham. (2006). Glia-neuron interactions in the nervous system of *Caenorhabditis elegans.* Current opinion in neurobiology *16,* 522-528.

Shao, Z., Watanabe, S., Christensen, R., Jorgensen, E. M., and Colon-Ramos, D. A. (2013). Synapse location during growth depends on glia location. Cell *154*, 337-350.

Shi, Y. C., Yu, C. W., Liao, V. H., and Pan, T. M. (2012). Monascus-fermented dioscorea enhances oxidative stress resistance via DAF-16/FOXO in *Caenorhabditis elegans*. PLoS One *7*, e39515.

Simonetta, S. H. (2010). Towards an automatic method for toxicity and pharmacological testing in *C. elegans.* The worm breeder´s gazette *18,* 2.

Sleigh, J. N., Buckingham, S. D., Esmaeili, B., Viswanathan, M., Cuppen, E., Westlund, B. M., and Sattelle, D. B. (2010). A novel *Caenorhabditis elegans* allele, smn-1(cb131), mimicking a mild form of spinal muscular atrophy, provides a convenient drug screening platform highlighting new and pre-approved compounds. Hum Mol Genet *20*, 245-260.

Smith, R. A., Hartley, R. C., Cocheme, H. M., and Murphy, M. P. (2012). Mitochondrial pharmacology. Trends Pharmacol Sci *33*, 341-352.

Smith, R. A., Hartley, R. C., and Murphy, M. P. (2011). Mitochondria-targeted small molecule therapeutics and probes. Antioxid Redox Signal *15*, 3021-3038.
Smith, S. W., Latta, L. C. t., Denver, D. R., and Estes, S. (2014). Endogenous ROS levels in *C. elegans* under exogenous stress support revision of oxidative stress theory of life-history tradeoffs. BMC Evol Biol *14*, 161.
Soukas, A. A., Kane, E. A., Carr, C. E., Melo, J. A., and Ruvkun, G. (2009). Rictor/TORC2 regulates fat metabolism, feeding, growth, and life span in *Caenorhabditis elegans*. Genes Dev *23*, 496-511.

T

Tank, E. M., Rodgers, K. E., and Kenyon, C. (2011). Spontaneous age-related neurite branching in *Caenorhabditis elegans*. J Neurosci *31*, 9279-9288.
Tauchi-Sato, K., Ozeki, S., Houjou, T., Taguchi, R., and Fujimoto, T. (2002). The surface of lipid droplets is a phospholipid monolayer with a unique Fatty Acid composition. J Biol Chem *277*, 44507-44512.
Tauskela, J. S. (2007). MitoQ--a mitochondria-targeted antioxidant. IDrugs *10*, 399-412.
Thieringer, H., Moellers, B., Dodt, G., Kunau, W. H., and Driscoll, M. (2003). Modeling human peroxisome biogenesis disorders in the nematode *Caenorhabditis elegans*. J Cell Sci *116*, 1797-1804.
Toth, M. L., Melentijevic, I., Shah, L., Bhatia, A., Lu, K., Talwar, A., Naji, H., Ibanez-Ventoso, C., Ghose, P., Jevince, A.*, et al.* (2012). Neurite sprouting and synapse deterioration in the aging *Caenorhabditis elegans* nervous system. J Neurosci *32*, 8778-8790.

V

Van Raamsdonk, J. M., and Hekimi, S. (2009). Superoxide dismutase is dispensable for normal animal lifespan. Proc Natl Acad Sci U S A *109*, 5785-5790.
Van Veldhoven, P. P., and Baes, M. (2013). Peroxisome deficient invertebrate and vertebrate animal models. Front Physiol *4*, 335.
Ventura, N. and Rea, S.L. (2007). *Caenorhabditis elegans* mitochondrial mutants as an investigative tool to study human neurodegenerative diseases associated with mitochondrial dysfunction. Biotechnol *2*.

W

Wanders, R. J., and Waterham, H. R. (2006). Biochemistry of mammalian peroxisomes revisited. Annu Rev Biochem *75*, 295-332.

Ward, J. D., Mullaney, B., Schiller, B. J., He le, D., Petnic, S. E., Couillault, C., Pujol, N., Bernal, T. U., Van Gilst, M. R., Ashrafi, K., (2014). Defects in the *C. elegans* acyl-CoA synthase, acs-3, and nuclear hormone receptor, nhr-25, cause sensitivity to distinct, but overlapping stresses. PLoS One *9*, e92552.

Waters, A.M., and Beales, P.L. (2011). Ciliopathies: an expanding disease spectrum. IPNA *26*, 1039-1056.

Watts, J. L., and Browse, J. (2002). Genetic dissection of polyunsaturated fatty acid synthesis in *Caenorhabditis elegans*. Proc Natl Acad Sci U S A *99*, 5854-5859.

Y

Yang, H. C., Chen, T. L., Wu, Y. H., Cheng, K. P., Lin, Y. H., Cheng, M. L., Ho, H. Y., Lo, S. J., and Chiu, D. T. (2013). Glucose 6-phosphate dehydrogenase deficiency enhances germ cell apoptosis and causes defective embryogenesis in *Caenorhabditis elegans*. Cell Death Dis *4*, e616.

Yang, W., and Hekimi, S. (2010). A mitochondrial superoxide signal triggers increased longevity in *Caenorhabditis elegans*. PLoS Biol *8*, e1000556.

Yokota, S., Togo, S. H., Maebuchi, M., Bun-Ya, M., Haraguchi, C. M., and Kamiryo, T. (2002). Peroxisomes of the nematode *Caenorhabditis elegans*: distribution and morphological characteristics. Histochem Cell Biol *118*, 329-336.

Yoshimura, S., Murray, J., Lu, Y., Waterston, R.H., and Shaham, S. (2008). *mls-2* and *vab-3* control glia development, *hlh-17/*Olig expression and glia-dependent neurite extension in *C. elegans.* Development *135,* 2263-2275.

Z

Zhang, J., Bakheet, R., Parhar, R. S., Huang, C. H., Hussain, M. M., Pan, X., Siddiqui, S. S., and Hashmi, S. (2011). Regulation of fat storage and reproduction by Kruppel-like transcription factor KLF3 and fat-associated genes in *Caenorhabditis elegans*. J Mol Biol *411*, 537-553.

Zhang, P., Na, H., Liu, Z., Zhang, S., Xue, P., Chen, Y., Pu, J., Peng, G., Huang, X., Yang, F.*, et al.* (2012). Proteomic study and marker protein identification of *Caenorhabditis elegans* lipid droplets. Mol Cell Proteomics *11*, 317-328.

Zhang, S. O., Box, A. C., Xu, N., Le Men, J., Yu, J., Guo, F., Trimble, R., and Mak, H. Y. (2010). Genetic and dietary regulation of lipid droplet expansion in *Caenorhabditis elegans*. Proc Natl Acad Sci U S A *107*, 4640-4645.

Zimmermann, R., Strauss, J. G., Haemmerle, G., Schoiswohl, G., Birner-Gruenberger, R., Riederer, M., Lass, A., Neuberger, G., Eisenhaber, F., Hermetter, A., and Zechner, R. (2004). Fat mobilization in adipose tissue is promoted by adipose triglyceride lipase. Science *306*, 1383-1386.